

PONTIFICIA UNIVERSIDAD
CATÓLICA DEL PERÚ

Escuela de Posgrado



**Construction of radon chamber to expose
active and passive detectors**

Tesis para obtener el grado académico de Doctor en
en Física que presenta:

Jhonny Jonnatan Rojas Hanco

Asesor:

María Elena López Herrera

Lima, 2022

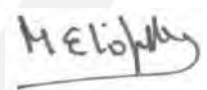
Declaración jurada de autenticidad

Yo, Maria Elena Lopez Herrera, docente de la Escuela de Posgrado de la Pontificia Universidad Católica del Perú, asesora de la tesis titulada *Construction of radon chamber to expose active and passive detectors* del autor Jhonny Rojas Hancco, dejo constancia de lo siguiente:

- El mencionado documento tiene un índice de puntuación de similitud de 13%, lo que está dentro del límite establecido. Así lo consigna el reporte de similitud emitido por el software *Turnitin* el 09/11/2022.
- He revisado con detalle dicho reporte y confirmo que cada una de las coincidencias detectadas no constituyen plagio alguno.
- Las citas a otros autores y sus respectivas referencias cumplen con las pautas académicas.

Lugar y fecha:

Lima, 17 de noviembre de 2022

Apellidos y nombres de la asesora: <u>López Herrera, María Elena</u>	
DNI: 07820505	Firma: 
ORCID: https://orcid.org/0000-0002-5028-4414	

© 2022

Jhonny Jonnatan Rojas Hanco

ORCID:0000-0002-3643-3399

All rights reserved except where otherwise noted.



Dedication

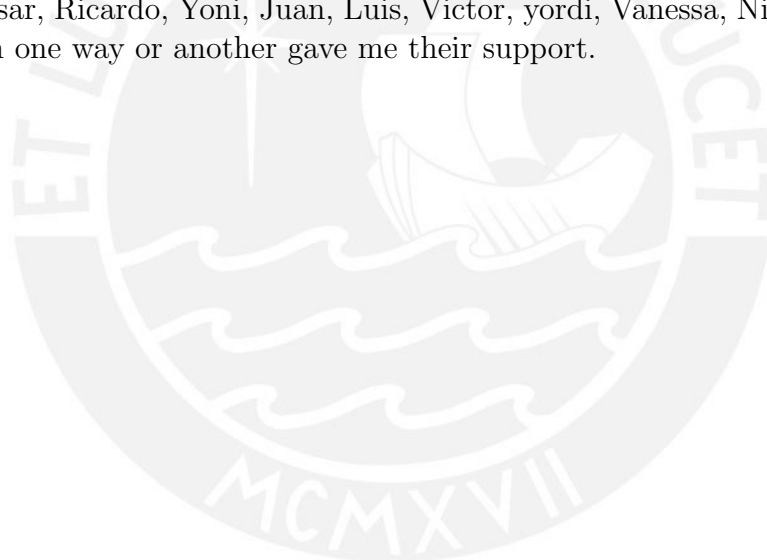
I dedicate this thesis to my parents, Roman and Vilma, to my siblings Fiorella, Cliver, and Flor, and also to my beloved nephews and nieces.



Acknowledgments

This research was supported by the Pontificia Universidad Católica del Perú (PUCP); and funds from CienciaActiva-CONCYTEC number 236-2015.

We appreciate the support of the Physics Faculty of Universidad Nacional Autónoma de México (UNAM) and Dosimetry Laboratory under the PUCP-UNAM Agreement 2016, also the Universidad Autónoma de Zacatecas (UAZ) to Nuclear Research Group led by Dr. Héctor V. who provided laboratory facilities, and the laboratory of Dr. Quindos for allowing us to perform an intercomparison. I would also like to thank Dr. María Elena Lopez H, Dr. Palacios, and Professor Patrizia for their guidance and consideration. A special thanks to the Electronic Engineer Hector Oscana. I would also like to thank all my colleagues of Grupo de investigación en Técnicas de Huellas Nucleares (GITHUNU-PUCP). Finally, to my friends who always supported and advised me during the research, Bertin, Felix, Omar, Marvin, Andres, Jessica, Rafael, Daniel, Cesar, Ricardo, Yoni, Juan, Luis, Victor, yordi, Vanessa, Niel, and Lou. B; and to all those who in one way or another gave me their support.



Abstract

In this research and development, we present the design and manufacture of a radon chamber (PUCP radon chamber), a necessary tool for the calibration of passive detectors, verification of the operation of active radon monitors as well as diffusion chamber calibration used in radon measurements in air, and soils. The first chapter is an introduction to describe radon gas and national levels of radon concentration given by many organizations. Parameters that influence the calibration factor of the LR 115 type 2 film detector are studied, such as the energy window, critical angle, and effective volumes. Those are strongly related to the etching processes and counting of tracks all seen from a semi-empirical approach studied in the second chapter. The third chapter presents a review of some radon chambers that have been reported in the literature, based on their size and mode of operation as well as the radon source they use. The design and construction of the radon chamber are presented, use of uranium ore (autunite) as a chamber source is also discussed. In chapter fourth, radon chamber characterization is presented through leakage λ , homogeneity of radon concentration, regimes-operation modes, and the saturation concentrations that can be reached. Procedures and methodology used in this work are contained in the fifth chapter and also some uses and applications of the PUCP radon chamber are presented; the calibration of cylindrical metallic diffusion chamber based on CR-39 chips detectors taking into account overlapping effect; transmission factors of gaps and pinhole for the same diffusion chambers are determined; permeability of glass fiber filter for ^{222}Rn is obtained after reach equilibrium through Ramachandran model and taking into account a partition function as the rate of track density. The results of this research have been published in indexed journals. Finally, the conclusion and recommendations that reflect the fulfillment aims of this thesis are presented.

Contents

Acknowledgments	III
Abstract	IV
Contents	V
List of Figures	VII
List of Tables	X
1	1
1.1 Introduction	1
1.2 Objectives and development aims	2
1.2.1 Main objectives	2
1.2.2 Specific objectives	2
2 A semi-empirical approach to estimate the LR-115 type 2 sensitivity in radon measurements	3
2.1 Range of alpha particle in air and Mylar film	4
2.2 Critical angle dependent on energy	7
2.3 Effective volume	8
3 Radon chamber design	12
3.1 Overview of some radon calibration chamber	12
3.2 Design of radon calibration chamber	16
3.2.1 Radon chamber features	17
3.3 Simulation of radon chamber	18
3.4 Building chamber	19
3.5 Radon chamber source	20
3.5.1 Radon emanation factor in soil grains	21
3.5.2 Radon emanation factor from soil applying Monte Carlo simulation	22
3.5.3 Autunite as radon source	23
4 Radon chamber test	25
4.1 Leakage test	25
4.2 Homogeneity test	26
4.3 Radon concentration regimes in the radon chamber	29
5 Use and applications of the radon chamber	33
5.1 Comparison of radon active monitors response	33
5.2 Calibration of metallic diffusion chambers based on $CR - 39^{TM}$ chips	44
5.2.1 Experimental procedure	44

5.2.2	Different exposures	45
5.2.3	Counting tracks	46
5.2.4	Calibration factor determination	51
5.3	An approach to the measurement of radon permeability and transmission factor using CR-39 detectors inside a diffusion chambers exposed in PUCP radon chamber	53
5.3.1	Transmission factor determination	53
5.3.2	Permeability of filter	54
6	Conclusions and recommendations	57
6.1	Conclusions	57
6.2	Recommendations	58
	Appendices	59
A		59
A.1	Radon and progeny effective volume code in Fortran 90	59
A.2	Macro CR-39 counting tracks base on ImageJ	64
A.3	Sikuli LR 115 type 2	65
A.4	^{226}Ra distribution in a grain of silicon oxide SiO_2	66
B		68
C	Academic Achievements	94
	Bibliography	95

List of Figures

2.1	After moving a distance d the final energy of the alpha particle is E'	4
2.2	R maximum and minimum in air with density of 0.00120 g/cm^3 within the energy window of the LR 115 type 2	5
2.3	Interaction of alpha particles with the $23\mu\text{m}$ thick Mylar	6
2.4	Range of alpha particles in air with density of 0.00120 g/cm^3 and Mylar	6
2.5	Critical angle $\theta_c(E)$ is the smallest angle at which the alpha particle must impact the detector to form the track.	7
2.6	Different critical angle vs. energy curves is obtained for different etching times by increasing the steps for energy and angle using Sikuli and Python taking into account the track's visibility of $1\mu\text{m}$	8
2.7	Scheme for determining which particles form tracks such that they meet the energetic and angular conditions.	9
2.8	Effective volume geometry of ^{222}Rn , ^{218}Po and ^{214}Po in front of LR 115 type 2 film (red line) see Appendix A.1.	9
3.1	General view of the radon chamber [1]	13
3.2	General view of the flow through radon chamber[2].	14
3.3	Ezeiza radon calibration chamber: 1m^3 acrylic glove-box [3].	14
3.4	Purpose-built radon chamber of Laboratory of Environmental Radioactivity, University of Cantabria [4].	15
3.5	IPEN radon chamber: "The radon chamber (aluminum tank) and the antechambers (glass beakers) are observed, were Radium 226 source was used" [5].	15
3.6	Complete schematic of the radon chamber A, with antechamber B, radon source, air bubbles, working volume and valves for different tests.	17
3.7	3D representation of the radon chamber with dimensions of $650 \text{ mm} \times 850 \text{ mm} \times 850 \text{ mm}$	18
3.8	First simulation gas air behavior at 1.0 L/min with radon chamber dimension using ANSYS software.	18
3.9	Build of radon chamber process.	19
3.10	Installation of radon chamber in the laboratory.	19
3.11	PUCP radon chamber working during an experiment.	20
3.12	Radon chamber tested.	20
3.13	^{222}Rn concentration time variation for two different environmental sample introduced in the purpose made chamber measured by AlphaGuard reference instrument.	21
3.14	^{226}Ra distribution in a grain of soil, considering non-uniform distribution in the same way as Stajic consider [6]. For this topic, review Appendix A.4 and B, where three equations are used to generate the radium distribution as shown and the subsequent determination of radon escape from the soil grain.	23
3.15	Radon source container of autunite sample.	23

3.16	Alpha spectrum of autunite.	24
4.1	the leakage lambda is determined from the exponential fit where the effective lambda is in h^{-1} , then using Equation 4.1 is in the order of $10^{-7}s^{-1}$	25
4.2	Distribution of Electrets inside of radon chamber.	26
4.3	Distribution of radon in the volume space with fans turned off.	27
4.4	AlphaGuard monitor measured the radon concentration during the homogeneity test with fans working.	27
4.5	Homogeneity test with fans working.	28
4.6	^{222}Rn concentration saturation at different flow rates.	29
4.7	The times required to reach equilibrium radon concentration can be observed as a function of flow rate.	30
4.8	Equilibrium ^{222}Rn concentration for different flow-rates.	30
4.9	Dynamic close mode. Growth of radon concentrations and the reduction of radon by the purge system operating at 5.0 L/min is observed.	31
4.10	Closed dynamic mode, where radon is accumulated in the source container for two weeks and then pumped into the radon chamber. In this way, a high concentration value is obtained instantaneously inside the radon chamber to expose detectors to high concentrations. In this mode, the performance of different active monitors can be evaluated since the concentration is maintained.	31
4.11	The radon is accumulated for 4 days in the container and then released into the radon chamber, such that it operates in open dynamic mode with a flow rate of 1.5 L/min. It can be observed how the radon concentration decreases until it finally reaches its equilibrium concentration.	32
4.12	This graph shows the operation of the chamber in hybrid mode, using both closed and open dynamic modes. With this it is possible to return to a previously set radon concentration value, as shown after a certain time the desired value is obtained, then the purge system of the chamber reduces the radon concentration with a flow rate of 5.0 L/min. In addition, a small peak is shown at the end of a controlled interruption of the purge system.	32
5.1	Experimental set-up for the comparison exercise.	34
5.2	Information provided by the radon chamber monitoring system based on e PIN diode S3204-09 (Hamamatsu) as an alpha particles detector developed by Baltuano et al [7].	34
5.3	Information provided by the radon chamber monitoring system.	35
5.4	^{222}Rn concentration is measured by AlphaGuard monitor (AG-2) considered as reference devise.	35
5.5	Environmental conditions during comparative monitors experiment given by AG-2 monitor as reference.	36
5.6	Pressure during comparative monitors experiment given by AG-2 monitor as reference.	36
5.7	A: Radon chamber background; B: Initial radon concentration in equilibrium secular.	37
5.8	AG monitors in flow mode.	37
5.9	RAD 7 behavior in flow mode. its measurements strongly dependent on humidity.	38
5.10	RTM measuments of radon 222.	38
5.11	RPM measuments of radon 222.	39
5.12	Comparative of active monitors response.	40
5.13	Response comparison of active monitors.	41
5.14	^{220}Rn , measurement by RAD7.	41

5.15	RTM ^{220}Rn measurements.	42
5.16	RPM ^{220}Rn measurements.	42
5.17	Path length of ^{220}Rn in air by Monte Carlo simulation (GITHUNU).	43
5.18	Experimental set up for calibration of cylindrical metallic diffusion chambers (radius of 3.05 cm, height of 0.792 cm) based on CR-39.	44
5.19	Passive monitors based on CR-39 chips.	45
5.20	Extractions and exposures of monitors to ^{222}Rn concentrations at second experiment.	46
5.21	Range track area histogram whit total tracks, avoiding damage and overlapping mix tracks in a given frame of CR-39 chip.	47
5.22	Range track area histogram whit total tracks of background in a given frame of CR-39 chip.	47
5.23	Range track area histogram whit total tracks in certain frame of CR-39 chip exposed.	48
5.24	Removing outliers to determine tracks density.	48
5.25	Considering tracks formed up to 3σ , then they will be outliers.	49
5.26	Tracks in diffusion metallic chambers with CR-39.	49
5.27	CR-39 background. Where circles represent outlier track density.	50
5.28	Track density of CR-39 inside metallic diffusion chamber exposed.	50
5.29	Correlation of track density readings by ImageJ MACRO39 and Politrack system.	51
5.30	Experimental response fit curve for CR-39 inside cylindrical metallic diffusion chamber.	52

List of Tables

2.1	Values of minimum energy E_{min} (MeV), maximum energy E_{max} (MeV), mean critical angle $\langle \theta \rangle$ (degrees), ^{218}Po air fraction f_1 that minimized the deviations between experimental sensitivity S_{exp} (cm) and simulated sensitivity S_{sim} (cm) in different radon diffusion chamber based in LR 115 type 2 detectors.	10
3.1	Features of radon chambers	16
3.2	Features of PUCP radon chamber	16
4.1	Radon chamber homogeneity values [8].	26
5.1	Radon concentrations for different active monitors.	40
5.2	First radon monitors exposures.	45
5.3	Second radon monitors exposures.	45
5.4	Results from monitor exposition to radon concentration at PUCP radon chamber.	51
5.5	Diffusion metallic chamber based on CR-39 chips calibration factor.	52
5.6	First results of transmission factor experiment.	54
5.7	Second results of transmission factor experiment.	54
5.8	Permeability experiment	55
5.9	Calibration factor(sensitivity of diffusion chambers based in CR-39 detectors).	55

Chapter 1

1.1 Introduction

The solar system was formed 4.5 billion years ago through nuclear reactions between protons, alpha particles, and high energy interactions following the rule of binding energy per nucleon and mass number[9]. This process allowed the creation of light and heavy elements, many of which were radioactive. Of the latter, only a few radioactive elements survive today due to very long half-lives[10]. These are reflected in the radioactive chains that can be found nowadays. One of these radioactive elements that are a consequence of the decay of the elements that make up the radioactive chains is a radon isotope which, as will be mentioned later, is a radioactive gas that contributes an environmental dose to human beings [11, 12].

The discovery of radon is attributed to Rutherford [13, 14] in current texts and also to Ernest Friedric Dorn [15]. It is now known that the authors discovered each radon isotope, ^{222}Rn and ^{220}Rn , separately. Then through a high voltage experiment in air, around 1901 Elster and Geitael noted the presence of radioactive substances and then radon in free air [16].

Three natural isotopes of radon namely, radon ^{222}Rn , thoron ^{220}Rn , and actinon ^{219}Rn resulting from the radioactive decay of the uranium, thorium and the actinium series. ^{222}Rn consists of the decay of ^{226}Ra , the direct parent of the ^{238}U series, while ^{220}Rn decomposes from ^{224}Ra , a member of the ^{232}Th series. The isotopes of radon are colorless, odorless, and tasteless noble gases, and they are naturally present in the atmosphere and in the soil. Actinon produces ^{223}Ra decay from the ^{235}U series, and is usually neglected because its presence is negligible in the atmosphere. Radon is spread as a gas element in the natural radioactive chain of the earth's crust. Radon emanates and exhales from rocks and soil and tends to concentrate in indoor places such as mines or underground homes. Other sources, including building materials and water extracted from wells, are less important in most circumstances [17].The main radiation dose received by the population comes from radon progeny. Many studies in Europe and North America suggest that radon progeny may cause lung cancers in the general population. The risk of developing lung cancer increases proportionately to increased exposure to radon progeny. Many people are exposed to low concentrations of radon, and most lung cancers with radon are produced at low levels. It has been determined that radon is the second leading cause of lung cancer in the population. The World Health Organization (WHO) gives indications on the maximum permitted concentration of radon in a residential home, and determining the level of radon concentration recommends it as an important component in a national health program [18].

A reference level represents the maximum accepted average annual radon concentration in a residential dwelling. It is an important component of a national radon program and should be established by countries at the national level. Action level refers to the annual average concentration in a home that is established by different organizations and if it is exceeded, must be taken actions to reduce radon concentration to below the limit [19, 18] <https://www.epa.gov/radon>.

Different national factors must be taken into account to establish a radon reference level, such as the distribution of measured radon concentration values reported on a map, the number of existing homes with high concentrations of radon, the average level of radon, and the prevalence of smoking. In light of the latest scientific data, WHO proposes a reference level of 100 Bq/m^3 to reduce the health risks of exposure to indoor radon [20].

Here in Peru for homes reference levels of radon are recommended between 200 Bq/m^3 to 600 Bq/m^3 and take action in homes and workplaces if radon concentration exceeds 1000 Bq/m^3 , then remediation measures should be taken to reduce radon concentration [21], [22].

A number of techniques have been used for measuring the concentrations of radon (^{222}Rn) and its progeny in the environment [23, 24].

With the above, there is a great need to measure not only radon concentrations but also its progeny properly, so the passive and active radon and progeny monitors must be calibrated and every so often tested to ensure proper measurement, therefore it is proposed and implement a radon chamber for these purposes in addition to studies of environmental radioactivity applications using radon the chamber.

1.2 Objectives and development aims

1.2.1 Main objectives

In this thesis, the objectives of research and development in radon measurements are:

- Design and construction of a radon chamber for detector calibration.
- Determination and verification of the parameters of the built radon chamber.
- Use of the radon chamber in specific application research.

1.2.2 Specific objectives

- Achieve different radon saturation concentrations inside the radon chamber.
- Passive detectors calibration as radon diffusion chamber based on CR-39 and LR 115 type 2 nuclear track detectors.
- Determine the permeability of glass microfiber filter without binder.
- Measure the experimental radon transmission factor by the pinhole method.

Chapter 2

A semi-empirical approach to estimate the LR-115 type 2 sensitivity in radon measurements

Basic concepts about the behavior of radon and its progeny in the air as the volume of the diffusion chamber must be taken into account as the secular and transient equilibrium of radon and its progeny. In addition, it is necessary to know a fundamental issue that has to do with the stability of nuclei in order to explain what type of nuclei are more likely to undergo nuclear disintegration by emitting alpha particles, particularly in the decay of radon and its progeny. Understand why under certain conditions, such as the presence of aerosols, and the exchange of air volume between a room and the outside is important to measure radon. For that, a balance factor between radon and its progeny can be measured. This factor is known as the equilibrium factor (FE), it is a very important parameter that allows us to know the proportion of the radon progeny present [25, 26, 27].

For such a measurement a passive monitor can be used such as diffusion chambers based on solid-state nuclear track detectors (SSNTD) like LR 115 type 2 or CR-39 among others. It is then possible to relate the number of tracks found in an SSNTD detector with those of radon and its progeny. It is well-known that LR-115 type 2 is a cellulose nitrate with an active part of 12 μm and a polyester base of 100 μm , which is used to detect radon and its progeny. Therefore, the sensitivity of such detectors must be determined experimentally or simulated.

Due to the need to know the calibration factor (CF) of the LR- 115 type 2 detectors in bare mode and in diffusion chambers of different geometries, Monte Carlo simulation is performed in a semi-empirical way. For this purpose, it is required to use input parameters, such as the energy window, the critical angle in dependence on its energy or its mean, the developing conditions, and the track counting criteria.

It randomly generates positions in space from which radon and progeny can decay by emitting alpha particles with a solid angle of 4π . These can be detected by the LR-115 type 2 film. The minimum distance for radon is about 5 mm and 30 mm for its most energetic decay product ^{214}Po . The maximum distance for detection is approximately 35 mm for Radon (α -energy: 5.59 MeV) and about 60 mm for its most energetic decay product ^{214}Po (α -energy: 7.83 MeV) http://www.gt-analytic.at/downloads_en/Kod_tech_det.pdf. Depending on certain energetic and angular conditions. It is necessary to show first the dependence of alpha particle range in the air on the energy under certain atmospheric considerations of a specific experiment.

2.1 Range of alpha particle in air and Mylar film

The interaction of alpha particles emitted by ^{222}Rn , ^{220}Rn and their respective progeny with air and Mylar is studied to determine how far the effective volumes of radon and its progeny are from the detector, which can be detected.

Through a TRIM and SRIM [28] program, the ranges are determined for different energies, a data treatment is performed obtaining final energies and distances traveled by the alpha particles in air.

A quadratic fit with $R^2 = 0.999$ of energy vs range is made. Then the energy is determined as a function of the distance traveled by the alpha particles under environmental conditions that are reflected in the air density.

The calculation of the energy of the alpha particles for different distances traveled as well as the final energies shown in Figure 2.1

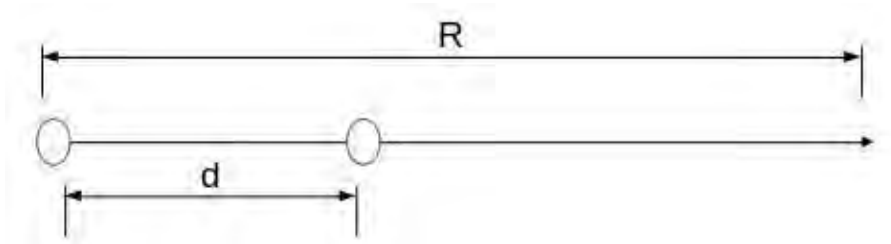


Figure 2.1: After moving a distance d the final energy of the alpha particle is E'

$$R(E') = aE'^2 + bE' + c \quad (2.1)$$

$$E' = \frac{-b + \sqrt{b^2 - 4ac'}}{2a} \quad (2.2)$$

The range (R) traveled in air by radon 222 alpha particles and its progeny is shown in Figure 2.2.

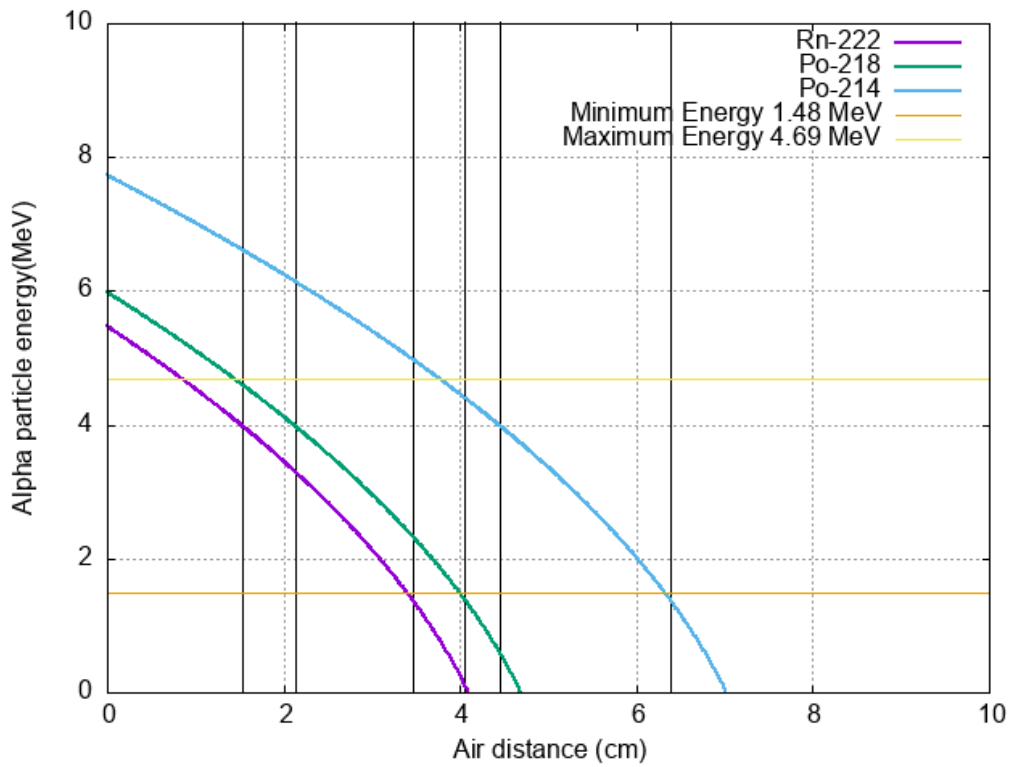


Figure 2.2: R maximum and minimum in air with density of 0.00120 g/cm^3 within the energy window of the LR 115 type 2

The atmospheric conditions for the simulation were such that they are all reflected in the density of air which was 0.00120 g/cm^3 . The graph is in correspondence to that obtained by Nikezic [29] and agrees with those reported by Glenn Knoll [30].

This same procedure can be applied considering other media such as Mylar for the detection of radon progeny, which can be deposited on the surface of Mylar and LR 115 type 2 film as show in Figure 2.3

2.1. Range of alpha particle in air and Mylar film

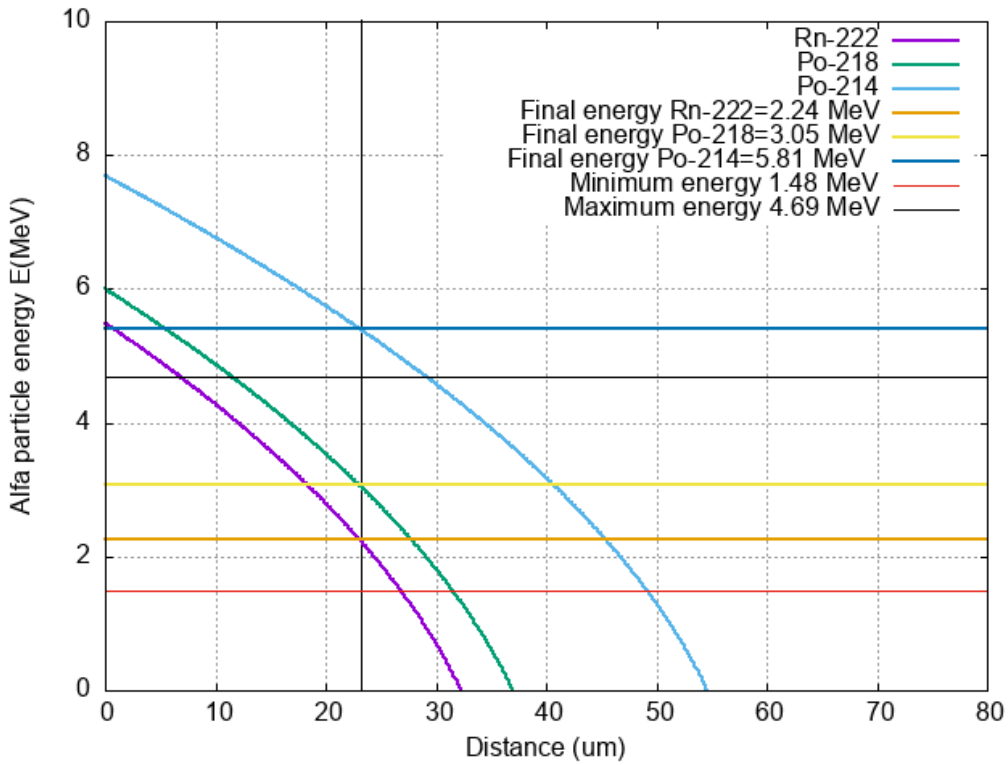


Figure 2.3: Interaction of alpha particles with the $23\mu\text{m}$ thick Mylar

Taking into account the air and the Mylar medium, we can determine the maximum distance at which the alpha particle must be found, so that on its way to the Mylar or film detector, it can arrive with a minimum of energy so that it can be registered as shown in Figure 2.4

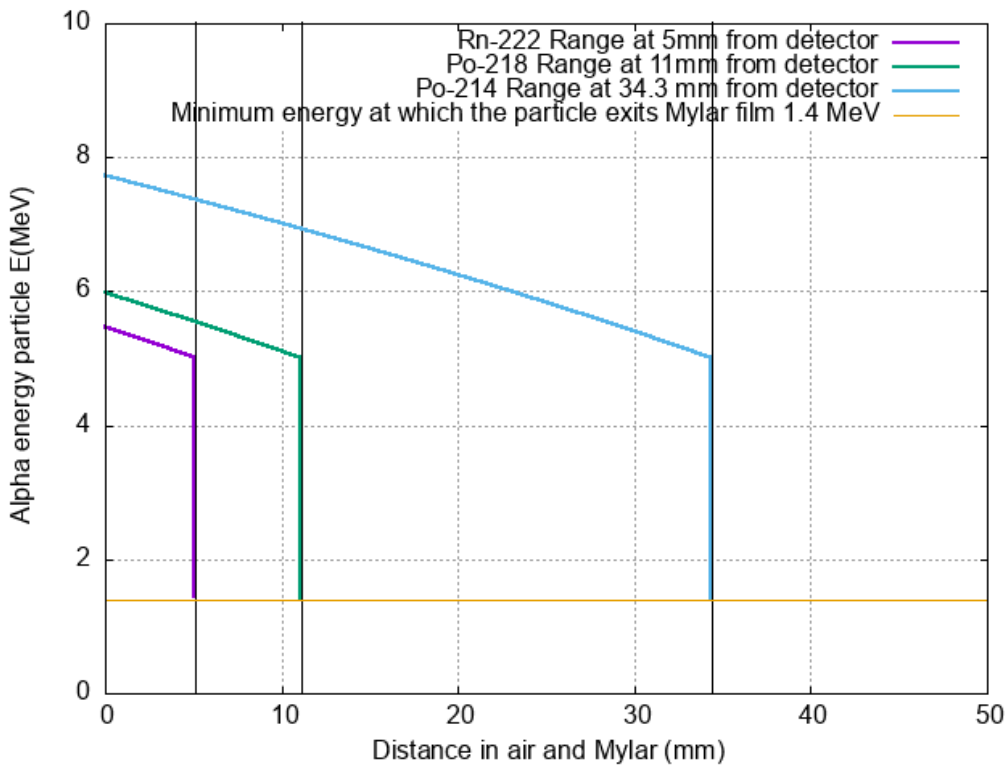


Figure 2.4: Range of alpha particles in air with density of 0.00120 g/cm^3 and Mylar

2.2 Critical angle dependent on energy

Once the maximum and minimum distances have been determined in dependence of the window energy, another important parameter that needs to be known is the critical angle whose value depends on the incident alpha particles energy on the detector, which is intrinsically related to the chemical treatment methodology and track visibility criteria. Software called TRACK-TEST [31] is used to generate a track profile based on the geometrical parameters, then alpha tracks major and minor axis are analyzed to establish whether alpha tracks particle is taking in account as visible. This consists of finding an intersection between the projected diameters, which must be greater than or equal to $1\mu m$. The track profiling program uses different models as Durrani and Bull [32], Durrani and Green [33]. Track formation depends strong of V-functions, witch is based on the residual range, whose value varies as the thickness of the LR-115 type 2 detector while changes the etching time. Then it is possible to determine critical angles and an energy window for which tracks are formed in the detector for a given etching time.

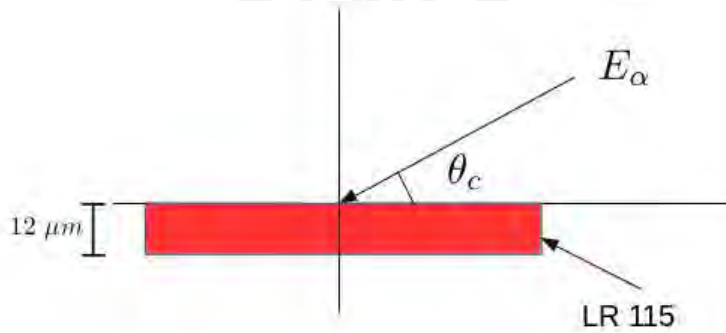


Figure 2.5: Critical angle $\theta_c(E)$ is the smallest angle at which the alpha particle must impact the detector to form the track.

According to the above, a curve of critical angles vs energies is obtained trough interactive software Sikuli [34]. Sikuli controls the Track Test program by a sequence of images in order to run it as many times as necessary (see Appendix A.3). The output data generated by the Track Test is immediately analyzed by an algorithm written in Python to determine whether or not a track is formed according to the energy and angle conditions, which must be greater than the critical angle. This is demonstrated in Figure 2.6

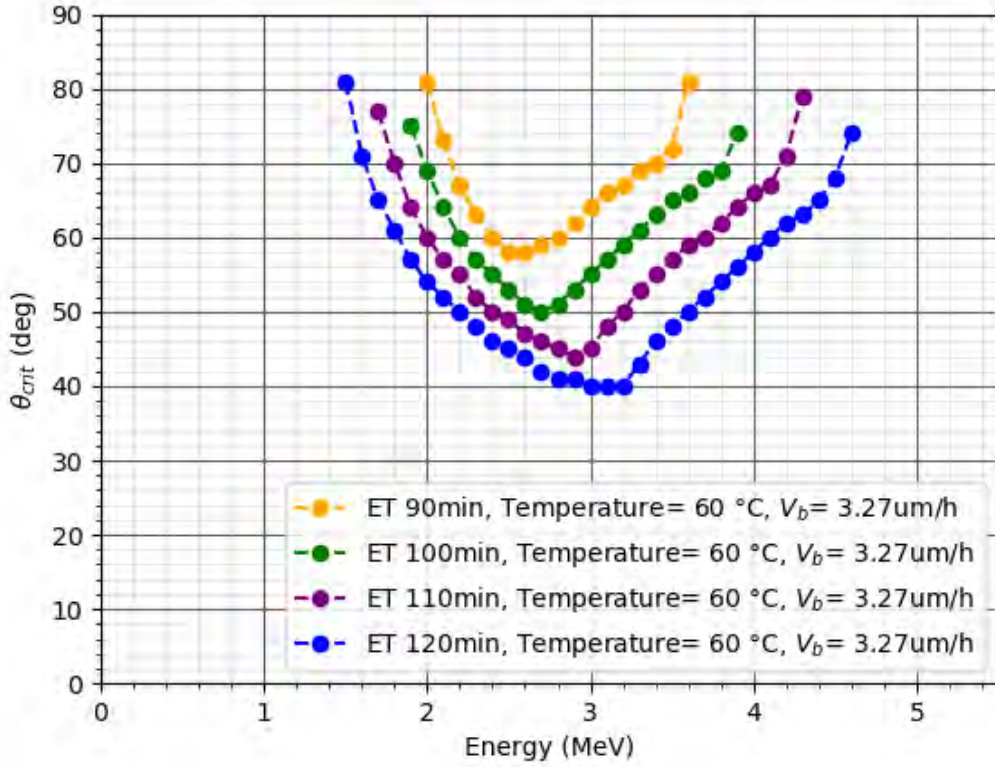


Figure 2.6: Different critical angle vs. energy curves is obtained for different etching times by increasing the steps for energy and angle using Sikuli and Python taking into account the track's visibility of $1\mu m$.

2.3 Effective volume

Once the critical angle vs energy is determined, a space is simulated where both ^{222}Rn and its short-lived progeny can be found.

A concept called effective volume is introduced which contains all the possible ^{222}Rn nuclei and progeny that have a non-zero probability of being detected by the LR-115 or CR-39, whose shape will depend on the type of detector, as well as whether it is used in bare mode or with diffusion chambers (taking into consideration the effective surfaces).

To do this, N random numbers are generated in a given space:

$$r = (r_{det} + d_{max})\sqrt{\epsilon_1} \quad (2.3)$$

$$\alpha = 2\pi\epsilon_2 \quad (2.4)$$

Where, r_{det} radio of the detector, d_{max} maximum distance at witch radon can be detected under critical angle vs energy condition, ϵ_1, ϵ_2 are random numbers, α is the angle at which the alpha particle hits the detector.

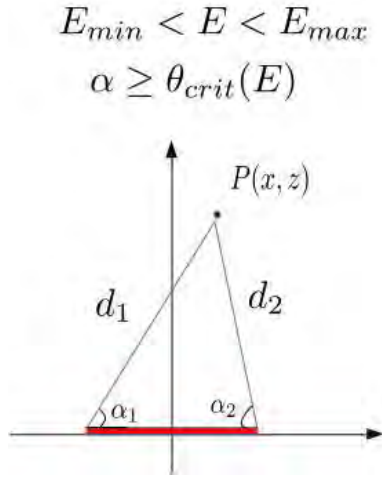


Figure 2.7: Scheme for determining which particles form tracks such that they meet the energetic and angular conditions.

Considering the critical angle and energy window conditions, it is possible to determine ^{222}Rn , ^{218}Po and ^{214}Po effective volume required to LR 115 type 2 film. A simulation of the points distributed in 3D space is performed to know the shape of the effective volumes. However, the figures presented are cross-sections. In addition, the code developed in Fortran is presented in Appendix B.

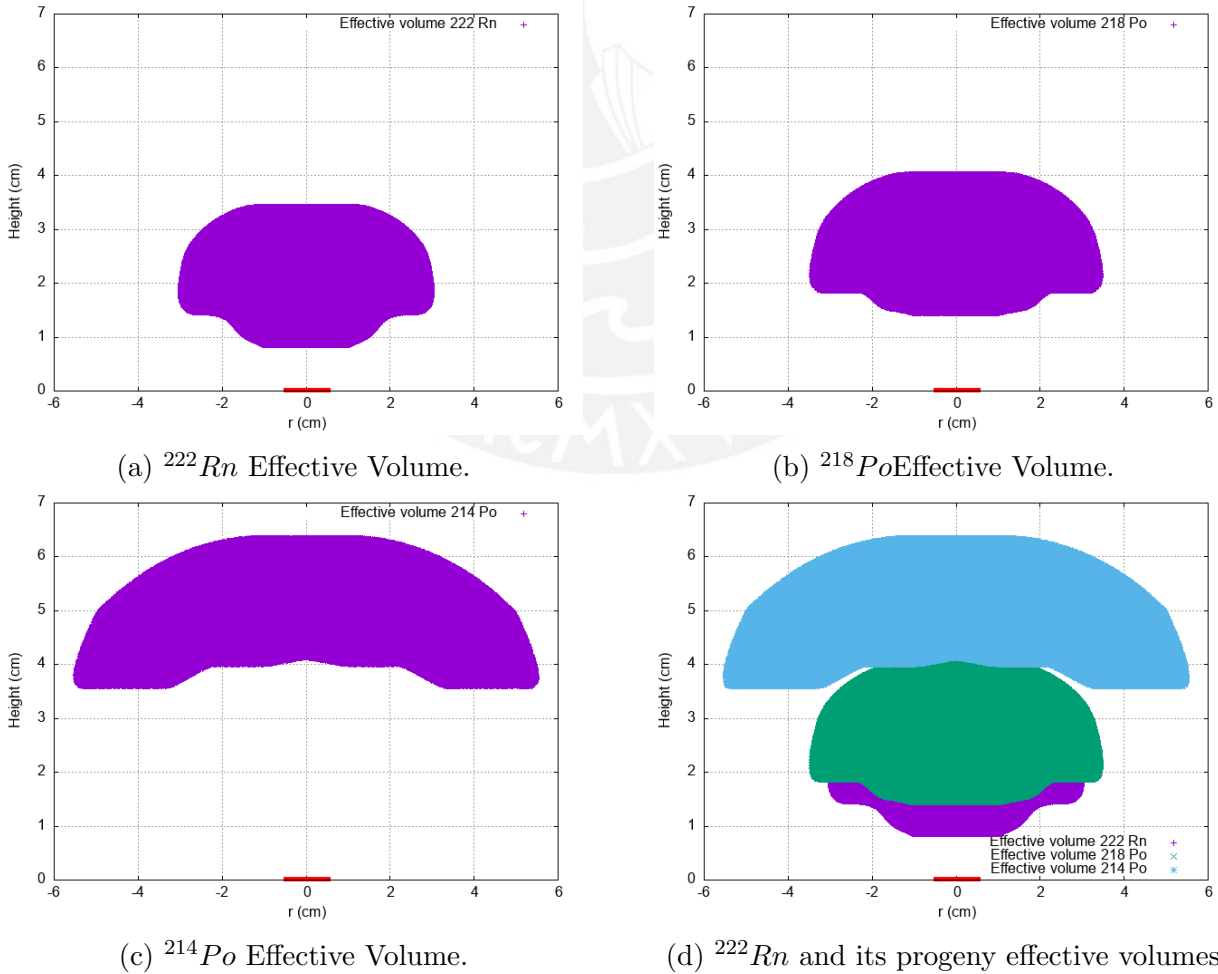


Figure 2.8: Effective volume geometry of ^{222}Rn , ^{218}Po and ^{214}Po in front of LR 115 type 2 film (red line) see Appendix A.1.

^{218}Po can be deposited on the surfaces of the diffusion chamber [35], s_{iw} measures the sensitivity of the detector to alpha particles emitted by this progeny, s_{ia} quantifies the sensitivity to alpha particles emitted in air by radon and fraction of polonium in air.

Then, the partial sensitivities of detector to the alpha particles emitted from air s_{ia} and walls s_{iw} can be calculated as follows.

$$s_{ia} = \frac{n_{Vi}V_{effi}}{N_{Vi}\pi r_d^2} \quad (2.5)$$

$$s_{iw} = \frac{n_{Si}S_{effi}V}{N_{Si}\pi r_d^2 A} \quad (2.6)$$

The calibration coefficient can be determined as the partial sum of the sensitivities multiplied by f factors representing the radon progeny in air and on surfaces. Where A and V are internal surface and internal Volume of the diffusion chamber, respectively. n_{Vi} and n_{Si} are number of alpha particles detected by the detector with r_d radius A . All the details can be found in the published article [36].

Some similar work has been done considering different energies and angles such that the response of detector and its geometry can be known [37]. However, the angles considered are iterated by 10 degrees, which means that the region of space found where an alpha emission can be detected is not defined with good accuracy. The contribution at this point is that the angular iterations are more accurate and the concept of critical angle is used such that it is the minimum possible whose function contains the etching condition in dependence on energy also defining the size and geometry of diffusion chambers. Then in this work, we also determine the optimal parameters for the shape of the tracks considering a simulated and experimental sensitivity.

Considering cone-shaped diffusion chambers whose dimensions are shown in Table 2.1, the sensitivities of the LR115 type 2 detector are simulated considering the fraction of polonium-218 in air, the average and energy-dependent critical angle. These parameters are iterated in such a way that the sensitivity is found as a function of them. The values of simulated sensitivities are compared with experimental values such that a minimum difference is obtained through the deviation, in such a way that the best parameters of critical angle, energy window, fraction of polonium in air are obtained such that they explain the experimental sensitivity found.

Table 2.1: Values of minimum energy E_{min} (MeV), maximum energy E_{max} (MeV), mean critical angle $\langle \theta \rangle$ (degrees), ^{218}Po air fraction f_1 that minimized the deviations between experimental sensitivity S_{exp} (cm) and simulated sensitivity S_{sim} (cm) in different radon diffusion chamber based in LR 115 type 2 detectors.

r_1 (cm)	r_2 (cm)	H (cm)	f_1	E_{min} (MeV)	E_{max} (MeV)	$\langle \theta \rangle$ (degrees)	S_{exp} (cm)	$\sum \sqrt{[S_{exp} - S_{sim}]^2}$ (cm)
2.75	4.5	13	0.1	1.8	4.1	53	0.34 ± 0.06	9.98×10^{-6}
2.1	3.55	6	0.1	1.2	3.9	50.5	0.35 ± 0.05	1.09×10^{-4}
2.55	3.45	7.7	0.1	1.2	3.7	55.5	0.28 ± 0.08	1.15×10^{-4}
1.5	1.5	4.8	0	1.8	4.1	65.5	0.12 ± 0.05	6.67×10^{-5}
		Mean	0.08	1.5	4.0	56.1		
		σ	0.05	0.3	0.2	6.6		
		Err. (%)	66	23	5	12		

The conversion factor (K) from track density to radon exposition (E_{exp}) is in the column S_{exp} in (cm) of Table 2.1.

$$K = \frac{\rho}{E_{exp}} \quad (2.7)$$

2.3. Effective volume

Units of K can be reduced and expressed in cm, then experimental sensitivity S_{exp} and conversion factor are equivalent.



Chapter 3

Radon chamber design

Radon and its progeny is considered by many organizations as the Environmental Protection Agency (EPA), the International Agency for Research on Cancer (IARC), world wide organization (WHO) as second carcinogen that can caused lung cancer. In United States researchers have estimated about 5000 to 20000 deaths every year due to radon [38], also epidemiological studies have carried out showing considerable correlation between radon and its daughters with the probability of Lung cancer [39, 40, 41]. Following this results many surveys about radon concentrations have reported [42, 43, 44]. We now know more accurately that the dose received is due to radon progeny [45, 46]. That's why the importance of measuring radon and its progeny properly by calibrating radon passive and active monitors.

The PUCP Nuclear Tracks Group (GITHUNU) <https://investigacion.pucp.edu.pe/grupos/githunu/> proposes implementing a radon laboratory where calibrations of the active and passive monitors can be carried out to diversify the methods of radioactivity measurement. Within the framework of the above, the construction of a radon chamber is proposed. This will allow us to perform studies such as the calibration of nuclear track detectors inside diffusion chambers, "cross check" of several active monitors, radon exhalation, as well as the determination of the radon diffusion coefficient, permeability in filters, under controlled conditions, etc.

Radon chambers allow the traceability of calibration instruments as well as for experimental research in different fields such as radio-protection, environmental monitoring, radon prospecting, etc.

This work began with the review and use of some radon chambers, with the support of the PUCP doctoral program and GITHUNU.

3.1 Overview of some radon calibration chamber

All radon chambers have been built to test and calibrate devices that measure radon and its progeny under controlled environmental conditions and are also intended to study radon decay products behavior. The measurements obtained must be traceable to a radium source or reference monitor. For that, there is a radon measuring system that has been maintained to measure radon properly called a primary national radon standard ^{222}Rn against international and national radium standards ^{226}Ra . Radon measurements performed at the National Institute of Standards and Technology (NIST) and radon transfer calibration standards are directly related to this national radon standard [47]. In this way, it is possible to build a one cubic meter NIST-traceable chamber using a standard glove box with four gloves and a transfer port [48].

Similarly, the Environmental Protection Agency (EPA) works with NIST-traceable radon chambers housed at the National Air and Radiation Environmental Laboratory (NAREL) in

3.1. Overview of some radon calibration chamber

Montgomery. They operate more than five radon chambers where the dimensions of the radon chambers are in the range of $3.6 m^3$ to $40 m^3$, where the source used is a radium-226 solution from NIST [49].

Some of these radon calibrations chambers like KRISS developed by Lee Jong-Man et al., can reach considerable sizes with a volume of $39.1m^3$, called room chambers, radon concentrations that can reach up to $250 \frac{kBq}{m^3}$, where the source used is a $3.7MBq$ Pylon ^{226}Ra used in flow mode, equipped with an aerosol generator [50]. Another large size chamber considered as a walking chamber is japanese radon toron reference chamber; it is $25 m^3$ volume, radon source is outside the chamber and active monitor AlphaGUARD is used no measured radon toron inside the chamber in mode flow-trough, also it has an aresol generator [51].

Many multipurpose radon chambers are built with solid glass as reported by Abdul R.H. Subber [52].



Figure 3.1: General view of the radon chamber [1]

In the Figure 3.1: The chamber is built of pixy glass and has volume of around $0.65 m^3$. It has a double locking system, that allows for samples removal without changing of radon concentration. A solid source of ^{226}Ra with a $122 kBq$ is used as radon source which is place at the top of the chamber and it is possible to reach different radon exposures [1].

3.1. Overview of some radon calibration chamber

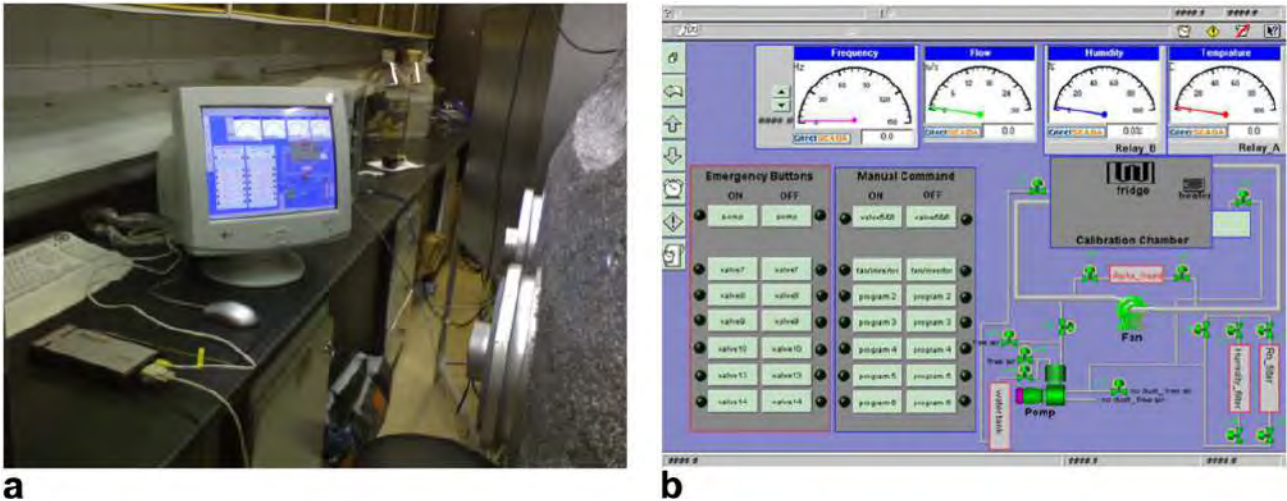


Figure 3.2: General view of the flow through radon chamber[2].

In the Figure 3.2: The chamber has a total volume of $0.498 m^3$, is cubic, parameters as temperature, humidity and flow are each regulated between $20^{\circ}C$ and $45^{\circ}C$, 10 and 70%, and 0.2 and $10 m^3/min$, respectively. Desired homogenous can be reached due to controllable speed fan. All the system is controlled by PLC (Programmable Logic Control) and the activity is measured by AlphaGuard monitor [2].



Figure 3.3: Ezeiza radon calibration chamber: $1m^3$ acrylic glove-box [3].

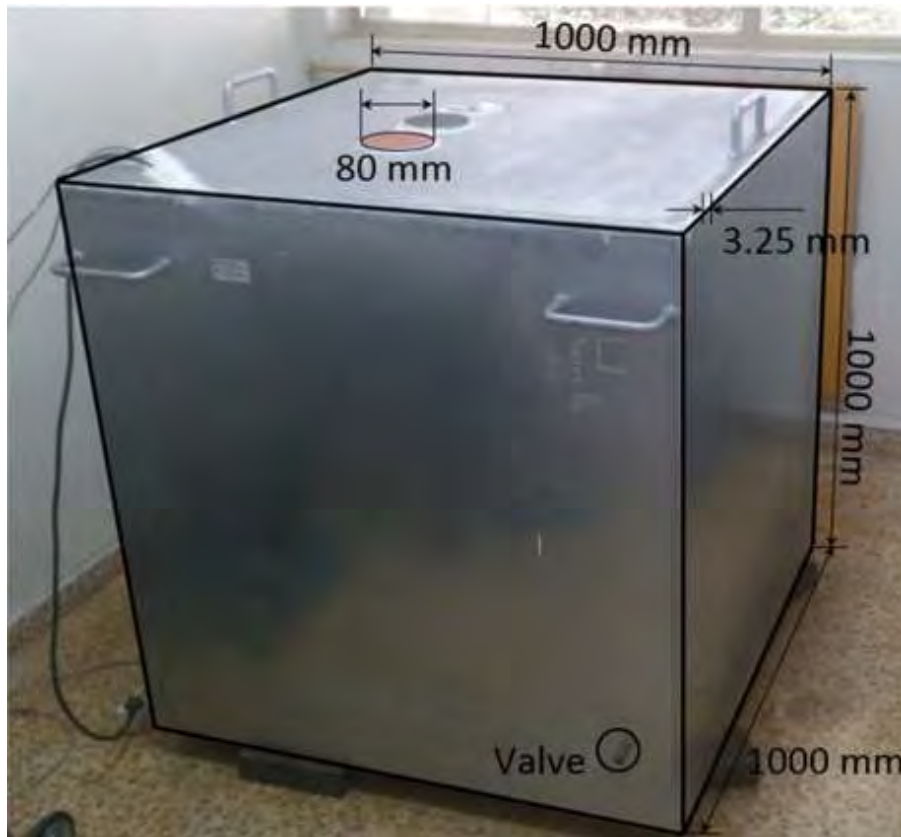


Figure 3.4: Purpose-built radon chamber of Laboratory of Environmental Radioactivity, University of Cantabria [4].

It is a chamber with a volume of 1 m^3 made of stainless steel, has a lid on the upper part through which different detectors can be placed or removed. It can reach radon concentrations of the order of kBq m^{-3} . This chamber does not use a traceable radon source but rather uses a traceable reference monitor for the international reference. In this chamber it is possible to evaluate the performance of active radon monitors [4].



Figure 3.5: IPEN radon chamber: "The radon chamber (aluminum tank) and the antechambers (glass beakers) are observed, were Radium 226 source was used" [5].

This review of radon chambers allowed us to study and understand how these types of radon flux chambers work.

3.2 Design of radon calibration chamber

The use of a radon chamber turns out to be an economical and reliable method of measuring known radon concentration in a constant climate. The method is intended to perform complex measurements, where the operation is safe without human intervention for a long period, which is supplied by a radon source that can be a reference and monitored by a traceable device.

According to the literature, there are three types of radon chambers which are flow-through, walk-in, and accumulation. Walk-in chambers have large volumes in the order of $25 m^3$ so that even personnel can enter the chamber and accommodate the detectors and are quite good at simulating the environmental conditions of a room. Flow-through types are used by professionals to test monitors, with considerable dimensions. Accumulation-type chambers are small-volume, lower-cost chambers where the monitors and source are enclosed in such a way that the radon growth is contained [53].

Then the chambers can behave as dynamic or static. Dynamic chambers are those with no constant concentration, but they are controlled by air pumps and flow meters to reach the required concentration. They can work in an open dynamic circuit and recirculated form. In dynamic open mode, radon leave the camber and is reintroduced into the chamber by air transfer. In the recirculated (closed) mode radon that is in the different parts of the chamber is reintroduced into the chamber in such a way that the ambient conditions are maintained [54].

To build a radon chamber for device calibration or research purposes it is important to consider the size, type, and working modes.

Table 3.1: Features of radon chambers

Type	Size	Modes	Cost
Accumulation-type	Small	Static	Chip
Flow-through	Considerable dimensions	Dynamic	Expensive
Walk-in	Large volumes	Static	Expensive

The PUCP radon chamber designed is a New-Multipurpose (flow-through and accumulation) type and can work in static and dynamic modes. It will allow us to perform a variety of detector exposure regimes as well as different applications such as correlations between environmental variables, filter characterization, detector sensitivity studies, etc.

Table 3.2: Features of PUCP radon chamber

Type	Size	Modes	Cost
New-multipurpose	Small	Static and Dynamic	Chip

It is an inexpensive and completely practical and safty to operate chamber under ambient conditions monitored by a wireless system based on a raspberry card [55], with an independent source of uranium ore, so that radon can be injected at different flow rates, depending on the saturation concentration and exposure, where the reference equipment is the AlphaGuard, with update calibration certified (<https://www.bertin-instruments.com/>).

The chamber is built of methacrylate [56, 57] where the leakage λ_{leak} is practically negligible as several studies report, where the leakage orders are about $10^{-7} s^{-1}$ Figure 4.1 and lower than ^{222}Rn decay constant term with order of $10^{-6} s^{-1}$.

3.2.1 Radon chamber features

The PUCP radon chamber built is a rectangular and multipurpose chamber where it is possible to work in accumulation and flow mode.

The radon chamber is made of 10 mm thick methacrylate, divided into two parts; the camera (A) with dimensions of 650 mm x 850 mm x 850 mm and the antechamber (B) where the shape is cylindrical with height and radius dimensions of 300 mm and 100 mm, respectively.

In chamber A, detectors are exposed at different concentrations, inside B the samples are placed before and after some planned experiments.

In chamber A, there is an environmental monitoring system composed of temperature, relative humidity and pressure sensors (BMP280). It also has two computer fans that can be controlled wireless by the computer. In addition, there are 13 gas metallic valves of 1/2 inch, which are used to operate the chamber, these permit to take air samples and connect different equipment, as well as to inject air with low radon concentrations in order to reduce the concentration inside the chamber A. Two Silica gel containers are connected to the chamber through hoses system to reduce humidity.

It also has two flow meters (0.0-15.0) Lpm (Gentec Stargas), one of them is connected to an adapted alternating pressure air pump (OTTO) at the source container, and the another is connected to a second similar pump to reduce concentrations if required or simply purge the chamber. In addition, it has two Jugitec-B rubber gloves to manipulated internal contents of the chamber from the outside.

Below is a 2D drawing of the radon chamber design with all its components and a 3D drawing of the chamber and antechamber Figures 3.6, 3.7

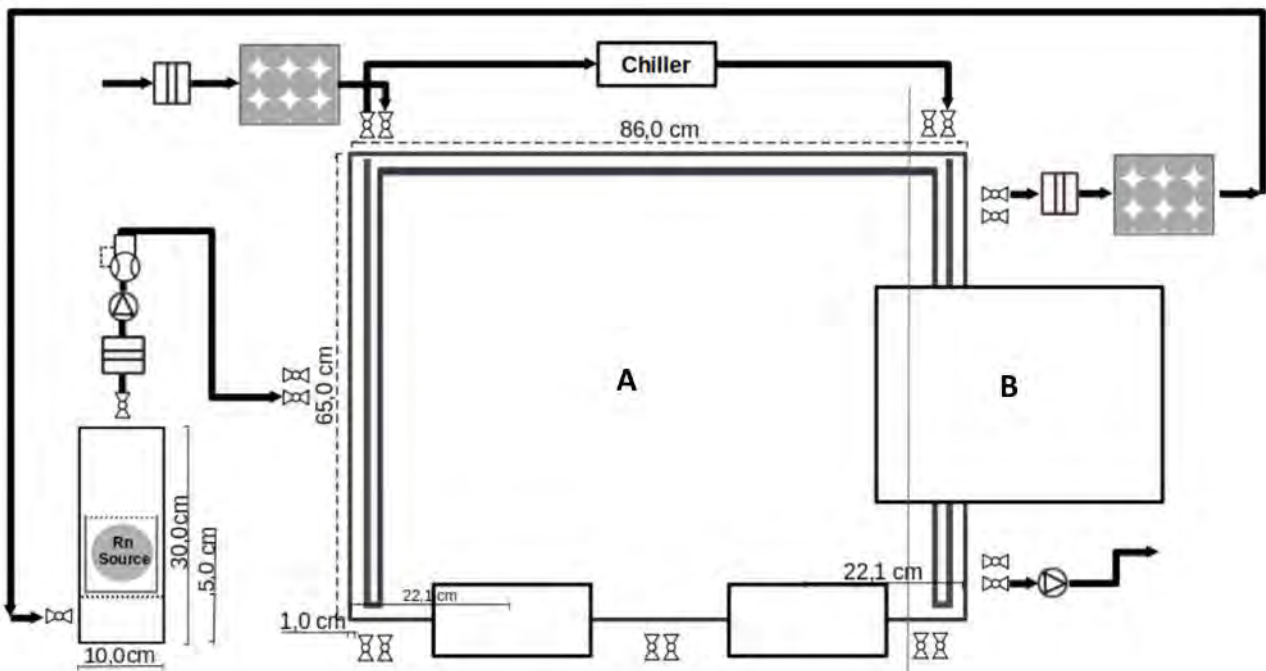


Figure 3.6: Complete schematic of the radon chamber A, with antechamber B, radon source, air bubbles, working volume and valves for different tests.

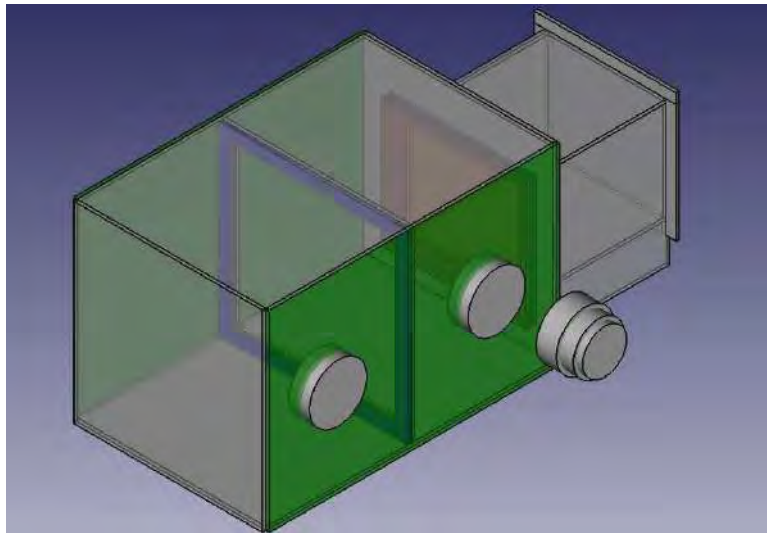


Figure 3.7: 3D representation of the radon chamber with dimensions of 650 mm x 850 mm x 850 mm.

3.3 Simulation of radon chamber

Computational fluid dynamics (CFD) software ANSYS – Fluent (R19.2) <https://www.ansys.com/academic>, where materials, boundary conditions like type of fluid, flow rate, grid number, and Navier Stoke equations considering non compressible fluid were taken account. As a first approximation, the radon chamber was simulated with the above-mentioned dimensions with a flow rate air inlet of 1L/min, to observe the behavior of the velocity gradients such that the net experimental radon chamber volume for the detector exposures can be determined.

This result can be observed in the Figure 3.8 where it is clearly noticed that for the simulated dimensions there is a uniformity in the central part of the chamber.

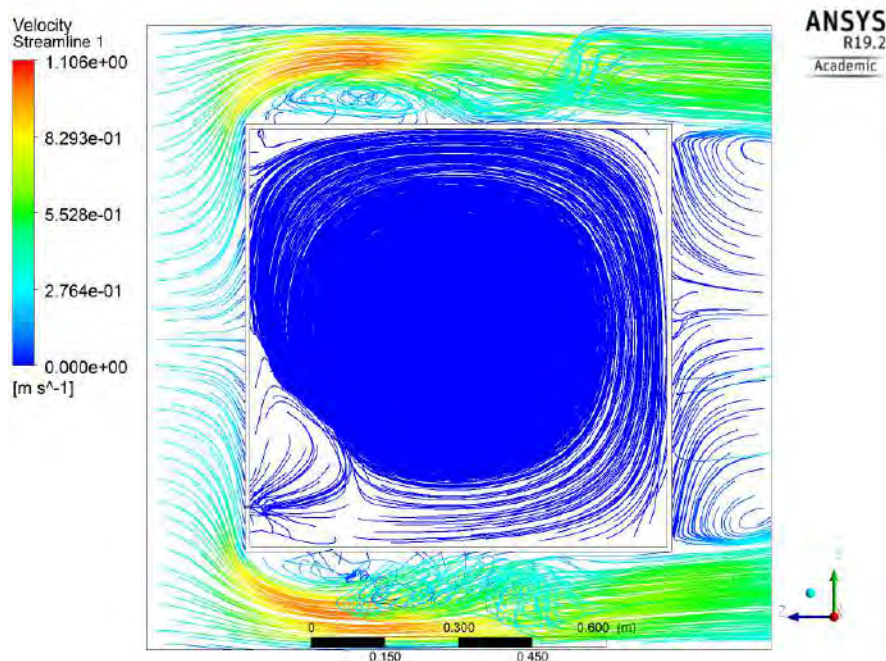


Figure 3.8: First simulation gas air behavior at 1.0 L/min with radon chamber dimension using ANSYS software.

3.4 Building chamber

The following shows construction of the chamber in the physics factory in a first stage and then the installation of the same in the radon room, where the radon concentration is low and the temperature and humidity are controlled, as is showed in Figures 3.9, 3.10



Figure 3.9: Build of radon chamber process.



Figure 3.10: Installation of radon chamber in the laboratory.



Figure 3.11: PUCP radon chamber working during an experiment.



Figure 3.12: Radon chamber tested.

3.5 Radon chamber source

A sample of soil or autunite ($Ca[(UO_2)(PO_4)]_2(H_2O)_{10-12}$) [58, 59] is used as a source of the radon chamber, which predominantly contains radium. These samples are then analyzed for radon supply potential by different monitors.

The radon source used can be affected by moisture, permeability to the exhalation of radon and therefore will affect the concentration of radon as literature reported [60, 61].

At first test, soil or autonite sample were used as radon sources in a cylindrical pilot chamber to find the saturation radon concentrations from samples, in order to estimate the concentrations that could be reached in the PUCP radon chamber, taking into account its volume. As shown in Figure 3.13, autonite sample in the cylindrical pilot chamber was called Radon-chamber-1 and with sample of soil it was called Radon-chamber-2. The working regime in this cylindrical pilot chamber was in accumulation mode and was tested by the AlphaGuard.

In this way the appropriate source for the PUCP radon chamber was established. The autonite sample was chosen as the radon source because the saturation concentration is higher than the soil sample and thus it is possible to obtain high, medium and low radon concentrations without changing the sample and the volume of the PUCP radon chamber. Therefore, it is possible, depending on the study to be performed, to have high, medium and low exposures in a very short time, as well as those same exposures in very long periods of time, as it commonly happens in field measurements.

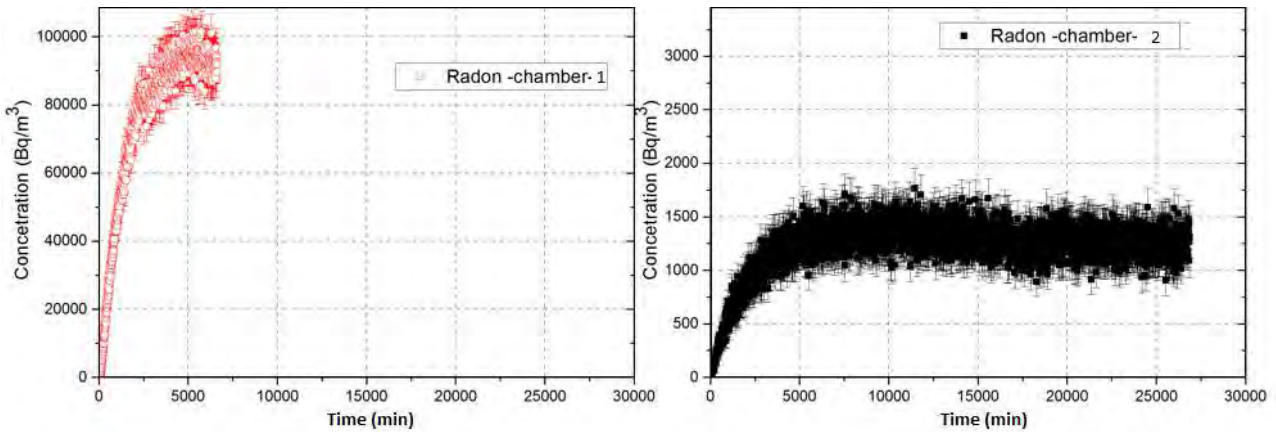


Figure 3.13: ^{222}Rn concentration time variation for two different environmental sample introduced in the purpose made chamber measured by AlphaGuard reference instrument.

3.5.1 Radon emanation factor in soil grains

The radon sources used in this study are granular samples, so it is necessary to analyze the properties of the grains in relation to radon supply. The most common radon radioisotopes are ^{222}Rn and ^{220}Rn generated by radium radioisotopes. It is known that by conservation of momentum in the radium alpha decay process, radon isotopes have a recoil energy of 86 keV ^{222}Rn and 103 keV ^{220}Rn energy by which they escape from the soil grains, transferring their kinetic energy to the medium. Another parameter in relation to radon production is the radium concentration in the soil grains.

Since radon is a very mobile gas, it can be released from the soil and rocks into the fissures or interstices (pores) of the soil grains, this phenomenon makes it very easy for radon to accumulate. Therefore, radon can travel long distances before decaying and it is quite likely to find considerable concentrations in dwellings posing a risk to the inhabitants. The mobility of radon through soil is controlled by the amount of water that is predominantly dissolution from the surrounding geological area [62, 63]. The water present in the soil pores (porosity) (by Monte Carlo simulation using neutrons is possible to measure the water content of soil see the approach in appendix B), grain size distribution, radium content, the way these are interconnected (permeability), and the transport processes through the soil define radon emanation. In other words, radon is transported from a grain of soil to a gaseous or liquid medium after the decay of radium alpha, due to the radon kinetic energy, and the transport in the pores is

facilitated by diffusion and convection [64]. The order of the diffusion length constant in these media is relatively low showing that transport by diffusion is relatively slow and this fact does not significantly affect the movement of radon [65, 66, 67]. Once released into the soil porosity, the efficiency of its release to the atmosphere depends on the porosity, the radon concentration in the pore spaces of soil and meteorological factors such as precipitation, pressure and temperature.

An important parameter to study is the emanation coefficient of the source. It define as the fraction of radon that escapes from the soil grains with respect to the total produced by radium decay and that is deposited in the pores of medium, it is a dimensionless parameter which is represented as a fraction or percentage.

There are many techniques to determine the emanation coefficient [68], for example to measure this factor in a porous material, which contains radium, a completely sealed chamber is used in which there is a soil sample which is kept for some days until equilibrium is reached after which it is pumped into another chamber which is connected to a Lucas cell [69, 70].

3.5.2 Radon emanation factor from soil applying Monte Carlo simulation

In the Monte Carlo procedure, a sphere of of radius R is assumed that emulates a soil grain of a certain diameter which contains a uniform radius distribution, those radon atoms generated at a depth equal to the radon path length have a non-zero probability of escaping to the surface, porosity or embedding in a neighboring grain. We assume a sphere circumscribed in the first sphere of smaller diameter with a difference between its radii equal to the radon path length. In this volume, random points are generated which represent the positions where atom radium decays and which will have an angle of 4π if radon is emitted. However, what is relevant is the calculation of the probability of escape of this radon atom from the grain, as the ratio that exists between the portion of the sphere of radius radius of the radon path length that protrudes from the sphere of radius R , on the surface of the sphere of radius. The points are generated by Monte Carlo method based on Stajic's work [6]. The process of radon emanation from soil grains is studied by quantifying the radon atoms escaping from the grain. Kinetic energy of ^{222}Rn and the range can reach in the soil are considered. The radon source is a dry sample which implies that the pores are filled with air, as a first approximation, ruling out moisture.

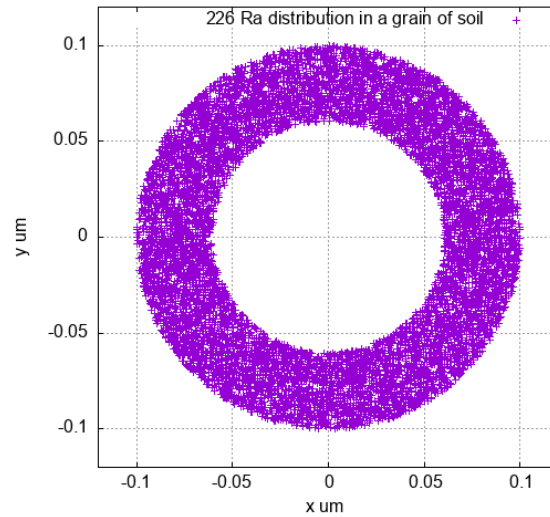


Figure 3.14: ^{226}Ra distribution in a grain of soil, considering non-uniform distribution in the same way as Stajic consider [6]. For this topic, review Appendix A.4 and B, where three equations are used to generate the radium distribution as shown and the subsequent determination of radon escape from the soil grain.

3.5.3 Autunite as radon source

Autunite, torbernite, and other autunite bunch minerals are uranium metals. Autunite was founded in France in 1852 [71]. It is a radioactive orthorhombic mineral, coming about from the aqueous modification of minerals [72, 68, 73] .

The radon source employed in this work are autunite sample of $[3.8072 \pm 0.0001]$ g and samples of this mineral of 0.659 g and 0.400 g were analyzed through gamma spectrometry, ^{226}Ra and ^{226}U content were determined, which have activities of 9586; 1943($Bq.kg^{-1}$) and 9053; 1364($Bq.kg^{-1}$) respectively. The radium content of the autunite sample was determined a second time by gamma spectroscopy, obtaining a value of ^{226}Ra (2096 ± 25) kBq/kg, which differs from that measured in the IPEN, this last value is consistent with the radon concentrations found in the sample in the secular equilibrium, then the emanation factor of the sample is calculated, which is around 0.3 - 0.5. This value will be further tested. Then, According to Barrenechea et al., [74] alpha spectra can be obtained from different uranium ore samples, which can be prepared as coarse and fine sources. There is also the option of having bulk sources.



Figure 3.15: Radon source container of autunite sample.

Below is the alpha spectrum autunite sample and it is possible to notice some vertical ladder lines with pronounced widths due to statistical fluctuations and low resolution, remembering that it is a granular source.

The horizontal axis of the channels can be transformed into energy by means of the linear equation obtained by energy calibration using a triple source of Uranium-233, plutonium-239, and Americium-241.

$$E = 1.84134Ch + 422.603 \quad (3.1)$$

Where, E(KeV) and Ch are Energy and channels, respectively. PUCP alpha qualitative spectrometer scheme of autunite source is shown in the Figure 3.16.

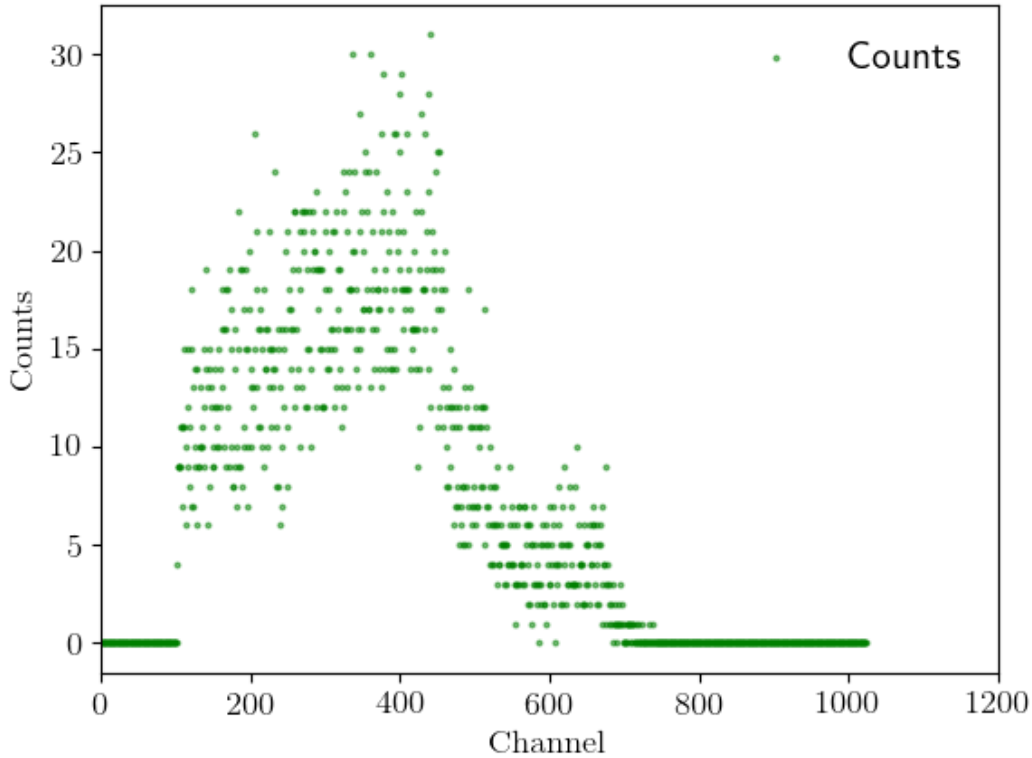


Figure 3.16: Alpha spectrum of autunite.

The alpha spectroscopy system used in this measurement has been developed by the Peruvian Institute of Nuclear Energy (IPEN) integrated Alpha Analyst™ of the Canberra brand with silicon detectors (PIPS) of 400 mm^2 diameters and a resolution of 18 KeV placed in double spectroscopy modules in their respective vacuum chambers), with a range up to 26.7 kPa. The energy range is from 0 to 10 MeV and with a resolution of 12 bits (granularity of 2.5 keV). The spectrometer is computer controlled by Amptek Dpp MCA software [75].

Chapter 4

Radon chamber test

Once the PUCP radon chamber was built, it was subjected to tests to guarantee the absence of leaks and ensure its homogeneity, with the aim of achieving its perfect functioning.

4.1 Leakage test

One of the main objectives is to ensure that the radon chamber does not leak or leaks as little as possible. One way to measure leakage is through the exponential growth or the decay of radon inside the chamber which should only be affected by the decay lambda. So if that factor is different only from the decay, it implies that there is a leakage lambda λ_{leak} and reverse diffusion. The latter is considered negligible since the uranium ore sample is very small [64, 77].

$$C(t) = C_0 \exp^{-\lambda^* t} \quad (4.1)$$

Where; $\lambda^* = \lambda_{222Rn} + \lambda_{leak}$, λ_{222Rn} , λ_{leak} are ^{222}Rn decay and leakage constant, respectively [76].

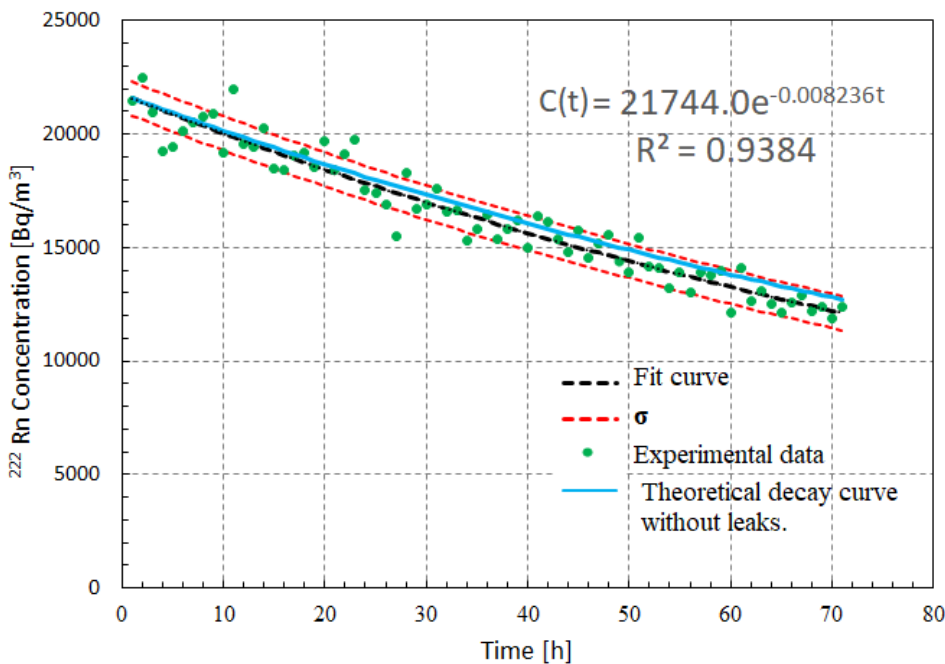


Figure 4.1: the leakage lambda is determined from the exponential fit where the effective lambda is in h^{-1} , then using Equation 4.1 is in the order of $10^{-7} s^{-1}$.

4.2 Homogeneity test

Radon chamber homogeneity is an important parameter that can directly influence the accuracy of radon detector calibration as well as experimental work in the measurement of radon and its progeny. The recommended values of this parameter is 1.5% to 10% according to different laboratories around the world [8]. This fact can be observed in the Table 4.1.

Table 4.1: Radon chamber homogeneity values [8].

Institutions	Homogeneity value (h)
International Radon Metrology Program (IRPM)	2.5%
Atomic Energy Commission of Syria (AECS)	10%
East China Institute of Technology (AECS)	< 3%
University of South of China	1.5% – 5%
Amirkabir University of Technology from Iran	10%

The homogeneity values test of Table 4.1 are determined by the following expression:

$$h = \frac{S}{\bar{C}} 100\% \quad (4.2)$$

Where S and \bar{C} are the standard deviation and the average radon concentration, respectively.

Therefore, it is necessary to guarantee an atmosphere such that the radon concentration is homogeneous in the experimental working volume. This is certain because PUCP radon chamber is built of methacrylate at the leakage is practically negligible as was showed in Figure 4.1.

Two radon test homogeneity were carried out. First with fans off and second with fans on. At first test, in working volume of the radon chamber, the homogeneity of radon concentrations is tested by using 10 Electrets detectors, distributed symmetrically and exposed in accumulation mode with fans off. The Electrets detectors difference voltage are evaluated to find the homogeneity of radon chamber as it is showed in the Figure 4.3



Figure 4.2: Distribution of Electrets inside of radon chamber.

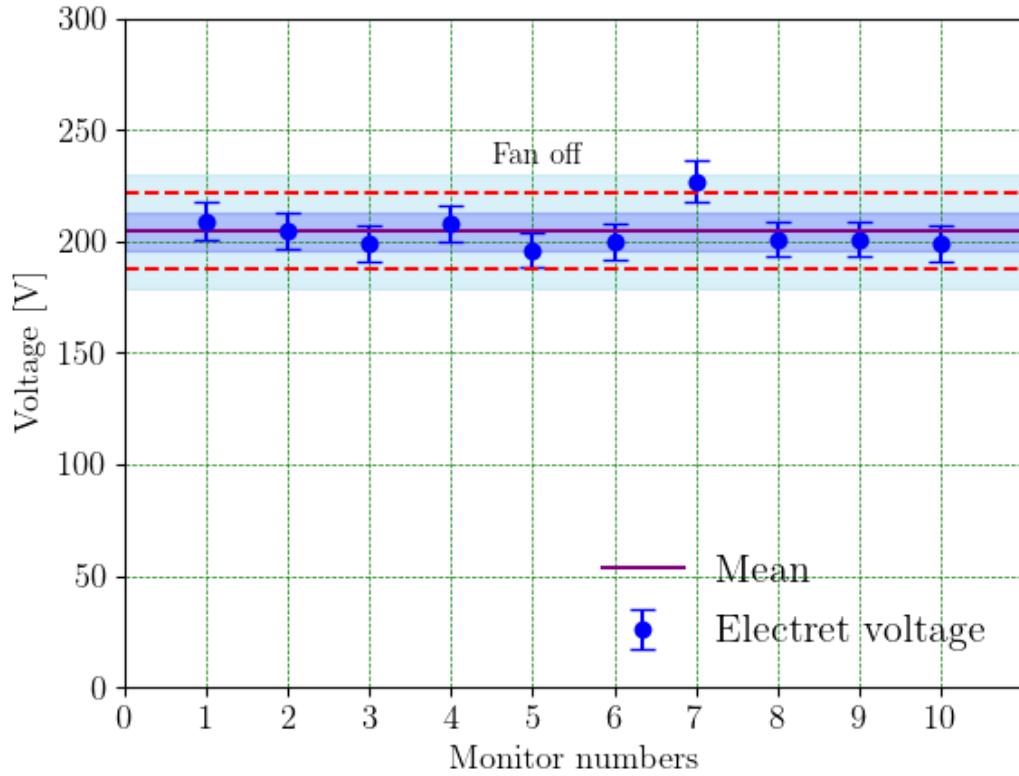


Figure 4.3: Distribution of radon in the volume space with fans turned off.

The homogeneity obtained in the PUCP radon chamber was 4.4%. This result is within the values reported as discussed in Table 4.1. This allows to perform detector exposures with good accuracy. SPER-1 Reader Of Electrets has been calibrated using a reference instrument traceable to the National Institute of Standards and Technology, reference instrument Fluke 23, Serial No. 52460870.

In a second test, two fans are used to distribute the radon homogeneously in the chamber, radon source is outside volume chamber and entering through system hoses and a flow meter measure flow rate of $(1.0 \pm 0.5) \frac{L}{min}$. The working regime used was in closed flow mode. The detector used to test the radon concentration in addition to Electrets https://www.radelec.com/radon_monitoring.html was AlphaGuard (ionization chamber), as a reference. Parameter of the environmental conditions were kept practically constant during the experiment.

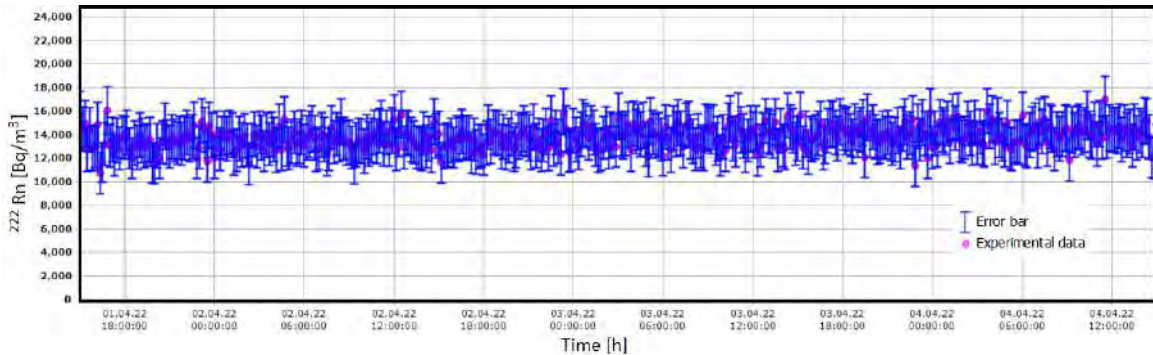


Figure 4.4: AlphaGuard monitor measured the radon concentration during the homogeneity test with fans working.

4.2. Homogeneity test

In this case, 5 Electrets detectors were distributed symmetrically to passively integrate the concentration inside volume chamber. Electrets difference voltage were measured at different positions, following the same procedure at the beginning, Electrets voltage were measured by SPER-1 reader and the results were as shown in Figure 4.5.

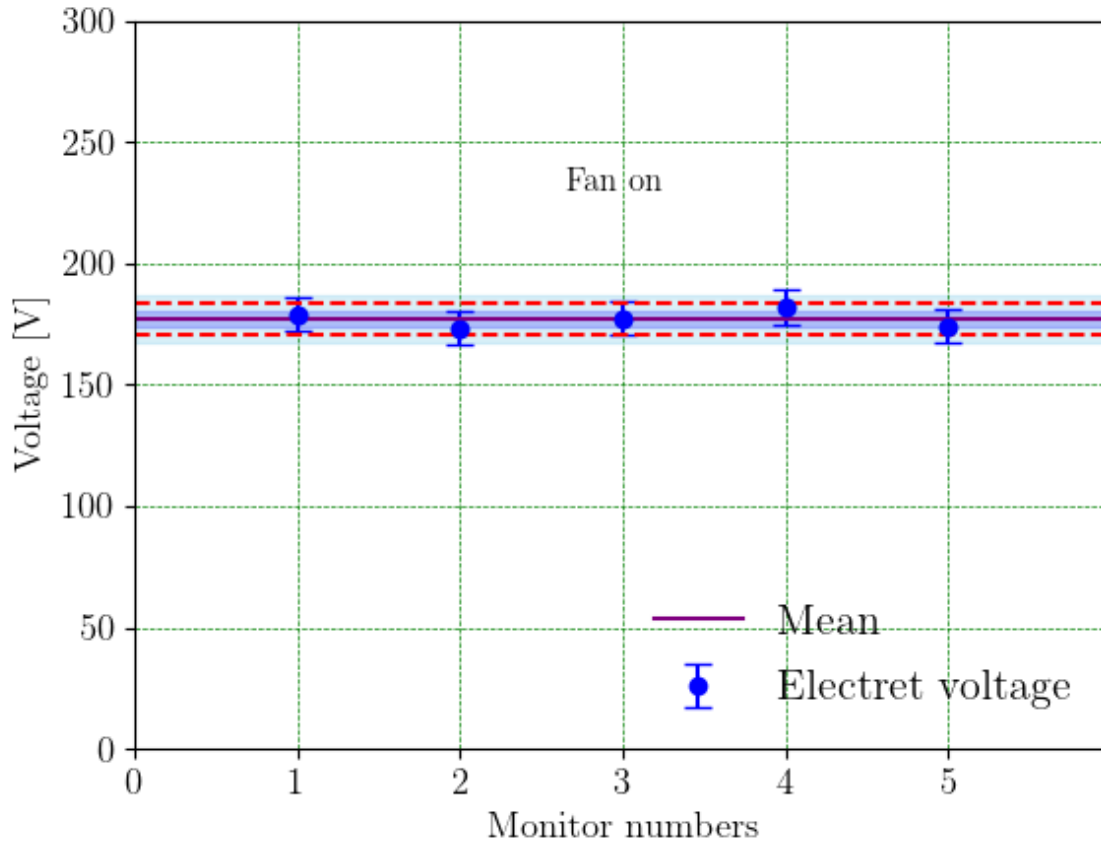


Figure 4.5: Homogeneity test with fans working.

The homogeneity obtained in the PUCP radon chamber was 1.8%. This result is within the values reported as discussed in Table 4.1. This allows to perform detector exposures with good accuracy. AlphaGuard response during this test showed a constant radon concentration 12 kBq/m^3 .

4.3 Radon concentration regimes in the radon chamber

Different radon concentration regimes were established in the PUCP chamber like regime or cumulative mode, in closed flow mode and open flow mode.

It is possible to study the behaviour of radon concentration inside the radon chamber by the following equation:

$$C(t) = C_i e^{-\lambda t} + \frac{\phi}{V\lambda} (1 - e^{-\lambda t}) \quad (4.3)$$

Where $C(t), C_i$ are the radon concentration at any given time and initial radon concentration. ϕ is the exhalation on the source, V is internal volume, λ represents the effective lambda of radon chamber [4].

The chamber in dynamic open mode allows to establish different saturation of radon concentration, for 1.0 L/min the ^{222}Rn concentration is greater than 2.0 L/min, 3.0 L/min and 4.0 L/min. For two last flow rates ^{222}Rn concentrations are similar. 4.6.

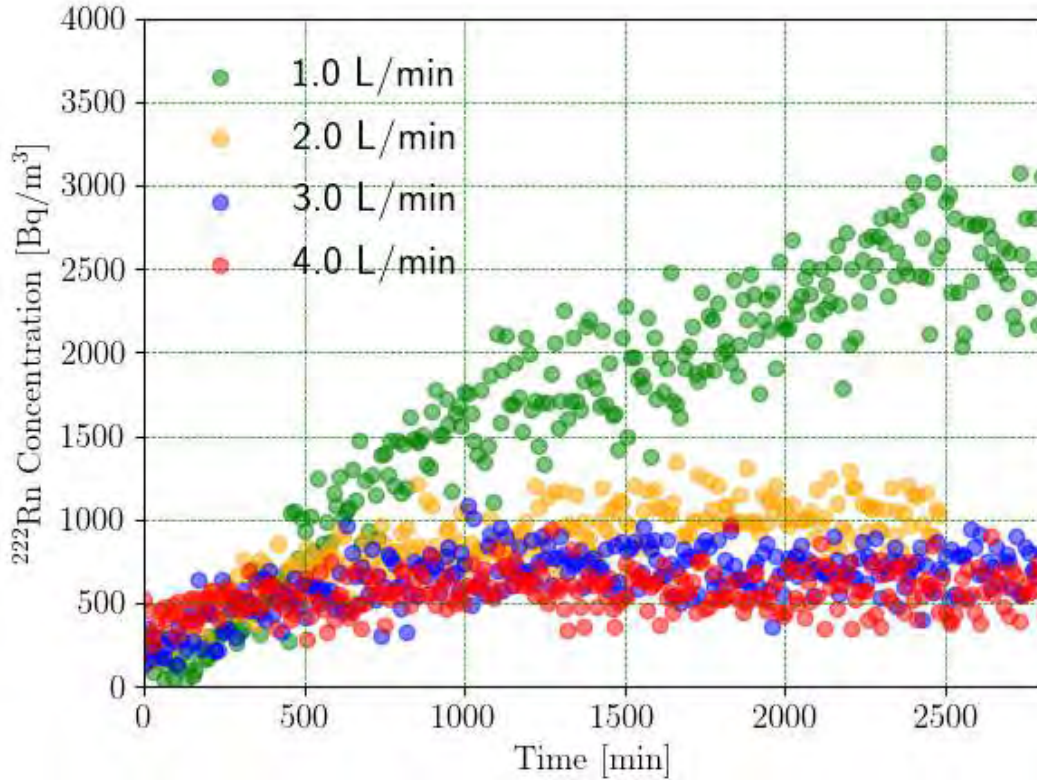


Figure 4.6: ^{222}Rn concentration saturation at different flow rates.

^{222}Rn concentrations found is quite similar to those measured indoors allowing carried out contrast study for long-term (months as measurements in homes).

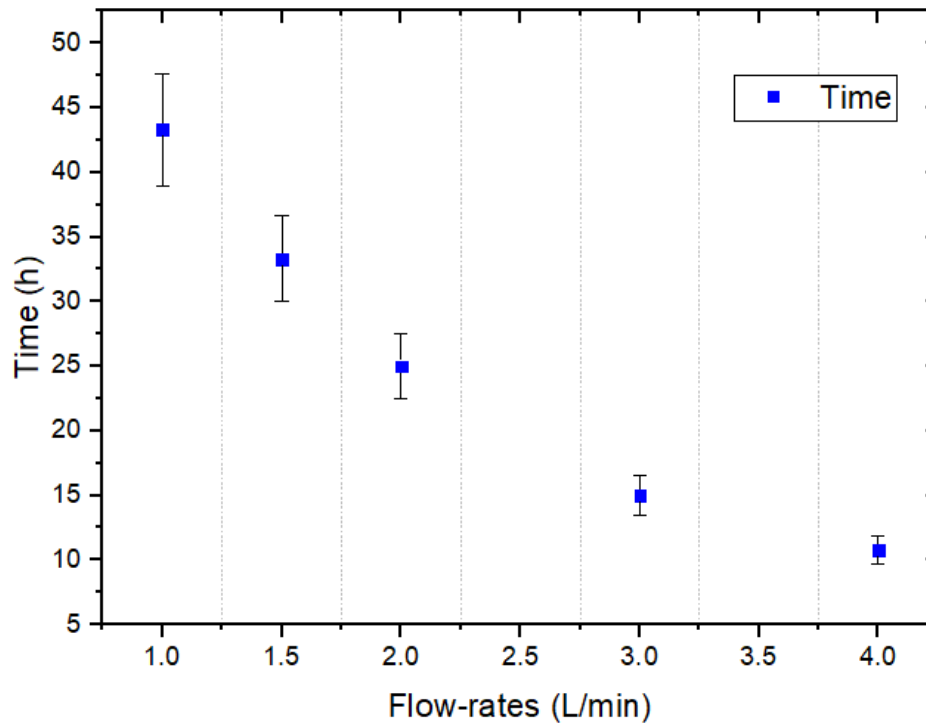


Figure 4.7: The times required to reach equilibrium radon concentration can be observed as a function of flow rate.

Radon concentrations comparable to those found in workplaces and homes can be achieved, for a flow rate of 4.0 L/min. It is therefore ideal for calibrating passive monitors exposed to these concentrations.

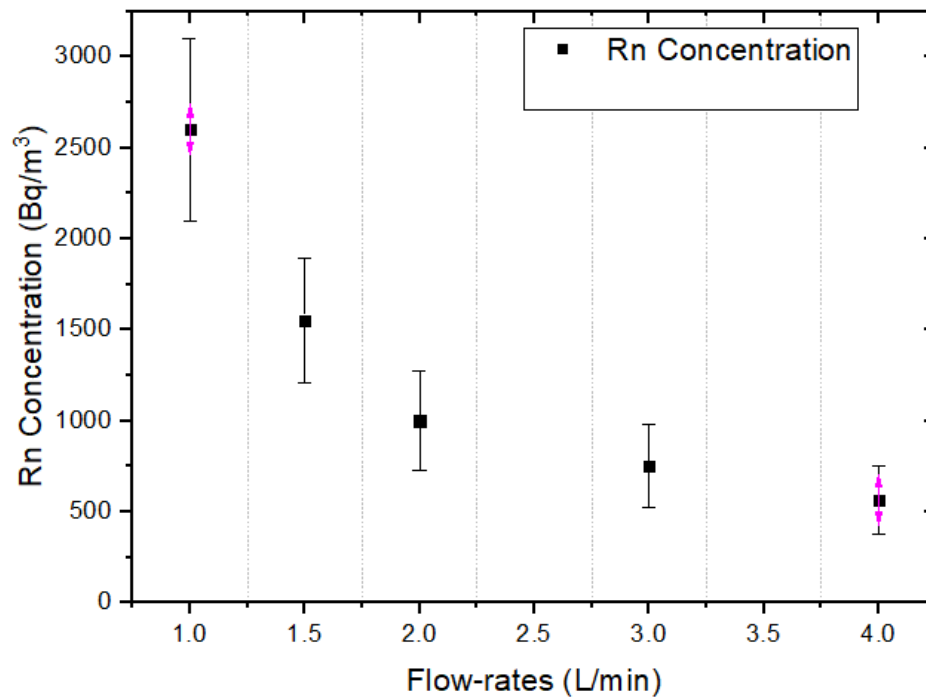


Figure 4.8: Equilibrium ^{222}Rn concentration for different flow-rates.

In dynamic close mode, higher concentrations can be achieved, however, it takes longer to reach an equilibrium concentration, growing observed is only due to the radon source pump

4.3. Radon concentration regimes in the radon chamber

which always works at 1.0 L/min and these concentration values can be used to expose detectors to high exposures in short times. On the right side of the graph, there is also an exponential drop in concentration, this is because in this experiment the purge system was used to reduce the radon concentration. The purging process takes on average about 24 h to reach levels comparable to background radon concentrations.

It can also be observed that the temperature is practically constant throughout the entire experimental procedure.

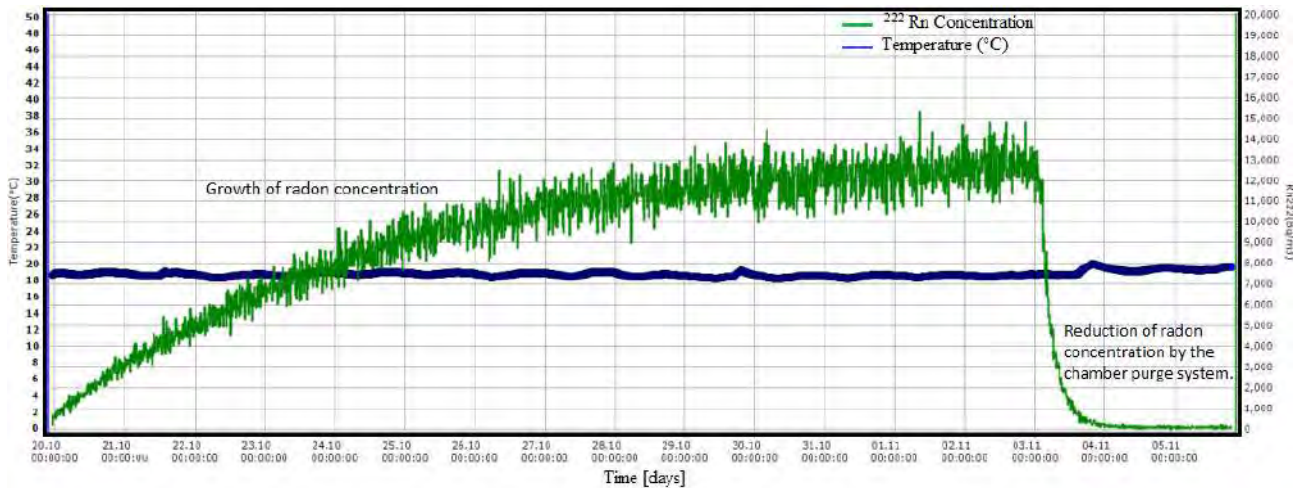


Figure 4.9: Dynamic close mode. Growth of radon concentrations and the reduction of radon by the purge system operating at 5.0 L/min is observed.

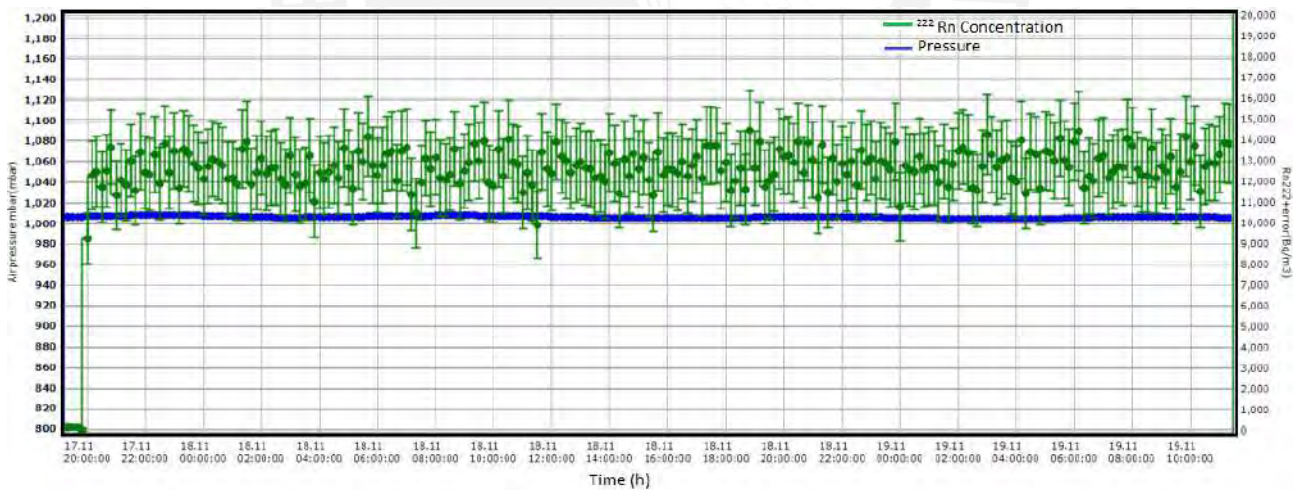


Figure 4.10: Closed dynamic mode, where radon is accumulated in the source container for two weeks and then pumped into the radon chamber. In this way, a high concentration value is obtained instantaneously inside the radon chamber to expose detectors to high concentrations. In this mode, the performance of different active monitors can be evaluated since the concentration is maintained.

4.3. Radon concentration regimes in the radon chamber

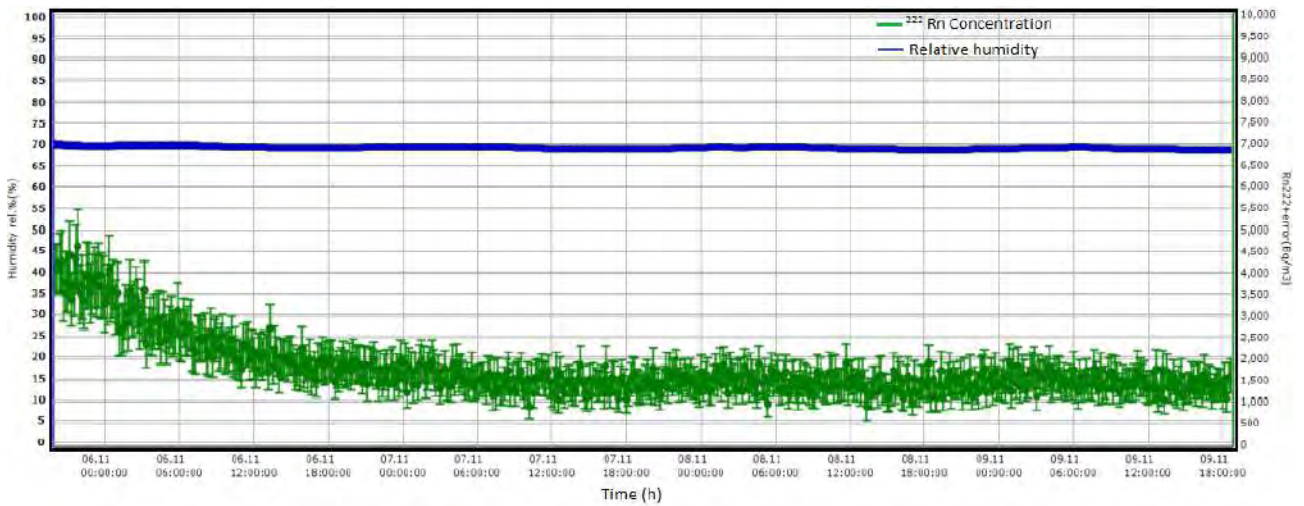


Figure 4.11: The radon is accumulated for 4 days in the container and then released into the radon chamber, such that it operates in open dynamic mode with a flow rate of 1.5 L/min. It can be observed how the radon concentration decreases until it finally reaches its equilibrium concentration.

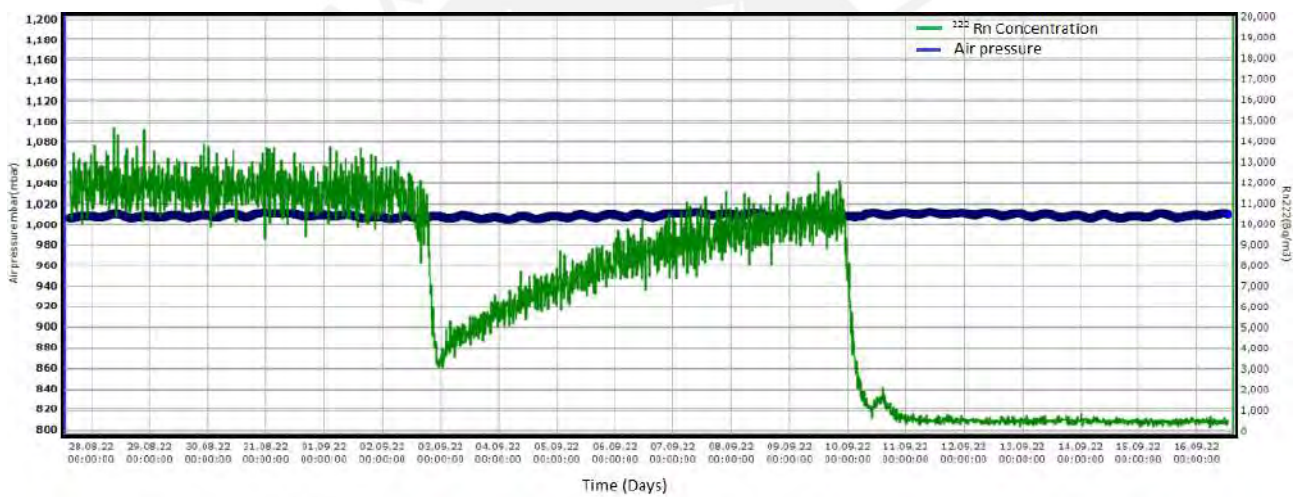


Figure 4.12: This graph shows the operation of the chamber in hybrid mode, using both closed and open dynamic modes. With this it is possible to return to a previously set radon concentration value, as shown after a certain time the desired value is obtained, then the purge system of the chamber reduces the radon concentration with a flow rate of 5.0 L/min. In addition, a small peak is shown at the end of a controlled interruption of the purge system.

Chapter 5

Use and applications of the radon chamber

Once the camera has been built and tested, we use it to carry out the following applications:

5.1 Comparison of radon active monitors response

The objectives that were sought to perform a comparison of active radon detectors were:

- Get the performance of measurements of radon monitors (AG-1, AG-2, RTM, RAD7, RPM) in equilibrium concentration of radon (close dynamic mode) and radon decay (static mode) where:
 - AG-1: AlphaGUARD Radon monitor (AG1), Bertin Instruments. PUCP code:B129766
 - AG-2: AlphaGUARD Radon monitor (AG2), Bertin Instruments. PUCP code:B289839
 - RTM 2200: Measurement System for radon/thoron, SARAD. PUCP code: B303833
 - RAD7: Real-time Continuous Radon Monitor with Spectral Analysis, DURRIDGE. PUCP code:B327057
 - RPM 2200: Radon and thoron progeny monitor (Working Level monitor), SARAD. PUCP code: B306625

Comparisons will be made taking into account: Initial radon concentration (C_0) and time of exposure.

- Determination of the equilibrium factor (FE).

The experimental set-up is shown in Figure 5.1

5.1. Comparison of radon active monitors response

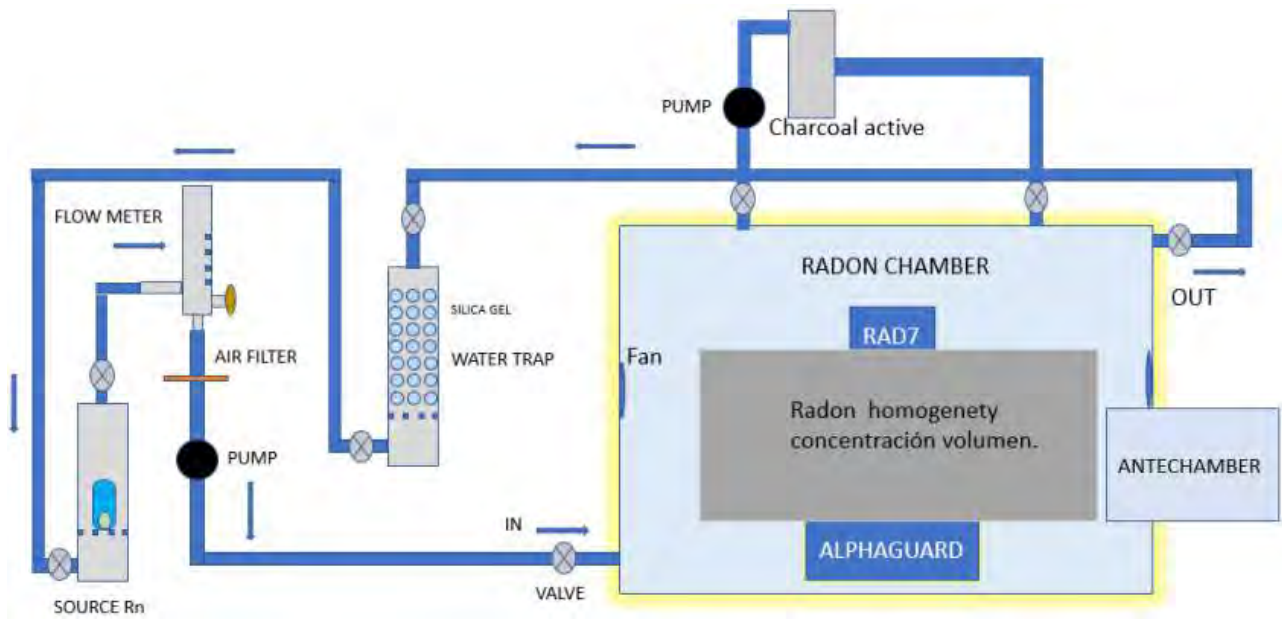


Figure 5.1: Experimental set-up for the comparison exercise.

While the detectors are exposed, the radon chamber monitoring system tests the conditions for radon concentration; and a silicon barrier detector provides information on the progeny of radon.

On the PC screen with the software that commands the operation of the chamber, you can see the information in real time: as shown in Figures 5.2 and 5.3, the information provided are; temperature, humidity, pressure and the peaks correspond progeny of ^{222}Rn , ^{218}Po and ^{214}Po .

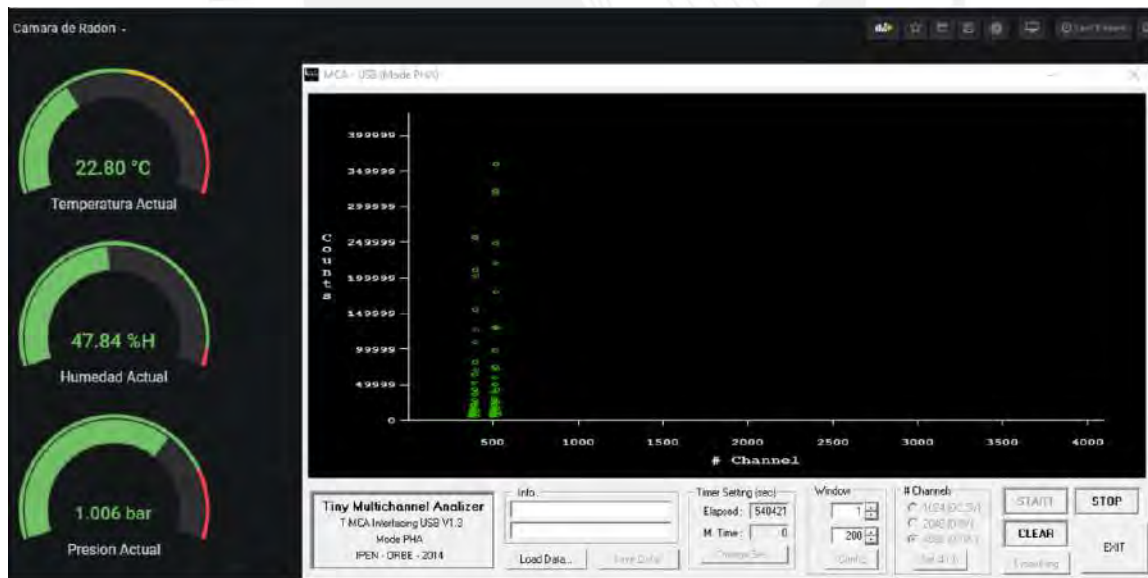


Figure 5.2: Information provided by the radon chamber monitoring system based on e PIN diode S3204-09 (Hamamatsu) as an alpha particles detector developed by Baltuano et al [7].

5.1. Comparison of radon active monitors response



Figure 5.3: Information provided by the radon chamber monitoring system.

For the active monitors comparison experiment, the AlphaGuard (AG-2) was taken as the reference, whose measurements of radon chamber concentrations during the experiment are shown in Figure 5.4.

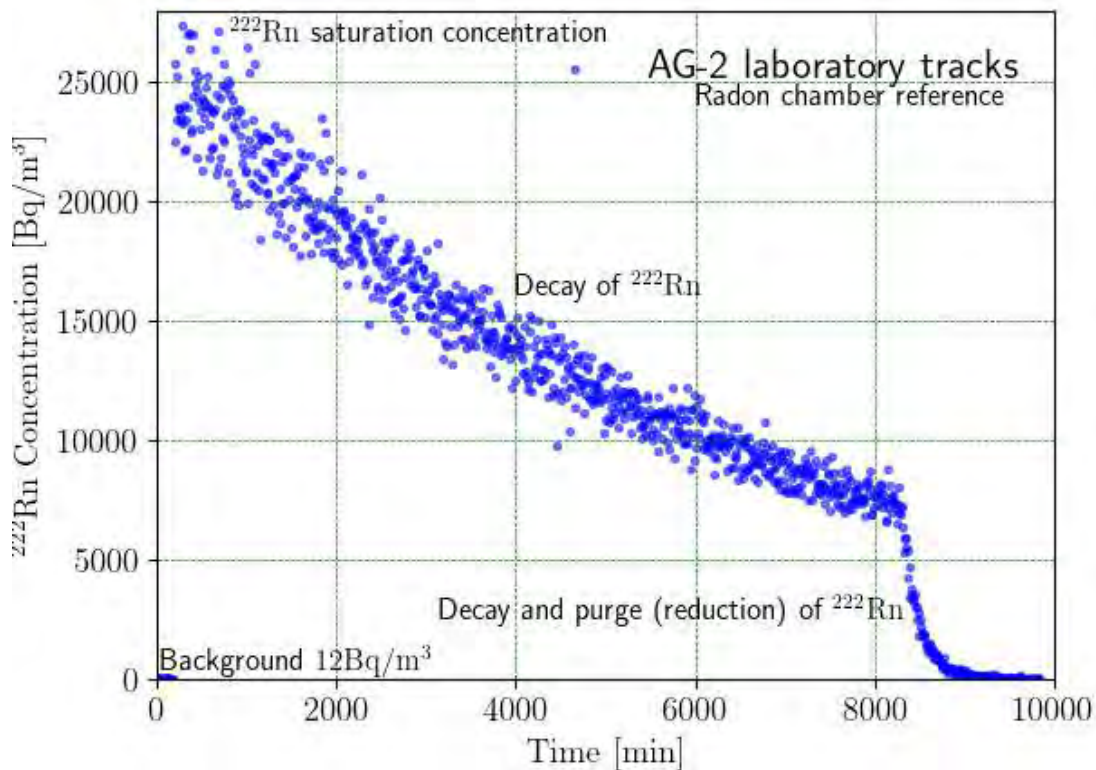


Figure 5.4: ^{222}Rn concentration is measured by AlphaGuard monitor (AG-2) considered as reference device.

The environmental conditions were also measured by the AG-2, which was set as a reference. Figures 5.5, 5.6 below shows the behavior of relative humidity and temperature. It was observed

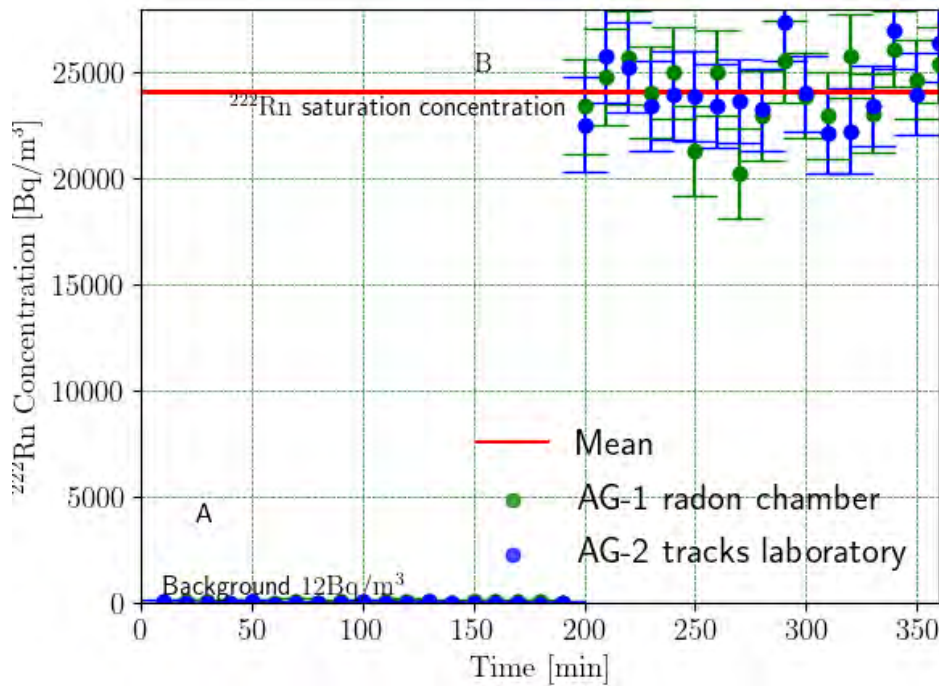


Figure 5.7: A: Radon chamber background; B: Initial radon concentration in equilibrium secular.

The obtained results are showed next. In Figure 5.8, it can be seen that the responses of Alpha Guard 1 and Alpha Guard 2 (AG-2 used as reference), they are optimal as expected, with a difference of 1.7% in measurement radon concentration levels.

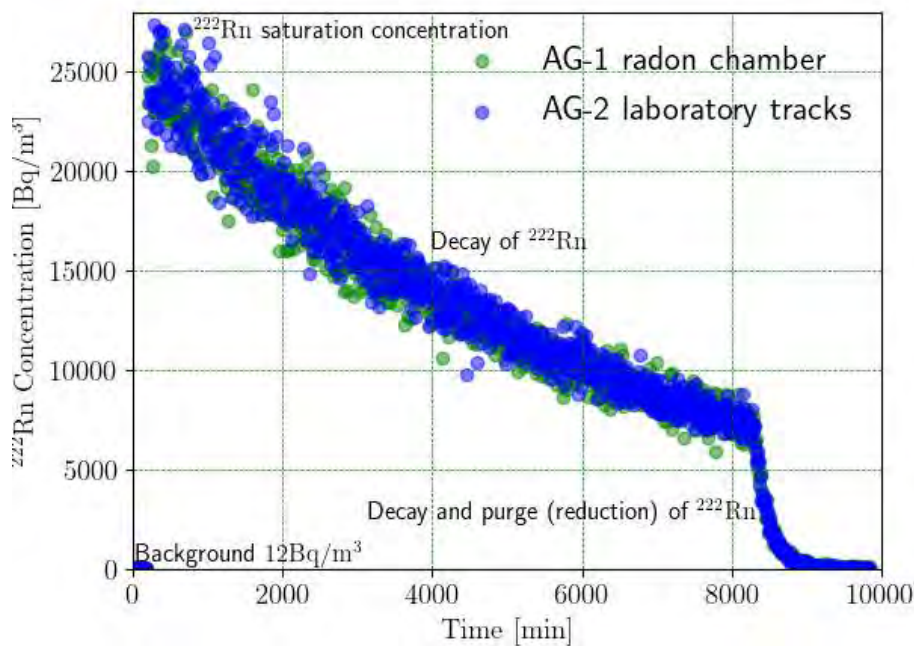


Figure 5.8: AG monitors in flow mode.

In the case of the result obtained with the RAD 7, Figure 5.9, there are inherent differences in the measurement system that is predictable, therefore presents a systematic error. It can be

5.1. Comparison of radon active monitors response

observed as constant in the first minutes in the presence of the source, then, in the absence of the source, only the decay is appreciated.

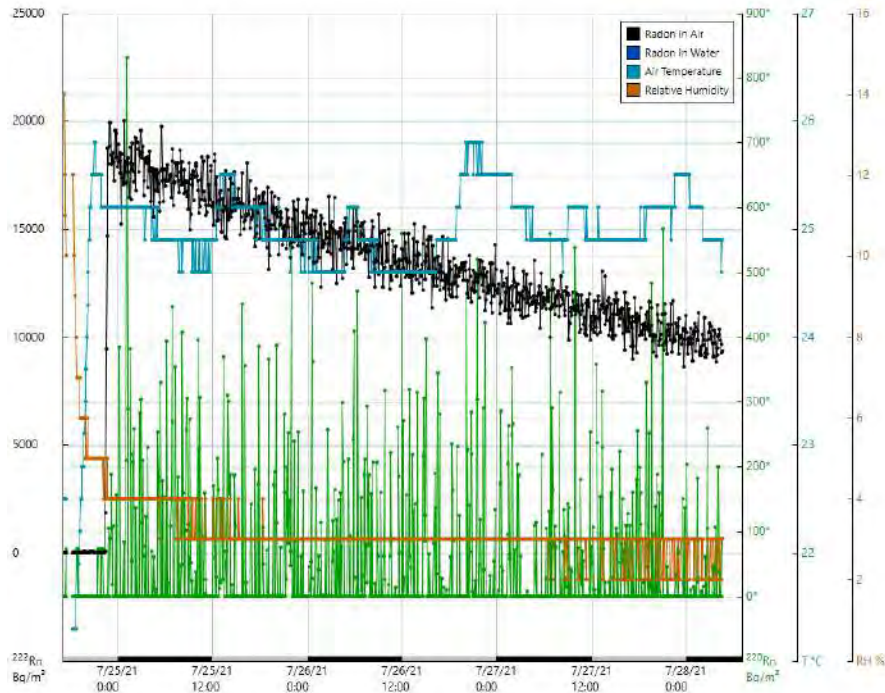


Figure 5.9: RAD 7 behavior in flow mode. its measurements strongly dependent on humidity.

After reaching low radon concentrations in the PUCP chamber and medium humidity conditions (30%HR to 70%HR), the results of the Sarad RTM and RPM monitors can be observed. Firstly, its responses are evaluated for low values, medium and high values of radon concentrations. The experiment was carried out in decay mode to observe the response of the monitors.

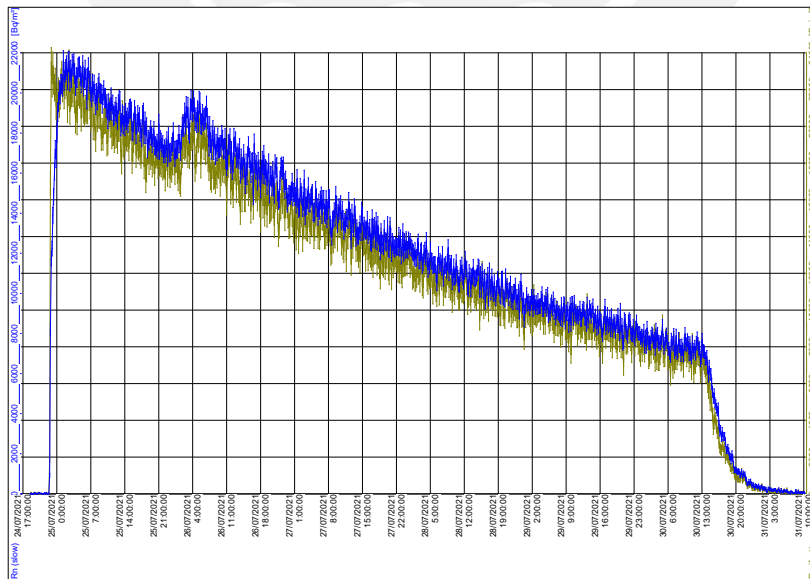


Figure 5.10: RTM measurements of radon 222.

As showed in Figure 5.10 Sarad RTM, behaves like the Alpha Guard reference monitors during the three stages of radon concentration evolution. We can note after 24h, a pronounced

pick due to a slight increase humidity, showing the high dependence on this parameter.

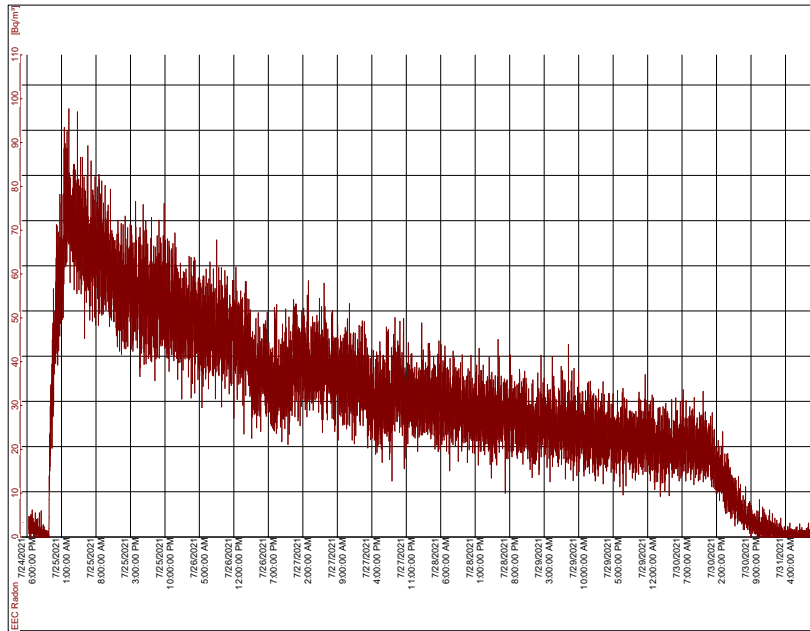


Figure 5.11: RPM measurements of radon 222.

The RPM monitor measures radon progeny, this graph Figure 5.11 shows the equivalent radon concentration, measurements have similar trend as the reference monitor. It is known that radon and its progeny are related through the equilibrium factor (FE). This can be determined by the relationship between the equilibrium equivalent concentration (EEC) of radon with its progeny and the radon concentration (C_{222Rn}) [78].

$$FE = \frac{EEC}{C_{222Rn}} \quad (5.1)$$

Due to the negligible presence of aerosols inside the radon chamber for this experiment and considering the dimensions of the chamber, a very small equilibrium factor is expected. Then with the data obtained from the RPM monitor and the AlphaGuard (AG-2) reference, a value of 0.004 is obtained, a very small value given the absence of aerosols.

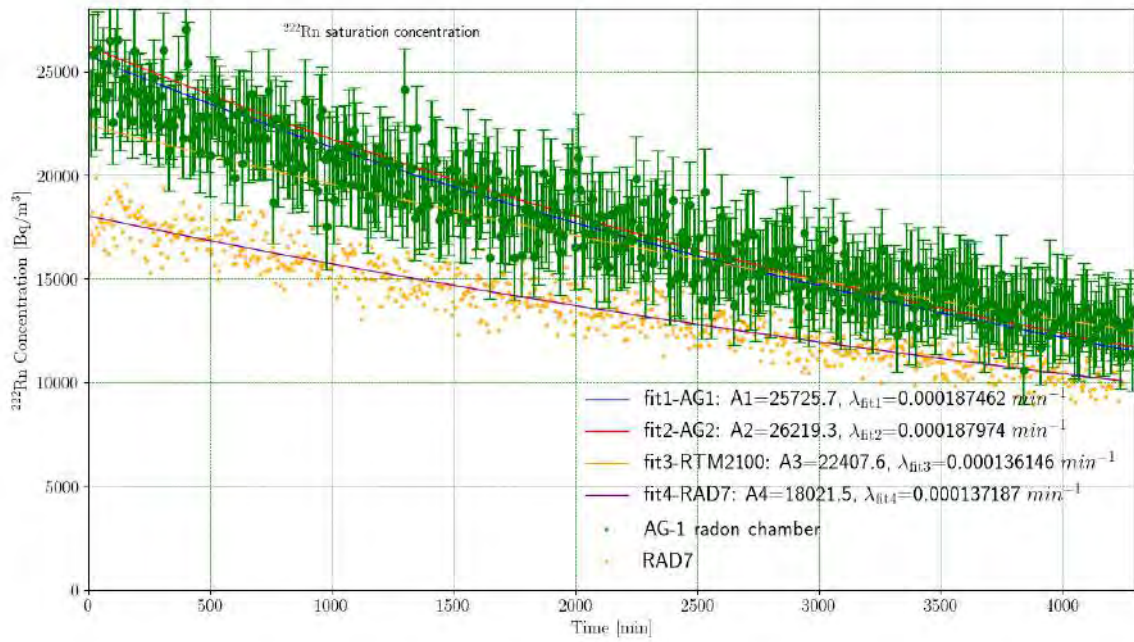


Figure 5.12: Comparative of active monitors response.

Comparison active monitors in decay mode shows good agreement between AG1, AG2, RTM. However, RAD7 response compared to the reference monitor AG2, it shows a percentage error of about 23 %. Reducing the difference for lower concentrations. An analogous result was also obtained by Chi-Feng Lin et al [79].

Table 5.1: Radon concentrations for different active monitors.

Monitors	$C(i)$ initial radon concentration Bq/m^3
AG1	23904.3 ± 2006.8
AG2	24007.3 ± 1798.2
RTM2100	21096.5 ± 2109.6
RAD7	18500 ± 1834

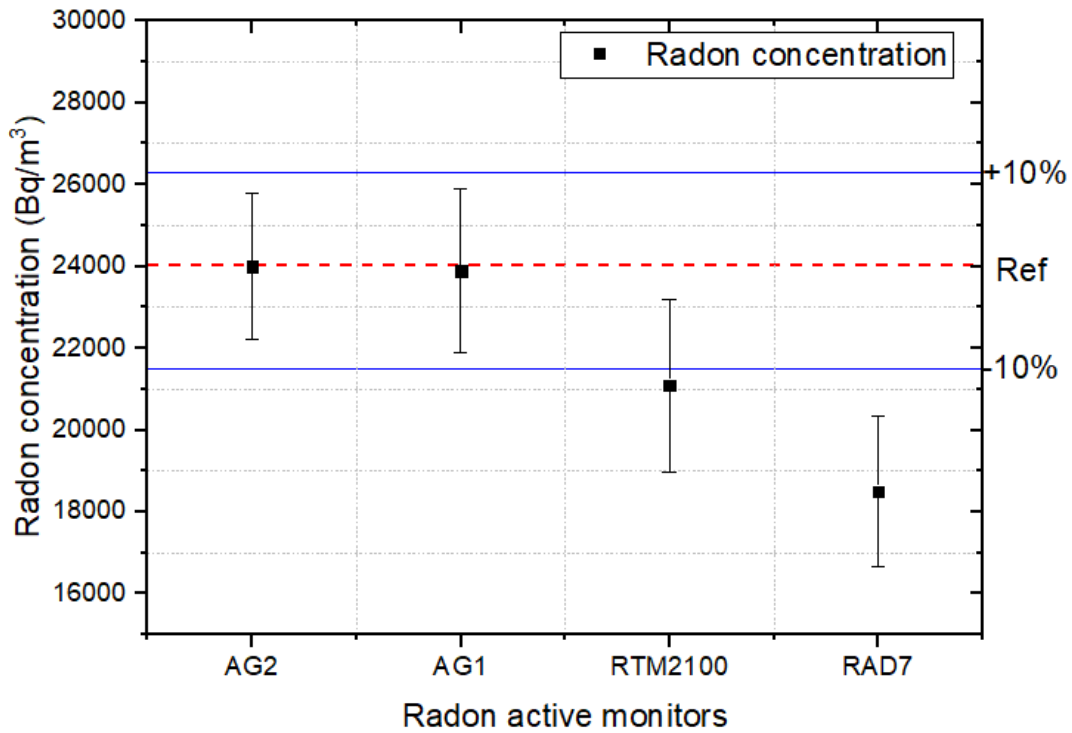


Figure 5.13: Response comparison of active monitors.

Similar graphs of ^{220}Rn were obtained with RAD7 monitor (Figure 5.14), RTM (Figure 5.15), RPM (Figure 5.16), the values found have the same order that the background which led us to conclude that its presence was not significant, ^{220}Rn comes from the same sample of autunite.

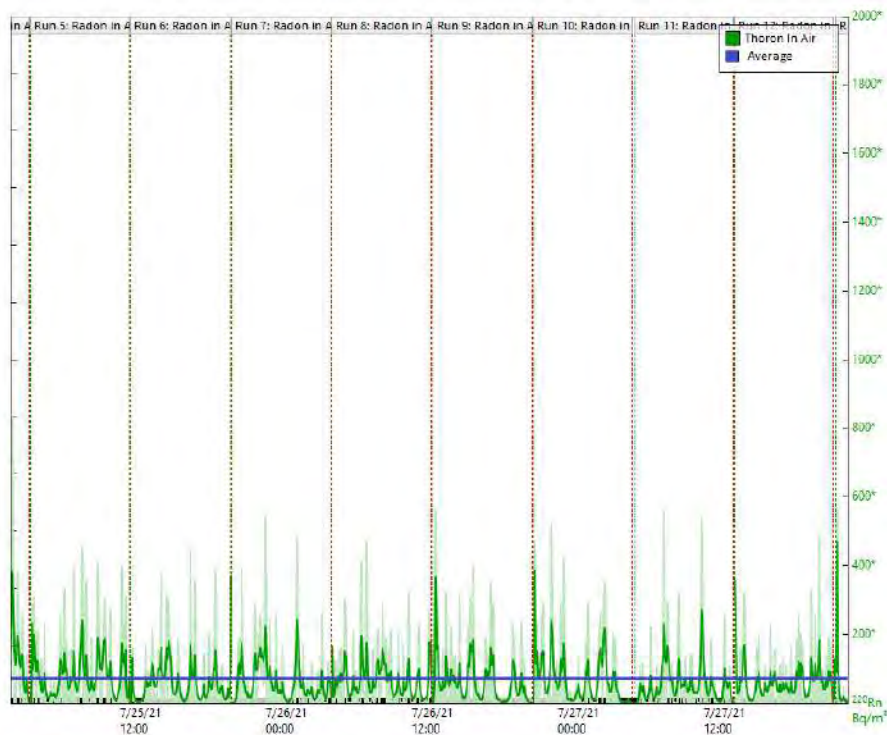


Figure 5.14: ^{220}Rn , measurement by RAD7.

5.1. Comparison of radon active monitors response

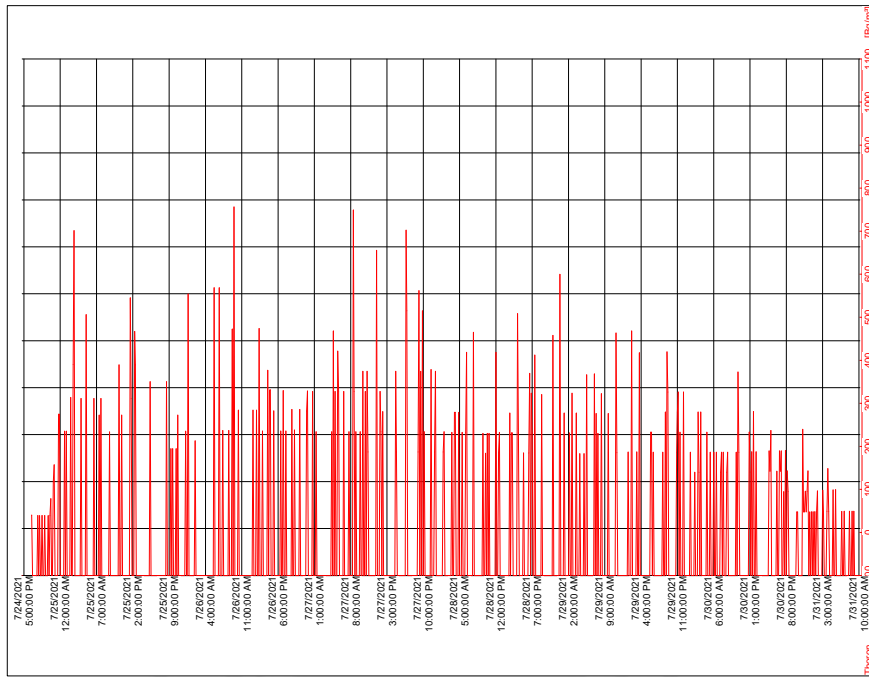


Figure 5.15: RTM ^{220}Rn measurements.

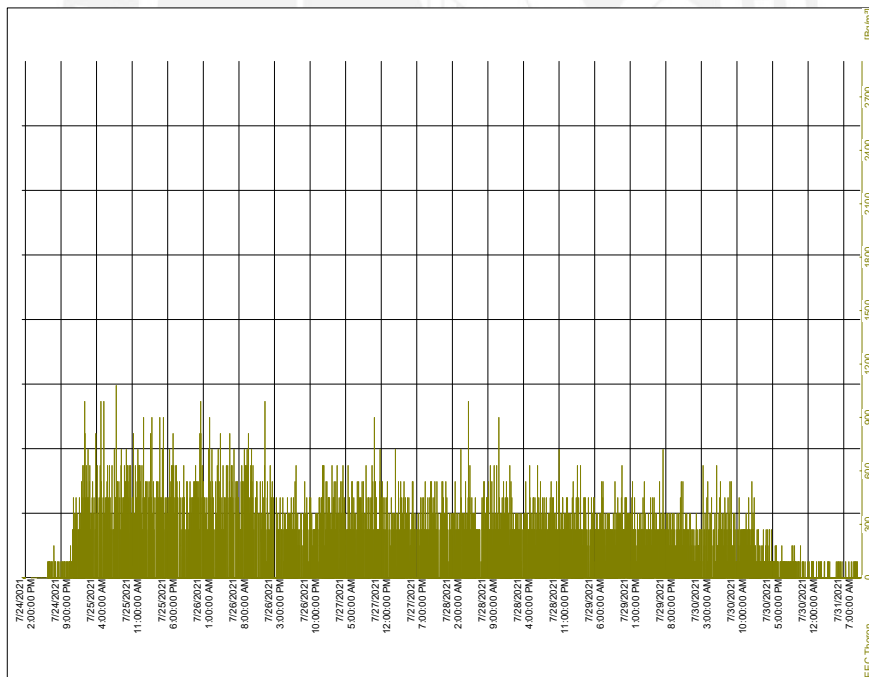


Figure 5.16: RPM ^{220}Rn measurements.

Also pointing out that the path length of ^{220}Rn in the air is in centimeters as it is demonstrated in Figure 5.17.

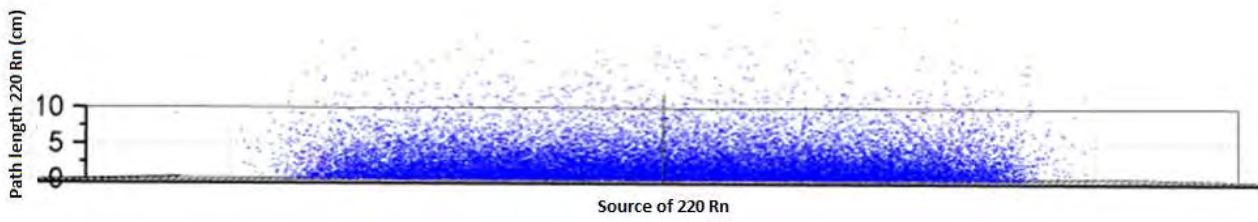


Figure 5.17: Path length of ^{220}Rn in air by Monte Carlo simulation (GITHUNU).



5.2 Calibration of metallic diffusion chambers based on $CR - 39^{TM}$ chips

Experimental calibration factor of metal radon chamber diffusion using $CR - 39^{TM}$ <https://www.tasl.co.uk/about.php> is carried out in the radon chamber at 5 radon exposures.

5.2.1 Experimental procedure

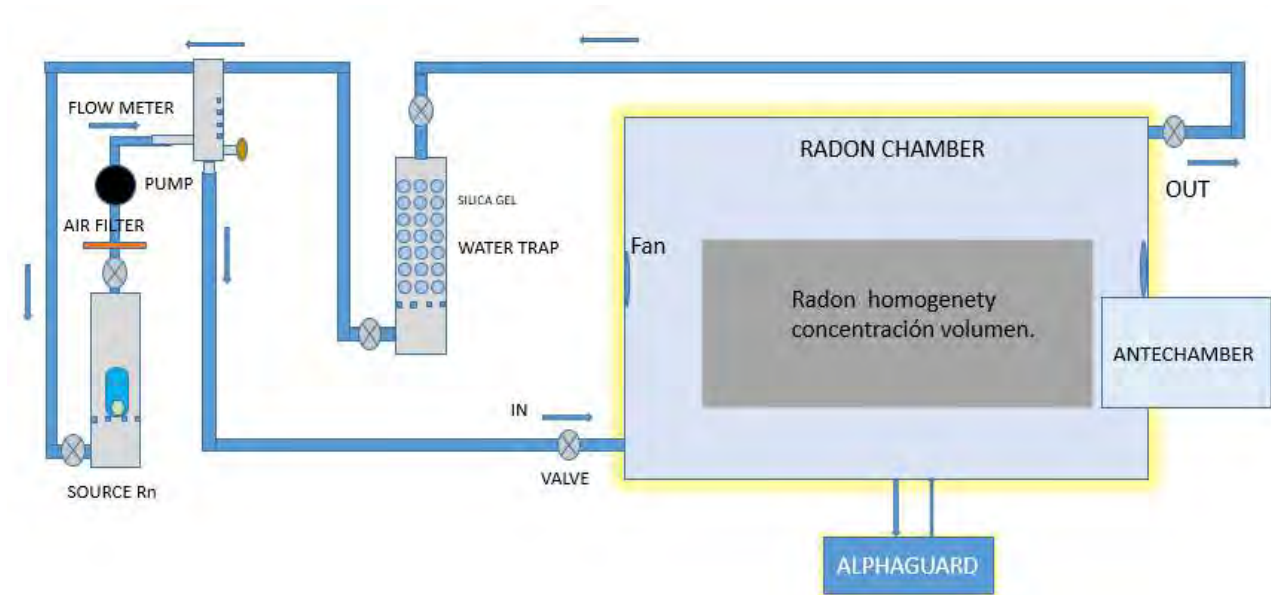


Figure 5.18: Experimental set up for calibration of cylindrical metallic diffusion chambers (radius of 3.05 cm, height of 0.792 cm) based on CR-39.

Experimental initial conditions:

Temperature: 22.1°C, humidity: 70.2% HR, pressure: 1004.7 mBar.

Monitors used in the experiment were:

20 CR-39 chips each inside metallic cylindrical diffusion chamber; 6 CR-39 chips each inside pinholes; 7 CR-39 chips each inside open metallic cylindrical diffusion chamber; 7 CR-39 chips each inside open metallic cylindrical diffusion chamber with filter; 2 CR-39 chips each inside metallic cylindrical diffusion chamber, closed and sealed with Teflon; 3 CR-39 chips each inside twin-chamber with filter; 7 CR-39 chips each inside classic twin chamber; 5 Electrets to evaluate the homogeneity.

The monitors (CR-39 chips in all configurations) were extracted in four sequences, in each sequence all parameter changes were measured, due to the dissolution effect of antechamber.

The monitors first extraction were used to measure the homogeneity of radon concentrations and to obtain first point of calibration metal cylindrical diffusion chamber.

The monitors second extraction were performed to obtain a second calibration point, also to measure filter permeability and transmission factor using pinholes.

The monitors third and fourth extractions were performed to obtain two more calibration points CR-39 chips inside the metallic cylindrical diffusion chambers.



(a) Open and close cylindrical diffusion chamber

(b) Pinholes and filter in cylindrical diffusion chamber.

(c) Twin diffusion chambers.

Figure 5.19: Passive monitors based on CR-39 chips.

The etching conditions of CR-39 detectors were NaOH 6.25 mol/L of an aqueous solution at $(97.3 \pm 0.1)^\circ C$ for 60 min, this procedure was carried out at GITHUNU-PUCP laboratory in the same way as reported by Caresana et al., 2020 [80].

5.2.2 Different exposures

All monitors based on CR-39 chips were exposed at decay process Table 5.2 and constant radon concentration Table 5.3. Then exposures were measured by AlphaGuard monitor.

Table 5.2: First radon monitors exposures.

Exposures	Radon exposition $kBqh/m^3$
1	361.1
2	712.2
3	942.2
4	1072.6
5	2716.5

Table 5.3: Second radon monitors exposures.

Exposures	Radon exposition $kBqh/m^3$
1	1000.4
2	2080.4
3	3978.9
4	6397.7

To get a linear response of CR-39 detectors, levels of low radon exposures were selected, where the efficiency of the detector was guaranteed. After that, CR-39 detectors exposed at high levels experience a reduction of their sensitivity because of the overlapping effect, then it is necessary to correct the values of density of tracks considering a polynomial way [81].

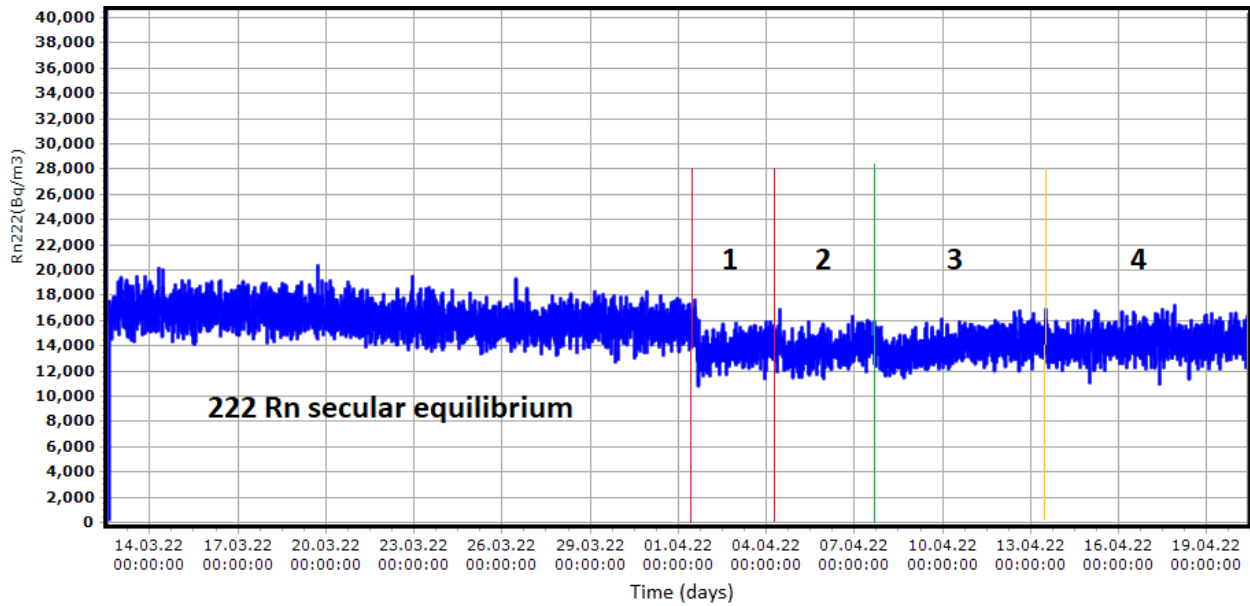


Figure 5.20: Extractions and exposures of monitors to ^{222}Rn concentrations at second experiment.

5.2.3 Counting tracks

ImageJ macro software was used to count tracks on CR-39 chip (see Appendix A.2), following similar procedure reported by [82]. One the must import thing is to find a factor convert between the pixel of image and micron unit it means calibrate, in order to get track area an the identify overlapping effect on the detector and make an appropriate track counting.

Using track by test software with input parameters it is possible to determine the minimum and maximum radius tracks and then area of tracks [31], it was around of $1200\mu m^2$. This data can be used to differentiate a overlapping and any kind of damage on detector. In the same way, CR39.m Matlab program by [83] was used compared that parameters finding some differences between them. Experimental results of geometric parameter by ImageJ <https://imagej.nih.gov/ij/download.html> macro is near the Tracks test program, it is showed in Figure 5.23, it is a profile track by Track Test and CR39.m and ImageJ diameter radio o track using calibration according microscopic vision in μm .

Then, after processing all the things discussed above, taking a random frame picture of CR-39 exposed, a histogram of area distribution is elaborated which shows the mixed contribution of radon and its progeny.

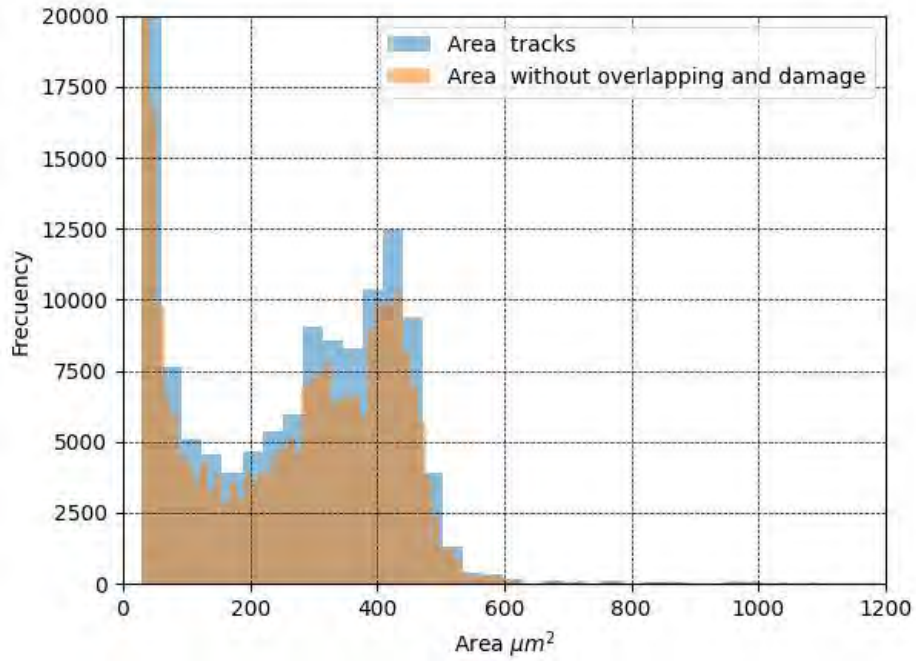


Figure 5.21: Range track area histogram whit total tracks, avoiding damage and overlapping mix tracks in a given frame of CR-39 chip.

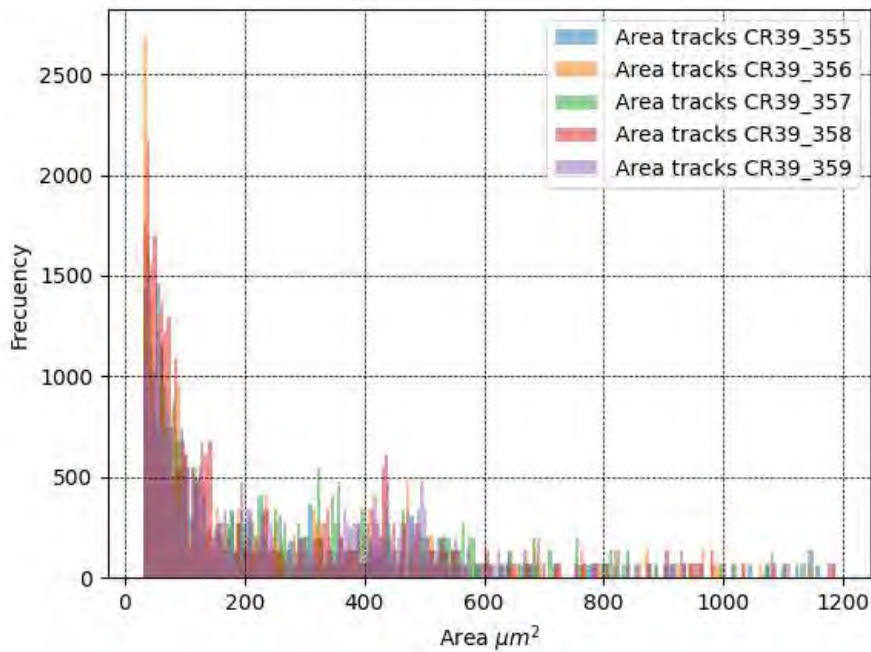


Figure 5.22: Range track area histogram whit total tracks of background in a given frame of CR-39 chip.

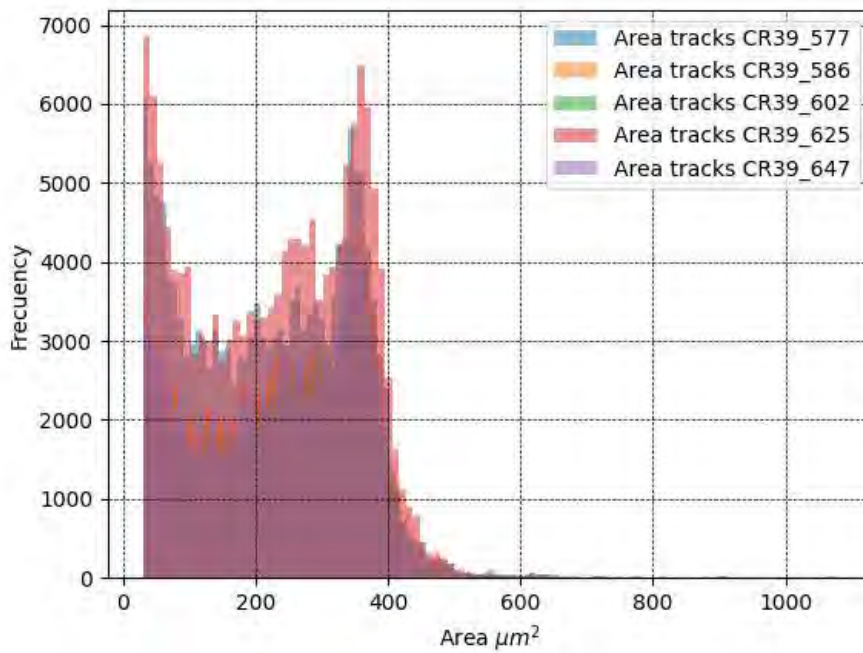


Figure 5.23: Range track area histogram whit total tracks in certain frame of CR-39 chip exposed.

The next step consist to determine track density of each frame detector and identify if there are any outlier data even considering track aperture area. For that purposed, box plot based on quartiles concept and Z score test is taking into account for improve data analysis. There is kind of difference when detecting outliers due to upper and lower limit on the box plot are equivalent to 2.75σ from average. It means some data could be out of the of the box plot limit but inside 3σ . Box plot generally is used for data that doesn't follow normal distribution and can be a little bit aggressive whit treatment of the data, in contrast, z scored is work very well for normal distribution. The last way is used to identified and eliminated outlier.

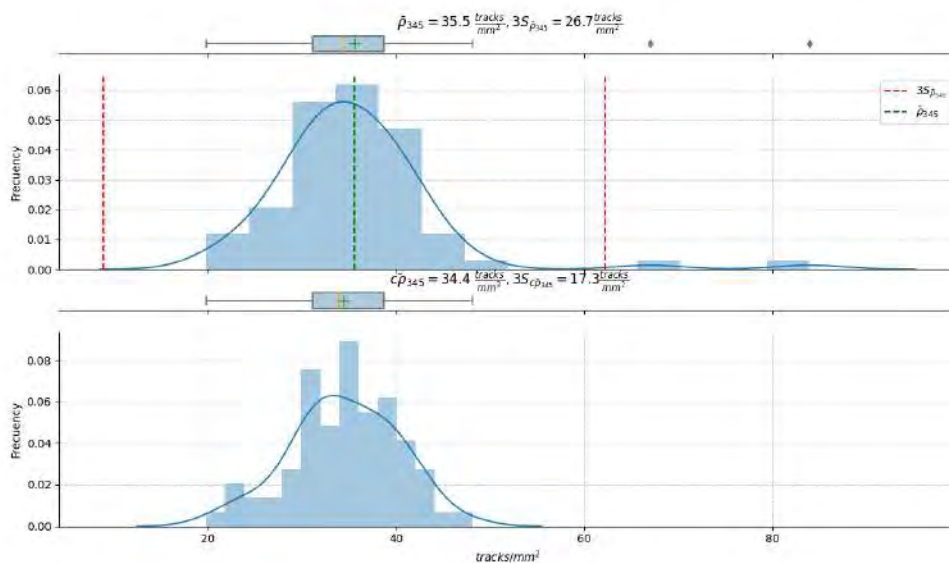


Figure 5.24: Removing outliers to determine tracks density.

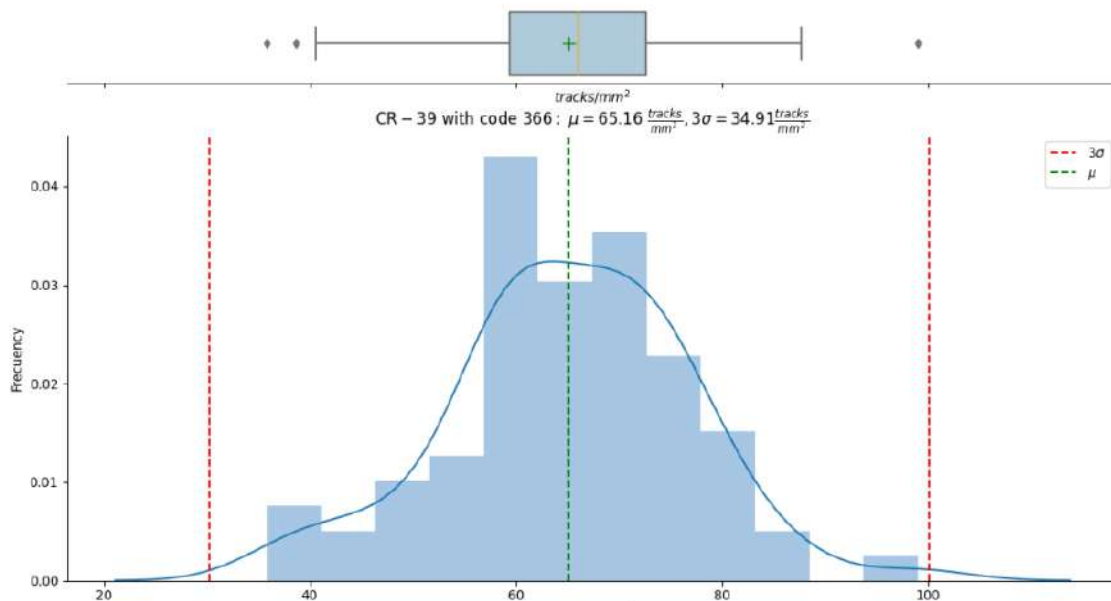


Figure 5.25: Considering tracks formed up to 3σ , then they will be outliers.

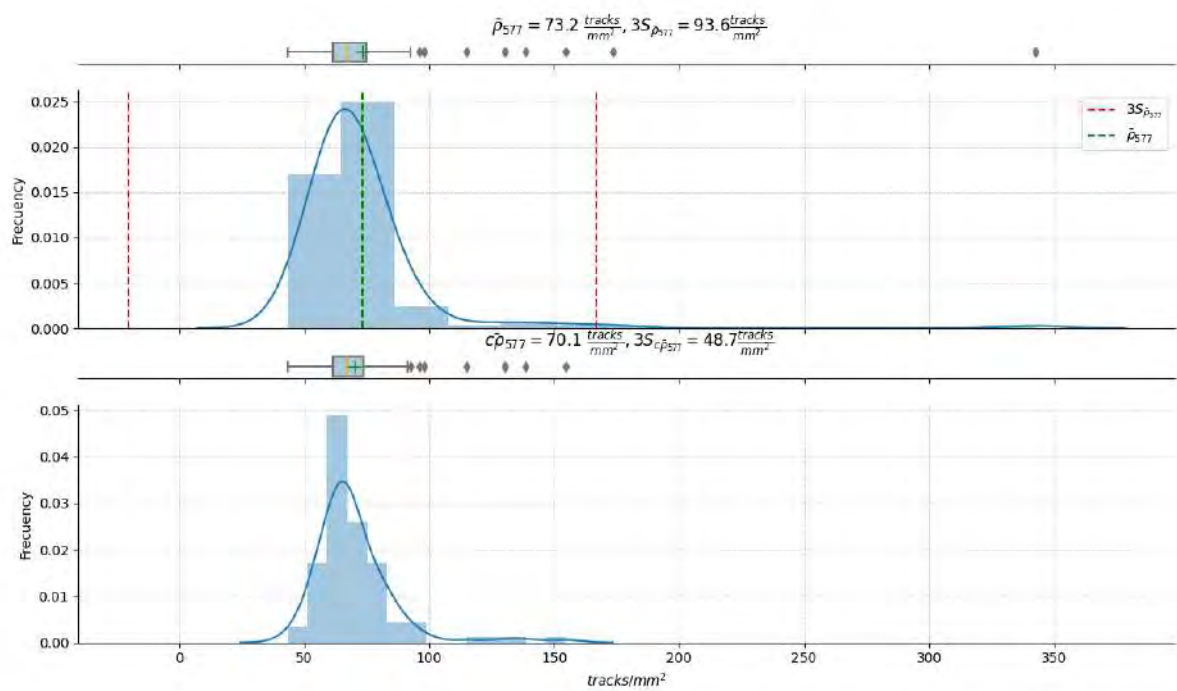


Figure 5.26: Tracks in diffusion metallic chambers with CR-39.

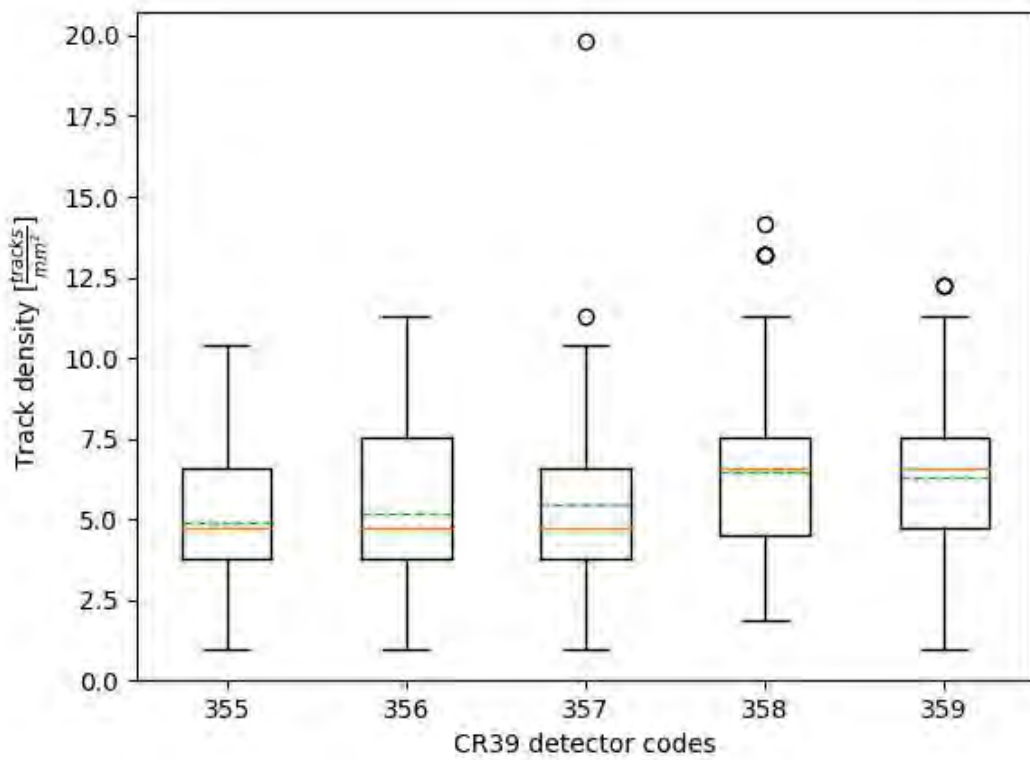


Figure 5.27: CR-39 background. Where circles represent outlier track density.

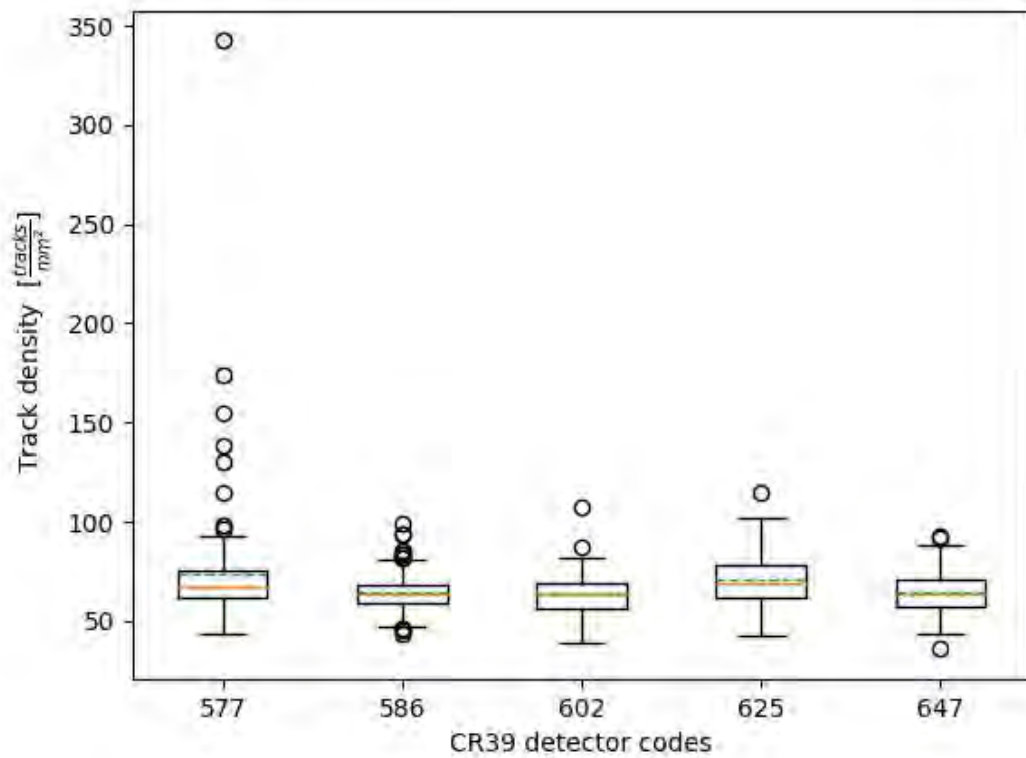


Figure 5.28: Track density of CR-39 inside metallic diffusion chamber exposed.

Once the count of tracks is done by means of macro called "MACRO39" based on software ImageJ, the results are compared with the readings made by the Politrack <https://miam.it/en/politrack/>, resulting in a strong linear correlation with $r=0.998$ indicating that there is an equivalence factor product of the differences in the reading methodology.

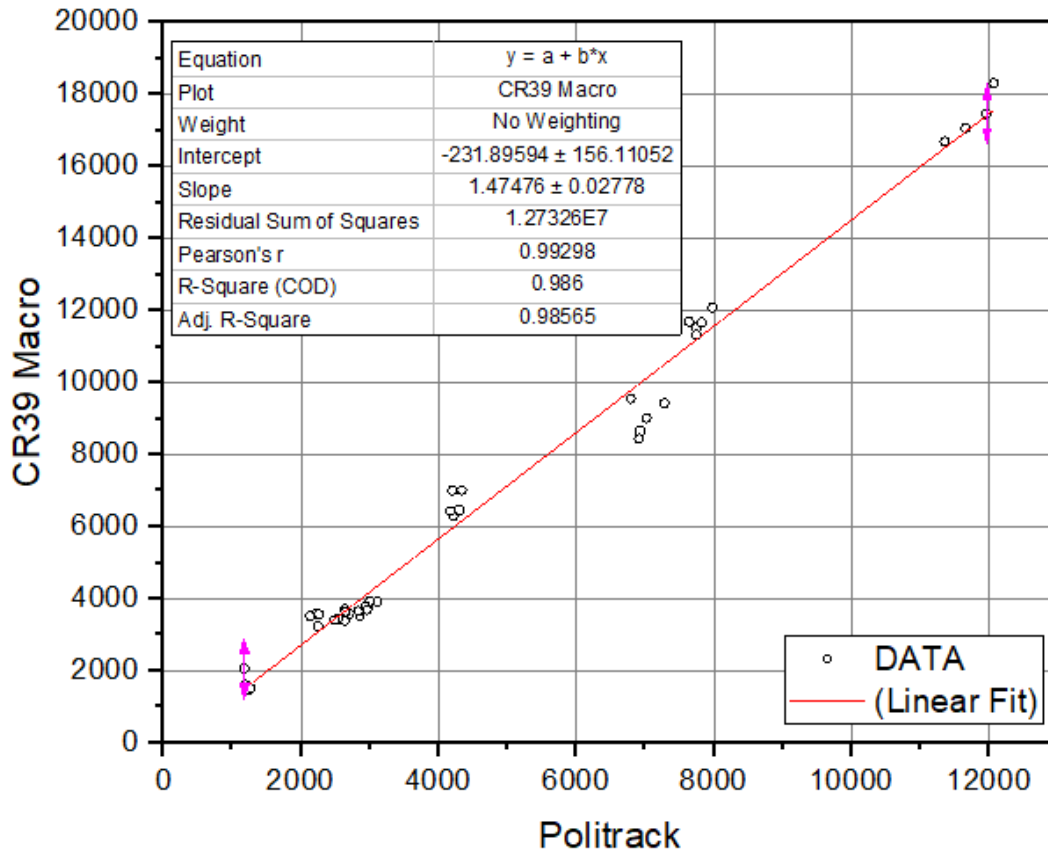


Figure 5.29: Correlation of track density readings by ImageJ MACRO39 and Politrack system.

5.2.4 Calibration factor determination

Table 5.4: Results from monitor exposition to radon concentration at PUCP radon chamber.

Exposures $kBqh/m^3$	Track density $[Tracks/mm^2]$	Uncertainty $[Tracks/mm^2]$
361.1	10.8	2.8
712.2	29.2	2.9
1072.6	32.6	3.6
2080.4	59.8	5.2
2716.5	84.6	6.4
3978.9	109.9	4.8
6397.7	167.2	6.2

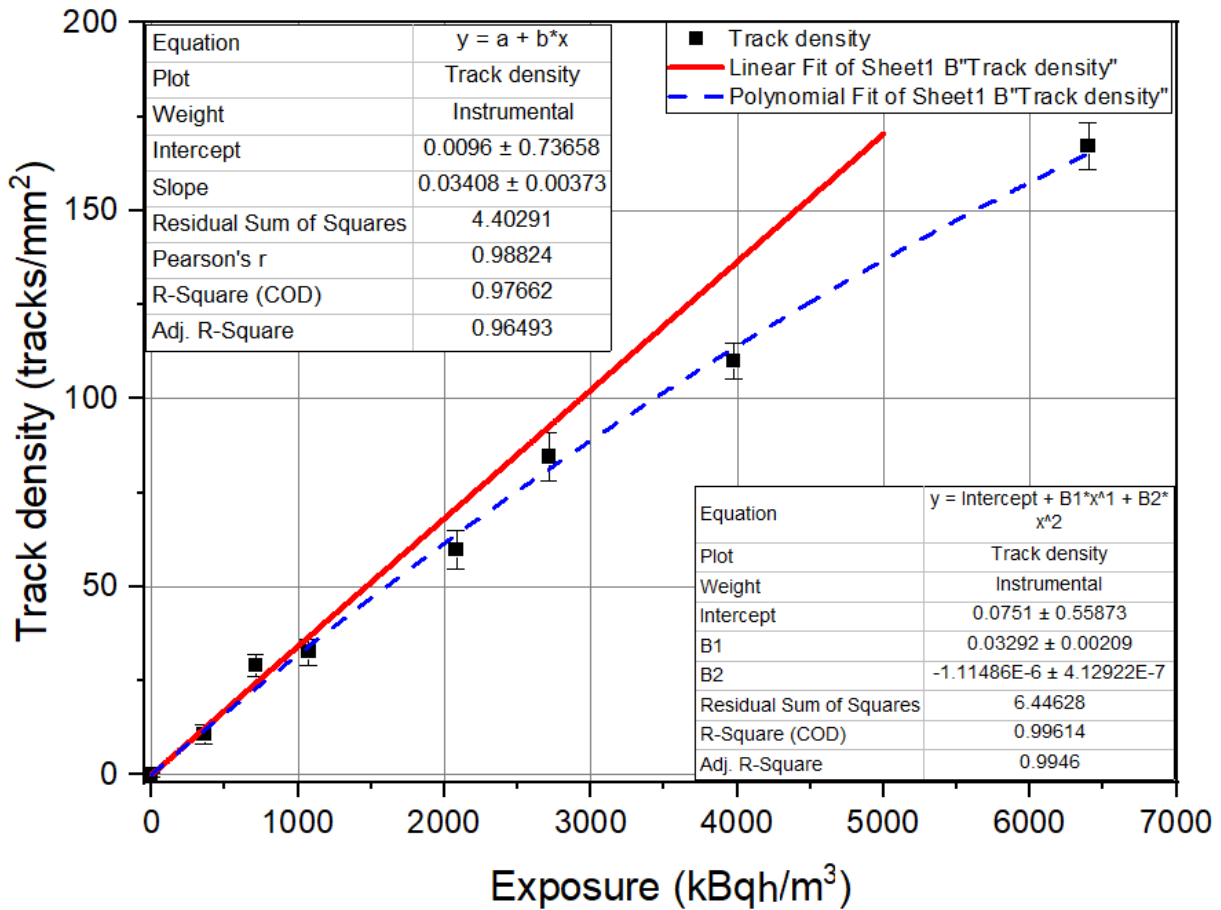


Figure 5.30: Experimental response fit curve for CR-39 inside cylindrical metallic diffusion chamber.

The experimental results show that the linearity in the calibration curve is only presented at low exposure points and for high exposition it is close to a cubic curve as reported by other authors as Daniele and Tommaso [84]. This is caused by the loss of detector sensitivity due to the effect of overlapping for high exposures, with the quadratic term taking precedence.

Table 5.5: Diffusion metallic chamber based on CR-39 chips calibration factor.

Calibration factor $\frac{\text{tracks}}{\text{mm}^2} / (\text{kBqh}/\text{m}^3)$
0.034 ± 0.004

Calibration factor CR-39 detector inside diffusion metallic chamber is getting from Figure 5.30, where lineal fit slope is taken as best converter from track density to exposure for radon concentration commonly found in homes and working places.

The following procedure is the same and analogous to the intercomparison performed in collaboration with the Environmental Radioactivity Group of Cantabria University (LaRUC) (Appendix B). In this measurement exercise, PUCP laboratory found exposures that were 1.13 times the reference exposures, with a coverage factor of 95%.

5.3 An approach to the measurement of radon permeability and transmission factor using CR-39 detectors inside a diffusion chambers exposed in PUCP radon chamber

In this section are determined the transmission factor through the pinhole method, permeability of a filter based on Ramachandran study [85].

Transmission factor is define as the ratio of inside and outside ^{222}Rn concentration.

$$F = \frac{C_s}{C_0} \quad (5.2)$$

Where, C_s and C_0 are radon concentration inside the pinhole chamber and outside air at the face of entry of the pinhole chamber, respectively.

5.3.1 Transmission factor determination

In this experiment, radon concentration fraction is detected by CR-39 chips, using pinhole, membrane filter and normal metallic diffusion chamber. The experiment was repeated twice.

The transition factor is determined from the equation of non-steady state diffusion model.

$$\frac{\partial C_i(t)}{\partial t} = J_i \frac{A_i}{V_{CM}} - \lambda C_i(t) \quad (5.3)$$

Where: C_i average radon concentration, J_i radon flux through membrane ($i = m$), by gap ($i = g$), pinhole ($i = p$), A_i (m^2) area of entrance holes, V_{CM} (m^3) is the internal volume of the metallic diffusion chamber and λ is decay constant of radon.

Using the Fick's first law of diffusion:

$$J_i = -D \frac{\partial C_i(t)}{\partial x_i} \quad (5.4)$$

Where: D (m^2s^{-1}) is the radon diffusion coefficient in air and the partial derive shows the change of radon concentration because of the position.

It is possible to rewrite the flux values according to the entrances. If membrane is used to cover the entrance of CM, flux can be express as:

$$J_m = -K \frac{\partial C_m(t)}{\partial x_m} \quad (5.5)$$

Replacing in the same way to the other cases in equation 5.4 and taking in to account equation 5.3, the concentration corresponding to the types of entrances is determined as:

$$\begin{aligned} C_m(t) &= \frac{C_0 \frac{A_m K}{V_{CM} d_m}}{\lambda + \frac{A_m K}{V_{CM} d_m}} \left(1 - \exp^{-\left(\lambda + \frac{A_m K}{V_{CM} d_m}\right)t} \right) \\ C_g(t) &= \frac{C_0 \frac{A_g D}{V_{CM} d_g}}{\lambda + \frac{A_g D}{V_{CM} d_g}} \left(1 - \exp^{-\left(\lambda + \frac{A_g D}{V_{CM} d_g}\right)t} \right) \\ C_p(t) &= \frac{C_0 \frac{A_p D}{V_{CM} d_p}}{\lambda + \frac{A_p D}{V_{CM} d_p}} \left(1 - \exp^{-\left(\lambda + \frac{A_p D}{V_{CM} d_p}\right)t} \right) \end{aligned} \quad (5.6)$$

Where: C_0 ($kBqm^{-3}$) is the radon concentration outside of CM and d_i (m) is the total distance that radon travel trough a membrane, gap or pinhole. At the beginning in Figure 5.20 the

5.3. An approach to the measurement of radon permeability and transmission factor using CR-39 detectors inside a diffusion chambers exposed in PUCP radon chamber

secular equilibrium is reached, it means the radon concentration inside CM keeps stable C_{S_i} . For that the equations 5.7 are independent of time:

$$\begin{aligned}\frac{Cs_m}{Co} &= \frac{\frac{A_m K}{V_{CP} d_m}}{\lambda + \frac{A_m K}{V_{CP} d_m}} \\ \frac{Cs_g}{Co} &= \frac{\frac{A_g D}{V_{CP} d_g}}{\lambda + \frac{A_g D}{V_{CP} d_g}} \\ \frac{Cs_p}{Co} &= \frac{\frac{A_p D}{V_{CP} d_p}}{\lambda + \frac{A_p D}{V_{CP} d_p}}\end{aligned}\tag{5.7}$$

Where $\frac{C_{S_i}}{C_o}$ is called radon transition factor [86]. Values for parameters like $D = 0.1 \text{ (cm}^2\text{s}^{-1}\text{)}$, $\lambda = 2.09 \times 10^{-6} \text{ s}^{-1}$, $A_p = 0.014 \text{ cm}^2$, $A_g = 7.562 \text{ cm}^2$, $d_p = 0.029 \text{ cm}$, $d_g = 0.922 \text{ cm}$ and $V_{CM} = 23.146 \text{ cm}^3$.

Table 5.6: First results of transmission factor experiment.

Setup experiment	Radon exposition $\frac{kBq}{m^3} h$	Track density $\frac{tracks}{mm^2}$
Diffusion chamber (gaps)		10.9 ± 2.5
Pinhole	361.1	10.2 ± 1.7
Membrane filters		20.1 ± 3.3

Table 5.7: Second results of transmission factor experiment.

Setup experiment	Radon exposition $\frac{kBq}{m^3} h$	Track density $\frac{tracks}{mm^2}$
Diffusion chamber (gaps)		59.8 ± 5.2
Pinhole	2080.4	53.9 ± 5.8
Membrane filters		127.8 ± 6.7

The transmission factor obtained according data from Tables 5.6, 5.7 for pinholes and gaps are 99.994% and 99.902%, respectively. However, for membranes the transmission factor is 1.904% it means this method should not be applied.

5.3.2 Permeability of filter

Permeability is an important physical feature of materials which is related with the apparent velocity of fluid flow through materials pores [64].

Authors as Pressyanov et al. [87], Ramachandran et al. [85], Wójcik and Zuzel [88] have measured and reported the permeability for some materials.

Open and metallic diffusion chamber cover by glass microfiber filter without binder <https://fanoia.com/en/filtros-microfibra-de-vidrio-y-cuarzo/>, exposed to radon in decay mode, are used to determine it's permeability. This filter is used in GITHUNU research and applications in order to retain moisture and aerosol preserving CR-39 and LR 115 type 2 nuclear track detectors. For that, the capability of radon flow through the filter (permeability) is measured.

Based on Ramachandran equation [85], it is possible to describe the behavior of radon concentration primary chamber (C_R), and radon concentration in membrane chamber (C_{GM}) showed in Figure 5.19b, expressed as equations 5.8.

5.3. An approach to the measurement of radon permeability and transmission factor using CR-39 detectors inside a diffusion chambers exposed in PUCP radon chamber

$$\begin{aligned}\frac{dC_R}{dt} &= -\lambda C_R + a - \frac{KA}{\delta V_R}(C_R - C_{GM}) \\ \frac{dC_{GM}}{dt} &= -\lambda C_{GM} + \frac{KA}{\delta V_{CM}}(C_R - C_{GM}) \\ a &= \lambda C_R\end{aligned}\tag{5.8}$$

Where: C_R, C_{GM} (Bq/m^3) are primary chamber and membrane chamber radon concentration, respectively. $\lambda(s^{-1})$ is the decay constant, K (cm^2s^{-1}) is the permeability constant, A (cm^2) surface area of membrane. V_R, V_{CM} are chamber and primary chamber volumes, respectively. δ cm is thickness of of membrane, a ($cm^{-3}s^{-1}$) is the gas production rate of the autunite sample.

When secular equilibrium is reached inside PUCP radon chamber, equations 5.8 can be considered:

$$\frac{dC_R}{dt} = \frac{dC_{GM}}{dt} = 0\tag{5.9}$$

Then, K can be calculated in term of knowing measured parameters like C_R and C_{GM} which is proportional to rate of ρ_R and ρ_{CM} track densities. In this way is possible to determine permeability.

$$K = \frac{\lambda\delta}{A\left(\frac{\rho_R}{\rho_{GM}} - 1\right)\left(\frac{1}{V_R} + \frac{1}{V_{CP}}\right)}\tag{5.10}$$

Table 5.8: Permeability experiment

Setup experiment	Radon exposition $\frac{kBq}{m^3}h$	Track density $\frac{tracks}{mm^2}$
Open diffusion chamber	712.2	79.5± 3.9
Membrane filters		40.9±2.8

We calculated the permeability using Equation 5.10 and data from Table 5.8. The value found is $[4.578x10^{-8} \pm 0.019x10^{-8}]cm^2/s$. It is in concordance with reported by Ramachandran et al. [85]; Arafa [89] where the order of 10^{-8} to 10^{-7} (cm^2/s).

We now proceed to determine the calibration factors or sensitivities of gap, pinhole, and membrane filter diffusion chambers, using the track density and exposure data Table 5.6, 5.7,5.8.

In the case of the gap diffusion chambers, the sensitivities have already been determined in Table 5.5.

Table 5.9: Calibration factor(sensitivity of diffusion chambers based in CR-39 detectors).

Diffusion chambers	Sensitivity S_{exp} (m)
Diffusion chamber (gaps)	0.009± 0.001
Pinhole	0.007±0.001
Membrane filters	0.020 ±0.001

These values are expressed in meter (m) units in order to compare them with the calibration factors determined and simulated by Nikezic using the program "computer program for the sensitivity calculation of CR-39 detector in diffusion chamber" [90]. Considering the geometric dimensions of the diffusion chamber and the detector, etching time, visibility, and V functions, the simulated sensitivity value for cylindrical metallic diffusion chamber gaps obtained was

5.3. An approach to the measurement of radon permeability and transmission factor using CR-39 detectors inside a diffusion chambers exposed in PUCP radon chamber

higher than the experimental, ($S_{sim} = 0.015 \pm 0.002$) m . The same result is observed in the Radout diffusion chamber where the simulated sensitivity value is twice the one reported by Caresana et al., [80].

This difference may be due to the etching conditions causing a V function different from those that Nikezic program use. For that, Hermosdorf said " these codes should be used carefully in respect on the choice of the sensitivity function" [91]. In this section as have been explained diffusion chambers (gap, pinhole and base en membrane) were etched under the same conditions as Caresana, it is inferred that the value simulated by the software is also high.



Chapter 6

Conclusions and recommendations

The thesis developed corresponds and contained design and construction of the radon chamber to expose passive and active detectors.

6.1 Conclusions

- In accordance with first main objective, design and construction of radon chamber (PUCP radon chamber) was completed successfully.
- The second main objective, the parameter that characterize the behavior of radon chamber were determine. These are within the expected range and in agreement with other research as shown discussed in section 3.
- One of the contributions of this thesis is the use of uranium ore (autunite) as a source for the radon chamber where ^{222}Rn concentrations show an acceptable behavior in repeated experiments, allowing to carry out three stable working regimes that will serve for the realization of various research studies.
- Uses and applications have been performed.
 - It has been possible to reach different levels of concentrations in close and open dynamic modes for different flow rates. It has also been possible to perform experiments such as comparing the response of active monitors in static mode and it has been found that by this method it is possible to identify which monitor needs to be calibrated considering a calibrated reference monitor. In addition, it was possible to determine the purging time of the chamber, establishing the necessary time to start new experiments.
 - We calibrated passive monitors (metallic diffusion chamber + CR-39), taking into account the tracks count with a macro developed in ImageJ, showing results, where the calibration points were low, medium, high and very high, such that the linear behavior was observed for exposures that would be found at home, then for higher exposures experimentally reflected the effect of saturation of the tracks (overlapping effect) decreasing the sensitivity of the monitor, taking preponderance the quadratic term.
 - The radon permeability in glass microfiber filter without binder was estimated, the value was found to be in the order of $(10^{-8} - 10^{-7})\text{cm}^2/\text{s}$ showing not only the validity of the procedure used as developed in the section but also the good performance of the radon chamber to carry out studies of this type.

- The transmission factor of the metallic and pinhole diffusion chambers was estimated using the model proposed by Sahoo. Acceptable values were found and they are in great relation with the track densities found, indicating that there will be a higher transmission factor in the presence of greater densities of traces. On the other hand, it was found that this method does not work properly in the case of filters.

6.2 Recommendations

- Develop the study of the behavior of radon concentrations as a function of temperature, since the radon chamber built has a temperature control system.
- Establish an automated system of the valves and air pumps of the radon chamber to reach different saturation concentration.
- The PUCP radon chamber is designed to be able to work with standard source, having the possibility of replacing the autunite as radon source.
- It is advisable to calibrate and test both active and passive monitors for every used diffusion chamber to guarantee accurate measurements.
- When operating the radon chamber, the air extraction system should be turned on when the antechamber is opened, and radon levels should be expected to be comparable to background levels when operating in the radon room. It is important to always test radon concentration levels outside the chamber for safe radon management.

Appendix A

All codes shown in this thesis were developed by the author.

A.1 Radon and progeny effective volume code in Fortran 90

Code developed by author of this thesis

subroutine energy2(xx,E1,Ei) ! !This subroutine computed the energy for distances less than the range

real(4), intent(in):: xx,E1

real(4), intent(out):: Ei

real(4)::A,B,dd,RP1,R1,Fp,R1X,F1,F2,F3

A=0.7065

B=3.6201

dd=0.5088

R1= A*E1**2. + B*E1+dd ! RANGE

RP1=-R1+(xx/0.1)

F1=(xx/0.1)

F2=sqrt(B**2.-4.*A*(RP1+dd))

F3=-B+sqrt(B**2.-4.*A*(RP1+dd))

if (F1.lt.R1 .and. F2.gt.0. .and. F3 .gt.0.)then

Ei=(-B+sqrt(B**2.-4.*A*(RP1+dd)))/(2.*A)

else

Ei=0.

end if

end subroutine energy2

!XXXXXXXXXXXXXXXXXXXXXXXXXXXXXXXXXXXX

subroutine ancritico2(Ei,acr)

real(4),intent(in)::Ei !E1 Energy of the incident alpha particles

real(4),intent(out)::acr !critic angle

real(4)::A,B,dd,D,E,F,G

integer::i

!Air density de 0.0012048 g/cm3

A=6.16157

B=-113.1883

```
dd=845.76998
D=-3287.5898
E=7021.67000
F=-7847.9744
G=3658.788045
```

```
acr=A*(Ei**6)+B*(Ei**5)+dd*(Ei**4)+D*(Ei**3)+E*(Ei**2)+F*Ei+G
```

```
end subroutine ancritico2
```

```
!XXXXXXXXXXXXXXXXXXXXXXXXXXXXXXXXXXXXXXXXXXXXXXXXXXXXXXXXXXXX
!XXXXXXXXXXXXXXXXXXXXXXXXXXXXXXXXXXXXXXXXXXXXXXXXXXXXXXXXXXXX
```

```
program voleff
```

```
real(4):: xx,yy,zz,theta,pi,h0,rd,dmax,dmin,phi,gam,beta,xs,R1,d1,d2,E1,te,dx,dd,Eii
real(4):: dp,tp
integer:: i,j,k,cont,nn,p,nt
real(4):: xi(1001),yi(1001),x(100000000),y(100000000),z(100000000)
real(4):: r(100000000) !Random coordinates points
real(4):: xc(10000000),yc(10000000),zc(10000000) !possible coordinates of tracks on the detec-
tor.
real(4):: rc(100000000),En(2),anc(2)
real(4):: xe(10000000),ye(10000000),ze(10000000)
real(4):: re(10000000) ! Points that belong to effective volume
real(4):: xp(10000000),zp(10000000),yp(10000000) ! Detected alpha particles coordinates points
real(4):: anginc(10000000),enrgia(10000000)
real(4):: b(1001,2),EF(2),tet(2),ang(2)
real(4):: ds(2),sens
pi=3.1415926536
h0=5.0
rd=1.
```

```
write(*,*) "(IN) Initial alpha particle as soon as 222 Rn decay or its progeny"
read(*,*) E1
write(*,*) "Number of events"
read(*,*) nt ! Total number of points generated
!XXXXXXXXXXXXXXXXXXXXXXXXXXXXXXXXXXXXXXXXXXXXXXXXXXXXXXXXXXXX !XXXXXXXXXXXXXXXXXXXXXXXXXXXXXXXXXXXXXXXXXXXX ! Distances and
energy data are read to calculate maximum  $d_{max}$  and minimum  $d_{min}$  distances.
```

```
open (unit=10,file='Rn222.txt',status='old') ! Here is where initial data is stored.
```

```
do i=1,1001
read (10,*,iostat=ierror) b(i,1),b(i,2) !
xi(i)=b(i,1) ! Traveled distances
yi(i)=b(i,2) ! Energy
```

```
if (yi(i) .gt. 4.675 .and. yi(i).lt. 4.695 ) then
dmin=xi(i)
!write(*,*) xi(i),yi(i)
end if
```



```
if (yi(i) .gt. 1.44 .and. yi(i).lt. 1.46) then
dmax=xi(i)
!write(*,*) xi(i),yi(i)
end if
end do
write(*,*) dmin, dmax
!XXXXXXXXXXXXXXXXXXXXXXXXXXXXXXXXXXXXXXXXXXXXXXXXXXXX
!XXXXXXXXXXXXXXXXXXXXXXXXXXXXXXXXXXXXXXXXXXXXXXXXXXXX
!Random points are generated according to the dimensions of the detector  $d_{min}$  and  $d_{max}$ 

do j=1,nt
open (unit=2,file='cilin.txt',status='unknown')
r(j)=(rd+dmax)*sqrt(rand())
theta=2*pi*rand()
z(j)=dmax*rand()
x(j)=r(j)*cos(theta)
y(j)=r(j)*sin(theta)
!print*, x(j),y(j),z(j)
write(2,*)x(j),z(j)
end do

!XXXXXXXXXXXXXXXXXXXXXXXXXXXXXXXXXXXXXXXXXXXXXXXXXXXX
!XXXXXXXXXXXXXXXXXXXXXXXXXXXXXXXXXXXXXXXXXXXXXXXXXXXX !Effective volume is generated
open (unit=8,file='vef222.txt',status='unknown')
open (unit=10,file='partdet222.txt',status='unknown')
open (unit=11,file='engvsag222.txt',status='unknown')
open (unit=12,file='anginciden222.txt',status='unknown')
open (unit=13,file='energias222.txt',status='unknown')
open (unit=14,file='puntosespacio222.txt',status='unknown')

cont=0.

do j =1,nt
ds(1)= sqrt( (r(j)+rd)**2 + (z(j))**2 )
ds(2)= sqrt( (r(j)-rd)**2 + (z(j))**2 )
tet(1)=asin(z(j)/ds(1))*(180/pi) ! Angle respect the detector surface and d1
tet(2)=asin(z(j)/ds(2))*(180/pi) ! Angle respect the detector surface and d1
!call energy(ds,E1,En)
!call ancritico(En,anc)

!cont=cont+1
!dx=1.0
do k=0,1000
dr=k*2*rd/1000
dd=sqrt( (r(j)-(-rd+dr))**2 + z(j)**2 )
te=asin(z(j)/dd)*(180/pi)
call energy2(dd,E1,Ei)
call ancritico2(Ei,acr)

if ((dmin;dd .and. dd;dmax) .and. (te;acr)) then
```

```

cont=cont+1
xe(cont)=x(j)
ye(cont)=y(j)
ze(cont)=z(j)
re(cont)=r(j)
write(8,*) re(cont),ze(cont)
exit
end if
end do
end do
nn=cont
write(*,*) nn ! Number of points of effective volume
call CPU`time(TIEMPO)
write(*,*)TIEMPO
!XXXXXXXXXXXXXXXXXXXXXXXXXXXXXXXXXXXXXXXXXXXX
!XXXXXXXXXXXXXXXXXXXXXXXXXXXXXXXXXXXXXXXXXXXX ! Number of particles hit the detector
p=0.
do k=1,nn
phi=2*pi*rand()
gam=acos(2*rand()-1)
beta=pi-gam
if (beta.le.pi/2.) then
xc(k)=xe(k)+ ze(k)*(tan(beta))*cos(phi)
yc(k)=ye(k)+ ze(k)*(tan(beta))*sin(phi)
zc(k)=0.0
rc(k)=sqrt( xc(k)**2+yc(k)**2 )

!XXXXXXXXXXXXXXXXXXXXXXXXXXXXXXXXXXXXXXXXXXXX
!XXXXXXXXXXXXXXXXXXXXXXXXXXXXXXXXXXXXXXXXXXXX if (rc(k)=rd)then !
dp=sqrt( (xe(k)- xc(k))**2 +(ye(k)-yc(k))**2 + (ze(k)-zc(k))**2 )
tp=asin(ze(j)/dp)*(180/pi)
call energy2(dp,E1,Eii)
call ancritico2(Eii,acr)
p=1
if ((dmin<dp .and. dp<dmax) .and. (tp<acr)) then

    p=p+1
xp(p)=xc(k)
yp(p)=yc(k)
anginc(p)=tp
enrgia(p)=Eii
write(10,*) xp(p),yp(p) ! Alpha track are form on the detector under critical and energy win-
dow conditions.
write(11,*) enrgia(p),anginc(p)
write(12,*) p,anginc(p)
write(13,*) p,enrgia(p)
write(14,*) xe(k),ye(k),ze(k) ! Points from effective volume that has a nos- zero !probability of
being detected by detector
end if
end if

```

```
end if
end do

      sens=2.*(p*dmax/nt)
write(*,*) sens,p

      end program
```



A.2 Macro CR-39 counting tracks base on ImageJ

```
dir1=getDirectory("Choose Source Directory");
dir2=getDirectory("Choose Destination Directory");
list=getFileList(dir1);
setBatchMode(true);
for(i=0;i<list.length;i++)
open(dir1+list[i]);
name=File.nameWithoutExtension;
saveAs("Tiff",dir2+i+"Original"+name);
setThreshold(0, 239);
setOption("BlackBackground", false);
run("Convert to Mask");
run("Dilate");
run("Dilate");
run("Fill Holes");
run("Watershed");
run("Set Scale...", "distance=2048
known=1190 pixel=1 unit= $\mu$ m global");
run("Analyze Particles...", "size=30-1200 circularity=0.70-1.00 show=Outlines display exclude
clear summarize record");
saveAs("Tiff",dir2+i+" CountMask1 "+name); close();
saveAs("Tiff",dir2+i+" Thresholded1 "+name);
selectWindow("Results");
saveAs("Results",dir2+i+name+"Results.csv");

selectWindow("Summary");
saveAs("Text",dir2+i+name+"Summary.txt");
run("Close");
```

A.3 Sikuli LR 115 type 2

```
def loopAngulo(i):  
j=74  
while j != 90:  
doubleClick("1509640412186.png")  
wait(1)  
type("K")  
type(Key.ENTER)  
wait(1)  
type("L")  
type(Key.ENTER)  
wait(1)  
type (str(i))  
type(Key.ENTER)  
wait(1)  
type (str(2.25))  
type(Key.ENTER)  
wait(2)  
type (str(3.2))  
type(Key.ENTER)  
wait(1)  
type (str(j))  
type(Key.ENTER)  
wait(1)  
type (str(1))  
type(Key.ENTER)
```



A.4 ^{226}Ra distribution in a grain of silicon oxide SiO_2

```
subroutine distance(x,y,theta,Rd,dist)
real, intent(in) :: x,y,theta,Rd
real, intent(out) :: dist
real:: A,B,T,d1,d2,discriminant,rt
```

```
    rt=sqrt(x**2+y**2)
    A=1.0
    B=2*(x*cos(theta)+y*sin(theta))
    T=rt**2 - Rd**2
    discriminant=B**2-4*A*T
```

```
    if( discriminant .gt. 0.0)then
d1=(-B+sqrt(discriminant))/(2*A)
d2=(-B-sqrt(discriminant))/(2*A)
```

```
    if (d1.gt.d2) then
dist=d1
!write(*,*) dist
else
dist=d2
```

```
    end if
```

```
    else
write (*,*) "complex solution"
end if
```

```
    if( discriminant .eq. 0.0)then
dist=d1
dist=d2
```

```
    end if
```

```
end subroutine distance
```

```
!XXXXXXXXXXXXXXXXXXXXXXXXXXXXXXXXXXXXXXXXXXXXXXXXXXXXXXXXXXXX
!XXXXXXXXXXXXXXXXXXXXXXXXXXXXXXXXXXXXXXXXXXXXXXXXXXXXXXXXXXXX
```

```
program emanation
```

```
real:: r,radiop,pi,phy,theta, dist,DD,density,EmFactor,TIME1, TIME2
real, allocatable:: x(:), y(:)
integer :: k,ks,i,nt
```

```
open(unit=14,file='2radio-distribution-SiO2.txt',status='unknown')
```

```
pi=3.1415926
```

```
DD=0.0396 !ion range in SiO2=0.0396um Rn-222
density=318309.886
```

```

do j=1,1
radio=2*j
nt= int(density*(radio**2.)*pi)
radiop=radio-DD ! ring thickness

allocate(x(nt))
allocate(y(nt))
!allocate(z(nt))

k=0
ks=0
do i=1,nt

r=((radio**2.-radiop**2.)*rand()+radiop**2.)**(1./2.)
phy=2.*pi*rand()

x(i)=r*cos(phy)
y(i)=r*sin(phy)
write(14,*) x(i),y(i)
!Radium decays and is emitted in random direction
theta=2.*pi*rand()
call distance(x(i),y(i),theta,radio,dist)
if (dist .gt. DD) THEN
k=k+1
x(i)=0.
y(i)=0.
end if

if (dist .lt. DD)THEN
ks=ks+1
X(i)=1.
y(i)=1.
!write(*,*)x(i),y(i)
end if
!write(*,*)theta,dist,ks,k
end do
EmFactor=real(Ks)/(real(nt))
write(*,*)nt,ks,k,EmFactor
iF (ALLOCATED (x)) DEALLOCATE (x)
iF (ALLOCATED (y)) DEALLOCATE (y)
Call CPU`TIME(TIME1)
!!write(16,*) nt,TIME1
end do
!iF (ALLOCATED (x(nt)) DEALLOCATE (x(nt))
!iF (ALLOCATED (y(nt))) DEALLOCATE (y(nt))
Call CPU`TIME(TIME2)
write(*,*) TIME2
end program

```

Appendix B





INTRODUCCIÓN

Las fuentes de neutrones como $^{241}\text{AmBe}$, ^{252}Cf , reactores nucleares y neutrones cósmicos, son usados para diversas aplicaciones, donde cada una de las fuentes tienen como característica principal el espectro de neutrones, además del mecanismo de como los neutrones son generados[1].

Existen diferentes métodos de detección de los neutrones, entre ellos tenemos a los detectores de trazas nucleares como los LR 115 (nitrato de celulosa) y el CR 39 (alil diglicol carbonato) los cuales son usados con algún tipo de convertidor [2]. El objetivo del trabajo es poder medir la presencia de neutrones debido a una fuente de $^{241}\text{AmBe}$ usando detectores de trazas nucleares y poder discernir trazas debido a la reacción (n,α) y fondo por la presencia radón y sus descendientes principalmente.

MATERIALES Y METODOLOGÍA

Se uso como convertidores boro-lucita y polietileno, para detectar neutrones en forma indirecta, mediante las reacciones nucleares $^{10}\text{B}(n,\alpha)^7\text{Li}$ cuya sección eficaz para neutrones es de $(\sigma=3840\text{ b})$ y (n,p) para neutrones rápidos produciendo partículas cargadas alfa y protones respectivamente. Las partículas alfa de la reacción antes mencionada son de 1.47 MeV, estas partículas alfas interactúan con el CR 39 y LR 115 donde pueden causar daños en la estructura polimérica y dejar trazas latentes al igual que los protones, el cual a través de un proceso de revelado químico (CR 39, $T=70^\circ\text{C}$, KOH a 6.1 N con un tiempo de grabado de 8 horas y media), (LR 115, $T=60^\circ\text{C}$, NaOH a 2.5 N con un tiempo de grabado de 1 hora y 45 minutos) pueden ser observadas con un microscopio óptico. Los detectores fueron irradiados con una fuente de neutrones de $^{241}\text{AmBe}$ cuyas características son, actividad inicial de 100 mCi, flujo de 6 $(\text{n}/\text{cm}^2\text{s})$ a 50cm [3]. Sin embargo, el experimento se realizó a 10 cm de la fuente durante 42 horas.

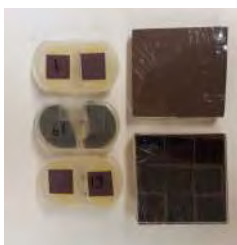


Figura 1: Diferentes configuraciones de los detectores tanto con CR 39, LR 115 con boro y polietileno.



Figura 2: Exposición de las diferentes configuraciones de detectores trazas nucleares una fuente de $^{241}\text{AmBe}$ a una distancia de 10cm.

La lectura de los detectores fue a través del software ImageJ donde se elaboro un macro el cual fue calibrado a las escalas del tamaño de las trazas, tomando ciertos criterios de visibilidad para poder discriminar trazas debido a las reacciones antes mencionadas y fondo.



Figura 3: Instrumentación necesaria para el procesamiento de datos luego de la exposición de los detectores a una fuente de neutrones; un baño María, un microscopio óptico, solución química de KOH y NaOH.



Figura 4: El conteo de las trazas, se realiza con el programa en ImageJ, a través de un macro, como se puede observar en la figura.

RESULTADOS

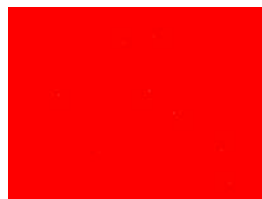


Figura 5: Distribución de huellas generadas en el detector LR 115 con boro natural y lucita, las huellas son los puntos blancos, estas son generadas por la interacción de las partículas alfa y el detector.



Figura 6: Distribución de huellas generadas en el detector CR 39 con boro natural y lucita, donde las trazas son los círculos con contorno oscuro. Se nota claramente que la morfología de las trazas son completamente diferentes a los observados en el LR 115, por tener diferentes parámetros tanto de ángulo crítico y ventana de energía además de su

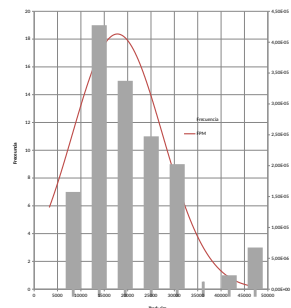


Figura 7: Distribución del tamaño de las trazas en el CR39 debido a la reacción (n,α) , cuyos valores están en el rango de $(10000 -35000)$ pixeles²

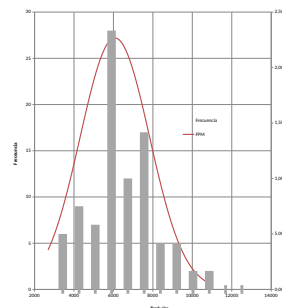


Figura 8: Distribución del tamaño de las trazas en el CR 39 debido al fondo del medio ambiente, cuyos valores están en el rango de $(3000-10000)$ pixeles²

CONCLUSIONES

Dado que la sección eficaz del ^{10}B para la reacción nuclear (n,α) de neutrones térmicos es bastante mayor que los rápidos y de acuerdo al espectro de neutrones de la fuente de $^{241}\text{AmBe}$ a 10 cm de la fuente donde el flujo es de 150 $(\text{n}/\text{cm}^2\text{s})$, la lucita debido a la presencia de núcleos ligeros en su estructura ha moderado los neutrones los cuales se reflejan en las trazas obtenidas en los CR 39, donde los diámetros son considerablemente mayores que las trazas del fondo, esto debido a la baja energía de las partículas alfa el cual se caracterizada por grandes diámetros como se muestra en las figuras 7,8.

La respuesta del detector LR 115 comparado a la respuesta del CR 39 mostró tener mayor eficiencia, esto debido al tipo de configuración y posición de la fuente respecto de la parte sensible del detector. Los resultados frente a la reacción (n,p) no fueron satisfactorios en el LR 115, no se pudo observar las trazas, mientras que en el CR 39 debido al alto fondo de los detectores existe una gran incertidumbre, en la discriminación de las mismas.

AGRADECIMIENTOS

Este trabajo fue realizado gracias al soporte de Concytec, al grupo de Huellas Nucleares de la PUCP (GITHUNU) y al cuerpo académico del profesor H.R. Vega Carrillo AUZ-México.

BIBLIOGRAFÍA

- [1] Vega-Carrillo, H. R., Manzaneres Acuña, E., Hernández Dávila, V. M., Mercado Sánchez, G. A., Gallego Díaz, E., & Lorente Fillol, A. (2005). Características dosimétricas de fuentes isotópicas de neutrones. Revista mexicana de física, 51(5), 494-501.
- [2] Alvarado, R., Palacios, D., Sajo-Bohus, L., Greaves, E., Barros, H., Nemeth, P., & Goncalves, I. F. (2010). Neutron flux characterization using LR-115 NTD and binary glass metal as converter. Revista Mexicana de Física, 56(1), 5-8.
- [3] Raquel Murillo, Héctor Vega. (2012). Dosis y espectro de los neutrones de $^{241}\text{AmBe}$, editorial académica española, ISBN: 978-3-659-05607-9.

INTRODUCTION

Neutron sources, such as 241Am/Be, 252Cf, nuclear reactors and cosmic neutrons, are used for diverse applications, where each of the sources has as main characteristic the neutron spectrum, in addition to the mechanism of how neutrons are generated [1]. The neutron-scattering method is widely used in agriculture, forestry, hydrology, and civil engineering, for measuring the water content of soil [2]. The neutron's sensitivity to specific types of atoms can be high, but it further depends on neutron energy which in turn decreases with every interaction[3]. A the aim of this work was to develop a simple model (soil and neutron source) to analyze the answer through neutron spectrum the water content in soil.

MATERIALS Y METHODS

A three-dimensional geometry is used, where the universe is a 1000 cm sphere, which is divided into two parts air and soil media. In the soil, there is a 500 cm deep seamer where the neutron source is placed at 125 cm 241Am/Be or 252Cf. The fluences in the z-axis are measured along the hole, to determine how backscattered neutrons affect the spectrum. The simulation was done through MCNP5, since neutrons undergo many interactions solve analytically does not become practiced.

Standard soil sample and soil sample of 5% and 50% water content was used.

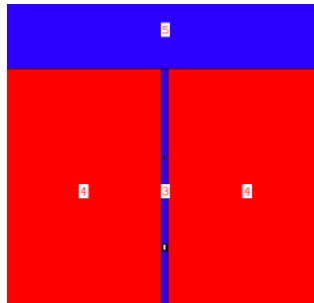


Figure 1: Geometry used in mcnp where 5 is air, 4 ground, 3 is the hole and the neutron source is the small white rectangle.

105 Earth, U.S. Average					
Element	Neutron ZA	Proton ZA	Weight Fraction	Atom Fraction	Density
O	8016	8016	0.513713	0.070604	0.0029581
Ne	11023	11000	0.008140	0.005578	0.000244
Mg	12000	12000	0.013303	0.011432	0.000501
Al	13027	13000	0.046263	0.053073	0.003256
Si	14000	14000	0.271183	0.231655	0.018635
Il	19000	19000	0.014327	0.007653	0.000335
Ca	20000	20000	0.051167	0.026664	0.001169
Ti	22000	22000	0.004695	0.002609	0.000106
Mn	25000	25000	0.000716	0.000272	0.000012
Fe	26000	26000	0.056283	0.027650	0.001043
Total			1.000000	0.000000	0.043927

Table 1: Chemical elements present in the soil with their respective molecular weights [4].

RESULTS

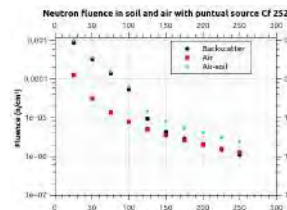


Figure 2: Contribution of the scattered neutron fluence due to 252Cf.

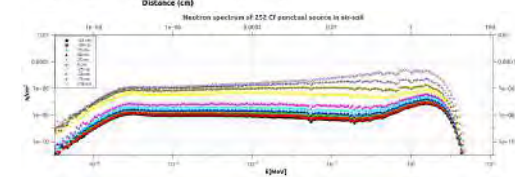


Figure 3: Fluence at different distances from 252Cf neutron source with respect to the z-axis in standar soil.

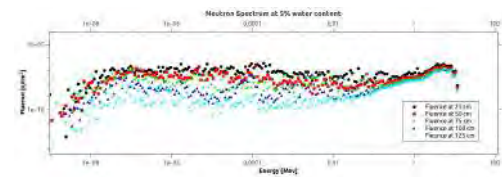


Figure 4: Fluence at different distances from 241Am/Be neutron source with respect to the z-axis in soil with 5% of water content.

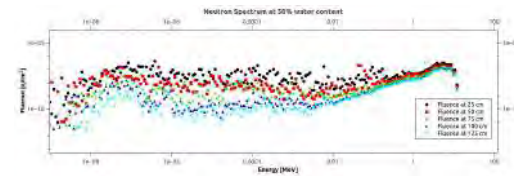


Figure 5: Fluence at different distances from 241Am/Be neutron source with respect to the z-axis in soil with 50% of water content.

CONCLUSIONS

As can be seen, there is a slight contribution of the neutrons dispersed to the total fluence due to the elements present in the soil. It is quite noticeable when the 252Cf source is used. For soil with 5% and 50% of water content it is observed that the flow to distances greater than 75 cm from the source there are no significant differences. However, for smaller distances there is a dispersion in the fluence due to the contribution of backscattered neutrons with 241Am/Be neutron source.

ACKNOWLEDGMENT

This work was carried out thanks to the support of Concytec, the group of Nuclear tracks of the PUCP (GITHUNU) and the academic body of Professor H.R. Vega Carrillo AUZ-Mexico.

BIBLIOGRAPHY

[1] Vega-Carrillo, H. R., Manzanares Acuña, E., Hernández Dávila, V. M., Mercado Sánchez, G. A., Gallego Díaz, E., & Lorente Fillol, A. (2005). Características dosimétricas de fuentes isotópicas de neutrones. Revista mexicana de física, 51(5), 494-501.
 [2] Li, J., Smith, D. W., Fityus, S. G., & Sheng, D. (2003). Numerical analysis of neutron moisture probe measurements. International Journal of Geomechanics, 3(1), 11-20.
 [3] Köhl, M., Schrön, M., Zreda, M., Schmidt, U., Dietrich, P., & Zacharias, S. (2015). Footprint characteristics revised for field-scale soil moisture monitoring with cosmic-ray neutrons. Water Resources Research, 51(7), 5772-5790.
 [4] McCann Jr, R. J., Gesh, C. J., Pagh, R. T., Rucker, R. A., & Williams III, R. G. (2011). Compendium of material composition data for radiation transport modeling. PNNL-15870 Rev. 1(4).

INTRODUCCIÓN

El isótopo Rn-222 es formado a partir del decaimiento del Ra-226, este gas radiactivo tiene mucha movilidad, puede desprenderse del suelo y las rocas a las fisuras o intersticios (poros) de los granos del suelo y mediante procesos de transporte como difusión y convección. Puede exhalar a la atmósfera, acumulándose en lugares cerrados como viviendas, lugares de trabajo, cuevas, etc, pudiendo representar un riesgo para la salud. Este proceso de desprendimiento del radón de los granos del suelo a los poros se denomina emanación de radón. Si se conocen parámetros como el factor de emanación, porosidad y contenido de Ra del suelo se puede calcular la concentración en los poros y por tanto estimar el radón exhalado por determinado mineral.

FUNDAMENTO

Solamente la fracción de radón que logra dejar los granos y entra en el volumen de los poros del suelo es considerado como radón que emana de los granos. Esta fracción es conocida como coeficiente de emanación o factor de emanación ϵ . Cuando el Ra decae, por conservación de momento el Rn tiene una energía cinética de 86 keV (Rn-222) y 103 keV (Rn-220). La distancia que puede moverse en un grano de mineral depende de la densidad y composición del material, los rangos para minerales comunes están (0.02-0.07 μm)[1]. Este mecanismo junto con el contenido de los poros llenos de agua o aire y la distribución de Ra, así como el tamaño de grano determinan la fracción de emanación [3].

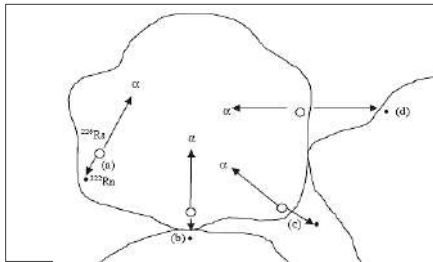


Figura 1: Proceso de emanación de radón de un grano de suelo, donde se observa tres posibles casos.

METODOLOGÍA

En la simulación, se asume un círculo de radio R el cual emula un grano del suelo que contiene una distribución uniforme de Ra-226, se generan N historias donde $(i=1,N)$ representan a los átomos de Ra, el cual decae generando un átomo de radón y una partícula alfa, aleatoriamente se genera un ángulo θ el cual define la dirección que seguirá el átomo de radón. Se asume SiO_2 o UO_2 como material del grano, donde el rango de energías 86.3keV (Rn-222) y 103keV (Rn-220) son 0.043 μm y 0.036 μm respectivamente el cual es calculado con SRIM-2013 [2], además se estudia un segundo caso donde el Ra está distribuido uniformemente en una sección de anillo del círculo de espesor igual al rango del Rn (D) en el material SiO_2 .

$$r_i = R(\xi_1)^{0.5} \quad (1)$$

$$\phi_i = 2\pi(\xi_2) \quad (2)$$

$$\theta_i = 2\pi\xi_3 \quad (3)$$

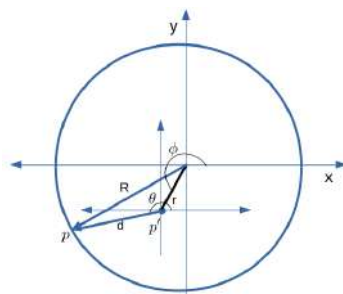


Figura 2: Modelo de proceso de emanación en 2-dimensiones, donde R es el radio del grano, ϕ y r determinan la posición del Ra, θ ángulo aleatorio el cual determina la dirección de emisión del átomo de Rn.

RESULTADOS

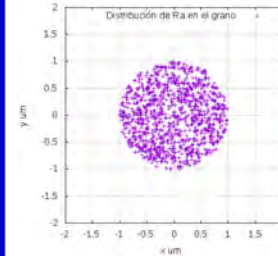


Figura 3: Distribución de átomos de Ra en un grano de suelo SiO_2 , con una distribución uniforme.

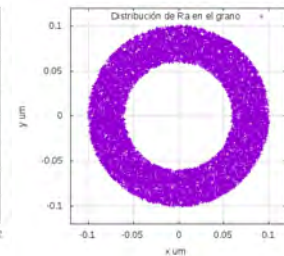


Figura 4: Distribución de átomos de Ra en un grano de suelo SiO_2 , con una distribución uniforme en un anillo con espesor igual al rango que el radón recorre en dicho material.

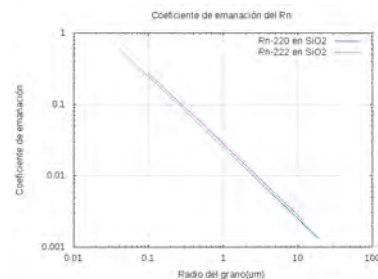


Figura 5: Coeficiente de emanación del Rn-222 y Rn-220 en SiO_2 , para una distribución uniforme de Ra, con diámetros diferentes.

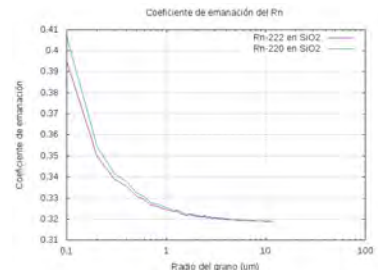


Figura 6: Coeficiente de emanación del Rn-222 y Rn-220 en SiO_2 , para una distribución uniforme de Ra en un anillo con espesor igual al rango que el radón recorre en dicho material, con diámetros diferentes.

CONCLUSIONES

Se observa que el coeficiente de emanación depende de la distribución del Ra en el grano así como del radio del mismo. Una distribución de Ra en un anillo de espesor igual al rango que recorre el Rn en el material, sugiere un mayor coeficiente de emanación el cual se condice con los medidos experimentalmente obtenidos en [1], dichas medidas encontraron las concentraciones de Ra no es uniforme en todo el grano, observándose una concentración en una capa fina en las cercanías de la superficie del grano. Por lo tanto, una distribución uniforme de Ra en todo el grano no refleja la distribución de Ra en el grano y su correspondiente ϵ .

AGRADECIMIENTOS

Este trabajo fue realizado gracias al soporte de Concytec y el grupo de Huellas Nucleares de la PUCP (GITHUNU).

BIBLIOGRAFÍA

- [1] Tanner, A. B. (1980). Radon migration in the ground: a supplementary review. Natural radiation environment III, 1, 5-56.
- [2] Ziegler, J. F. (2013). SRIM-2013 software package. see <http://www.srim.org>. Google Scholar.
- [3] Stajic, J. M., & Nikezic, D. (2014). Theoretical calculation of radon emanation fraction. Nuclear Instruments and Methods in Physics Research Section B: Beam Interactions with Materials and Atoms, 336, 19-25.



PONTIFICIA
UNIVERSIDAD
CATÓLICA
DEL PERÚ

Development of LR-115-based radon monitors and their calibration using soil as radon source in a radon Chamber and the comparison with Monte Carlo simulation

Jhonny Jonnatan Rojas Hanco

Dra. María Elena Lopez Herrera

Dr. Daniel Palacios

Pontificia Universidad Católica del Perú

May 2018

Contents



Introduction

- . Radón
- . Radioactive chain

Methodology detection

- . Pasive and active method
- . LR-115 type II.

Montecarlo simulation

- . Window energy
- . Critical angle
- . Effective volume

Experimental methodology

Experimental results.

Introducción Radon

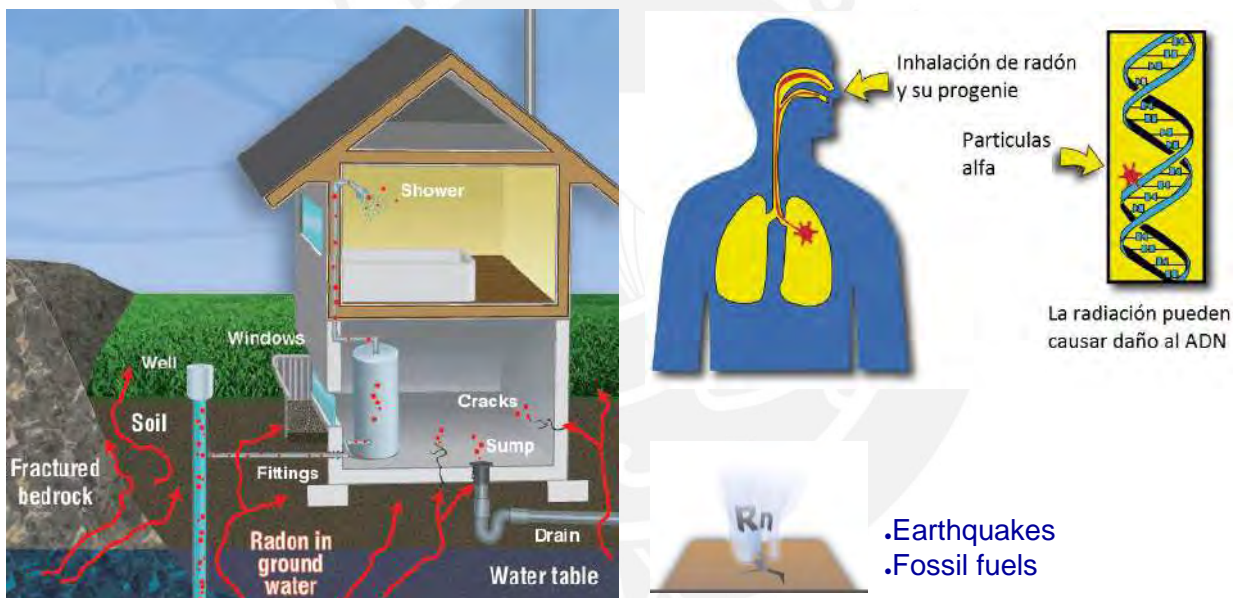


Figure1: Radon exhalation from soil, radon get into home Health Canada [1] .

Introduction

Radon

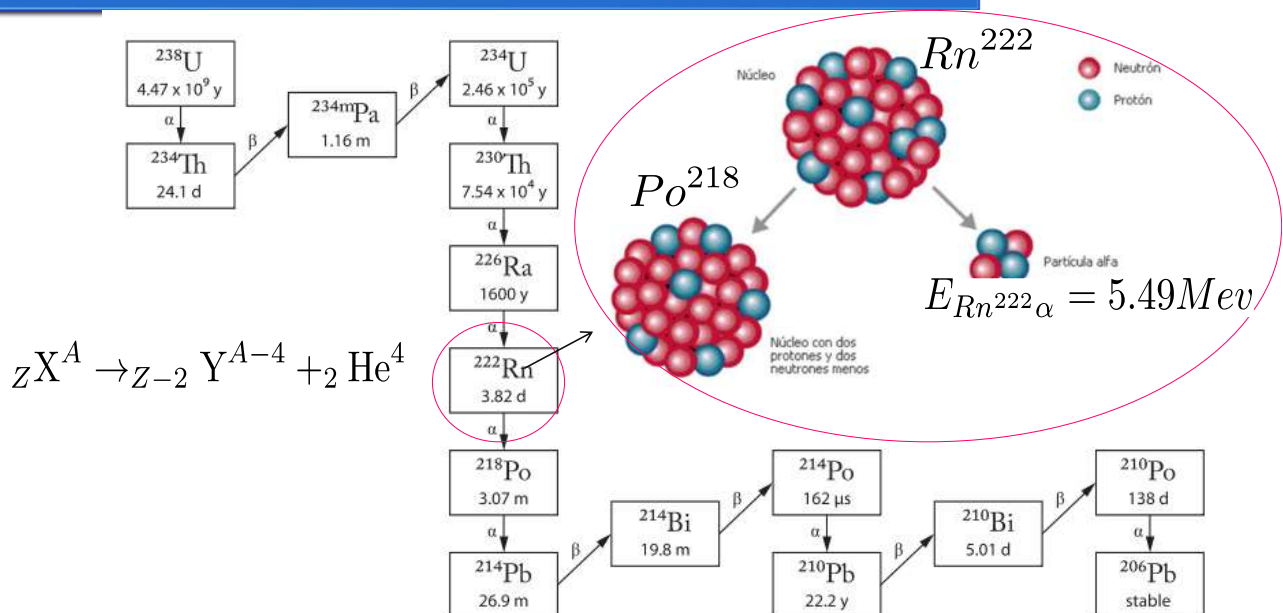


Figure2: Radioactive chain of U-238 [2].

Detection methodology

Pasive method (Nuclear track detectors)



Nuclear tracks due to alpha particles

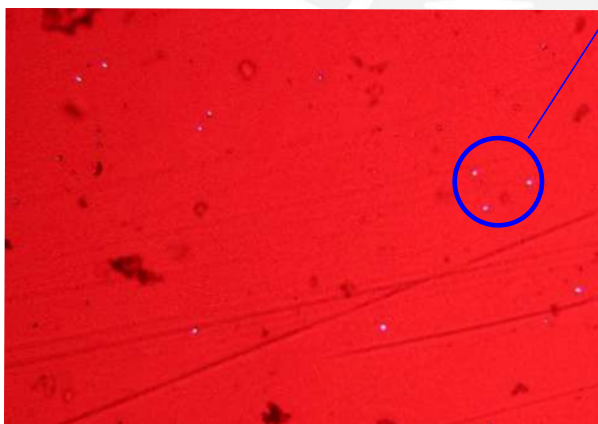


Figure3: LR 115 type II

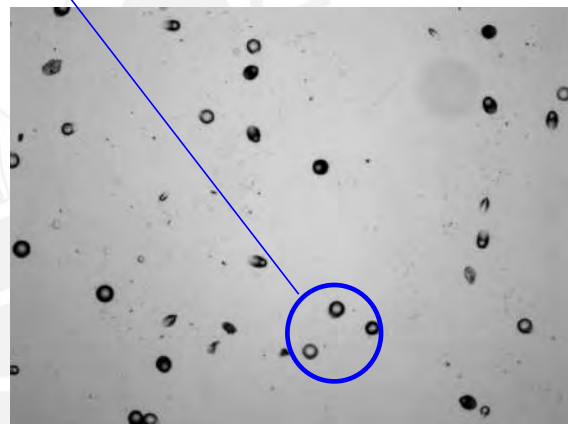


Figure4: CR 39

This detectors have different responses not only because the window energies, but also their structure.

Detection methodology

Active method

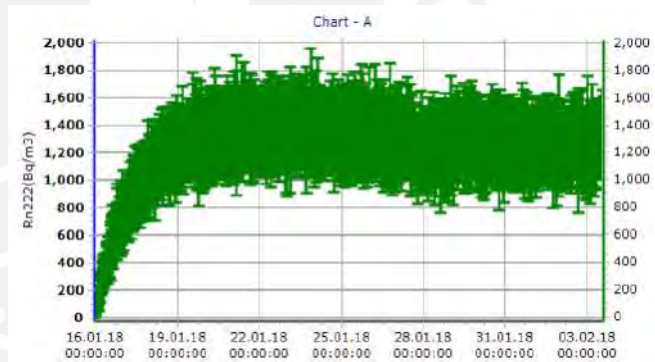


Figure5: **ALPHA GUARD**

Figure6: Radon concentration every 10 minutes.

Detection methodology LR-115 type II



It has a critical angle which depends on the energy and etching conditions.

$$\Delta E$$

$$\theta_{crit}(E)$$

Figure7: Cellulose nitrate film

The choice of the detector LR-115 is made in view of the fact that LR-115 detectors do not develop tracks originating from the progeny alphas deposited on them (Eappen et al., 1988; Nikolaev and Ilic, 1999; Durrani, 1997) and therefore are ideally suited for air concentration measurements (Eappen and Mayya, 2004)

Monte Carlo Simulation

Critical angle using track test program



```
ALLOWED  $V_t/V_b$  FUNCTIONS ARE AS FOLLOWS

THE FIRST ALLOWED FUNCTION IS
 $V_t/V_b = 1 + (A1 * \exp(-B1 * Y) + A2 * \exp(-B2 * Y)) * (1 - \exp(-B3 * Y))$ 
DEFAULT CONSTANTS ARE: A1=100; A2=5; B1=0.446; B2=0.107; B3=1

THE SECOND ALLOWED FUNCTION IS
 $V_t/V_b = 1 + (2.14 * \exp(-0.12 * Y) + 2.7 * \exp(-0.135 * Y)) * (1 - \exp(-Y))$ 

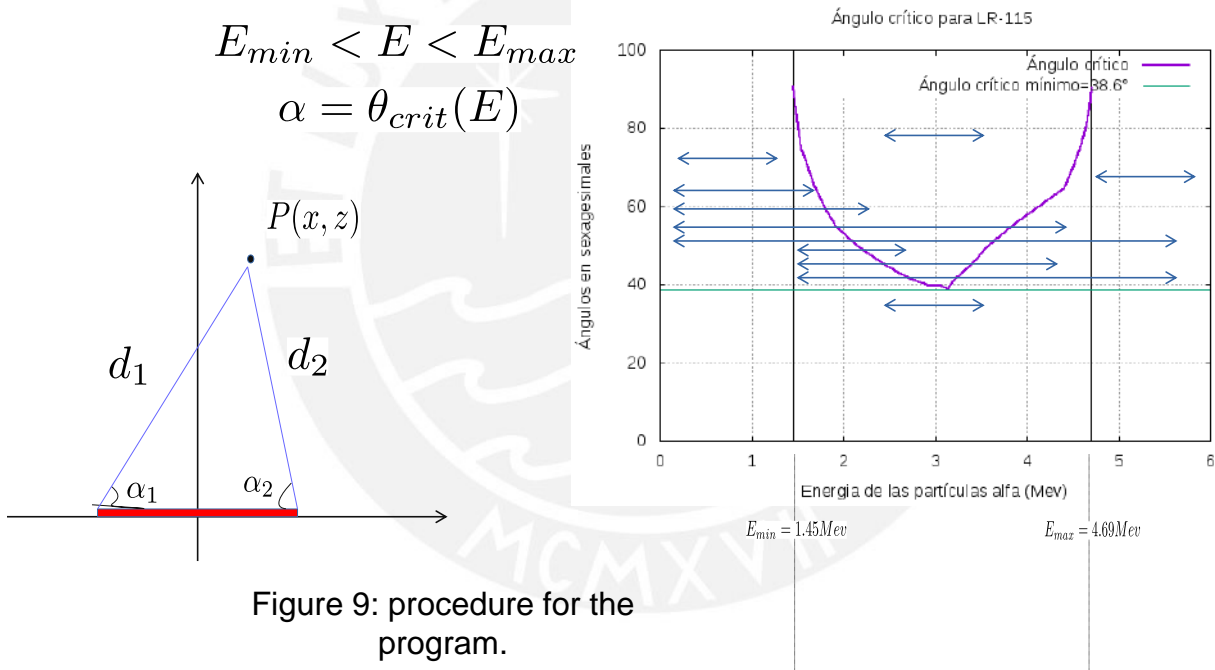
Y IS RESIDUAL RANGE OF ALPHA PARTICLE IN DETECTOR MATERIAL

TYPE 1 FOR FIRST OR 2 FOR SECOND FUNCTION
```

Figure 8: Track test program [4].

Monte Carlo simulation

Development of code to determine the effective volume



Monte Carlo simulation

Effective volumes of radon and its progeny

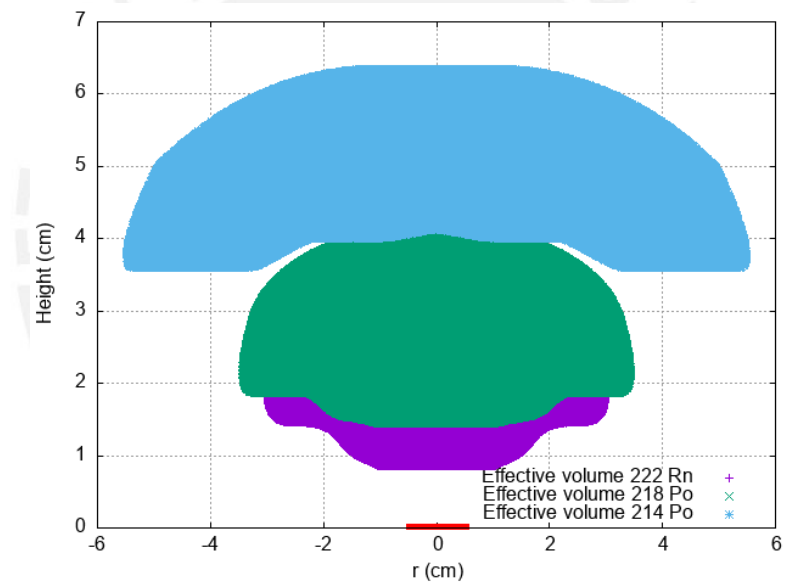


Figure 10: effective volume for bare mode L-115.

Monte Carlo simulation Thoron diffusion

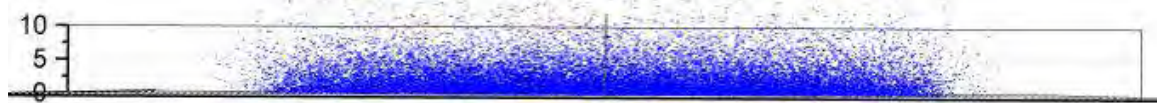


Figure11: Thoron exhalation of the soil or wall.

Experimental methodology

.G2 monitors and bare mode LR-115 type 2 detector

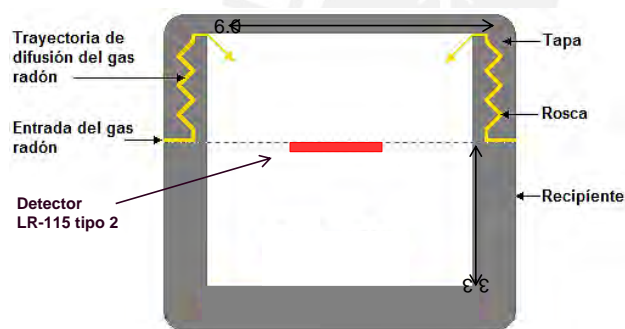


Figure12: Geometry of G2 monitor.

Figure13: General view of G2 monitors and bare mode LR-115 detectors.

Experimental methodology

.Two experiments were carried out:

.The first is the exposure of the G2 monitors and bare detectors (attached to the wall of the accumulation chamber) to three exposures which are low, medium, and high.

.The second is the exposure only of bare detectors to determine thoron influence.

Experimental methodology

.First experiment

The detectors were exposed to three radon exposures, 296.96, 704.40 And 8297.27 Kbqh/m³.

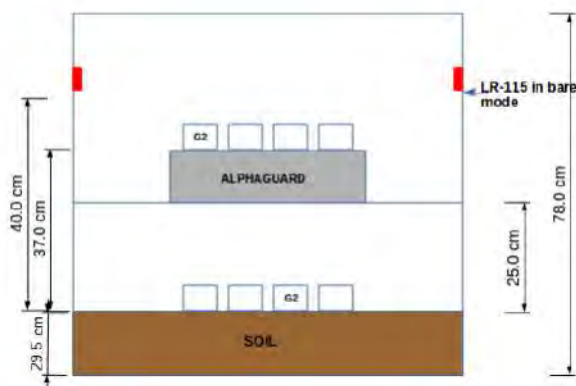


Figure14: Scheme of the First experiment.

Experimental methodology

.Second experiment

The bare mode LR-115 type 2 detectors were exposed to radon exposure of 544.88 Kbqh/m^3 .

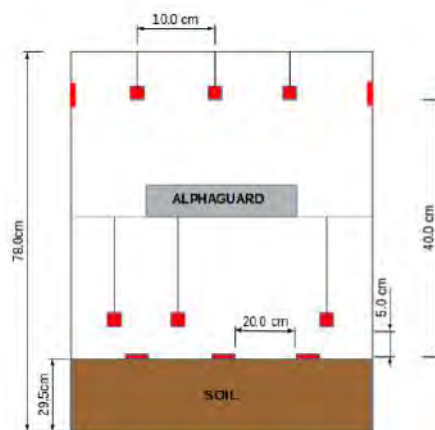


Figure15: Scheme of the second experiment.

Experimental methodology

Exposures

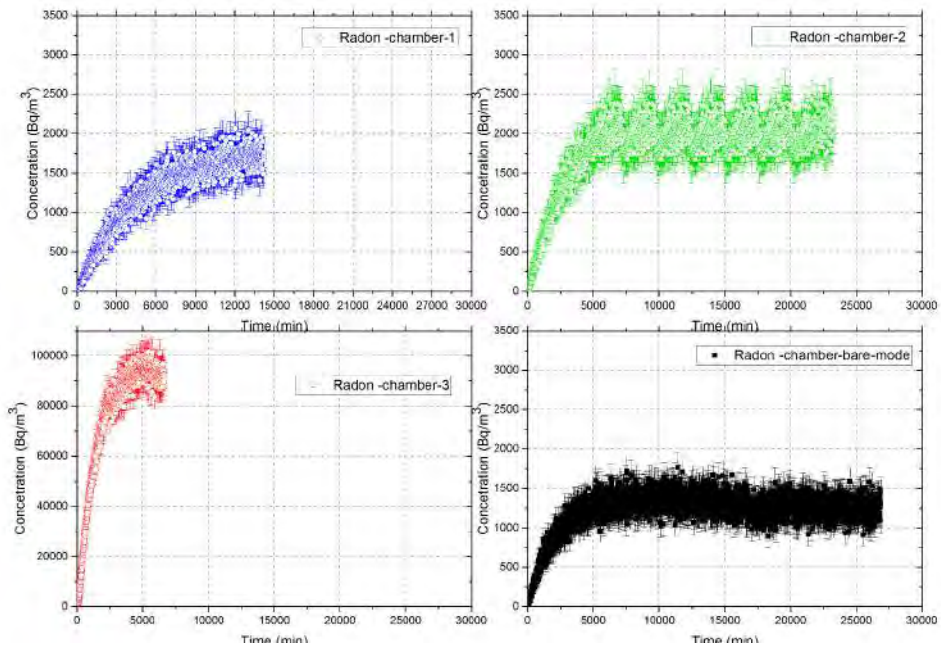


Figure 16: Different exposure in the radon chamber.

Experimental results

First experiment G2 calibration factor

$$CF_{G2} = 0.01291 \pm 0.00105 \frac{\text{Tracks/mm}^2}{\text{KBqh/m}^3}$$

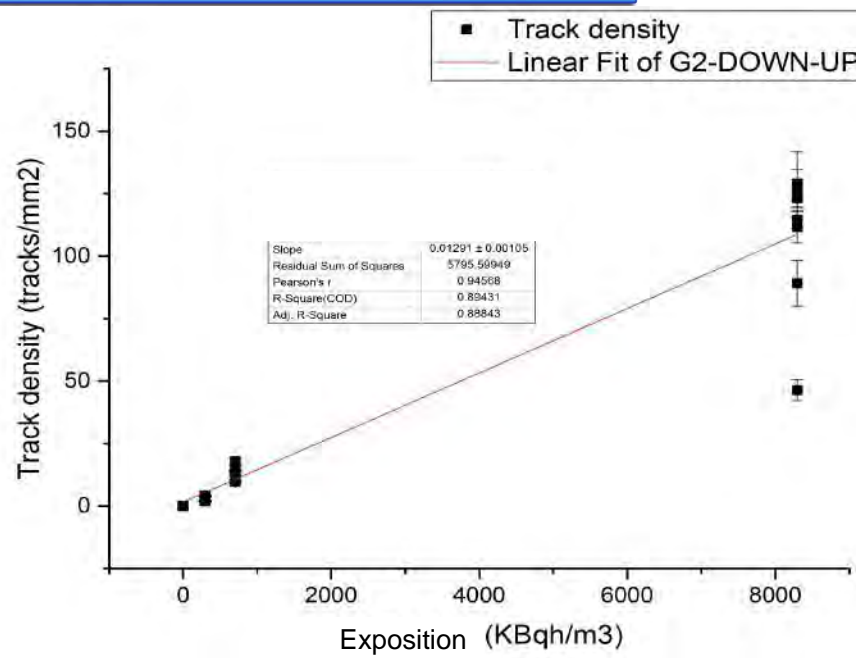
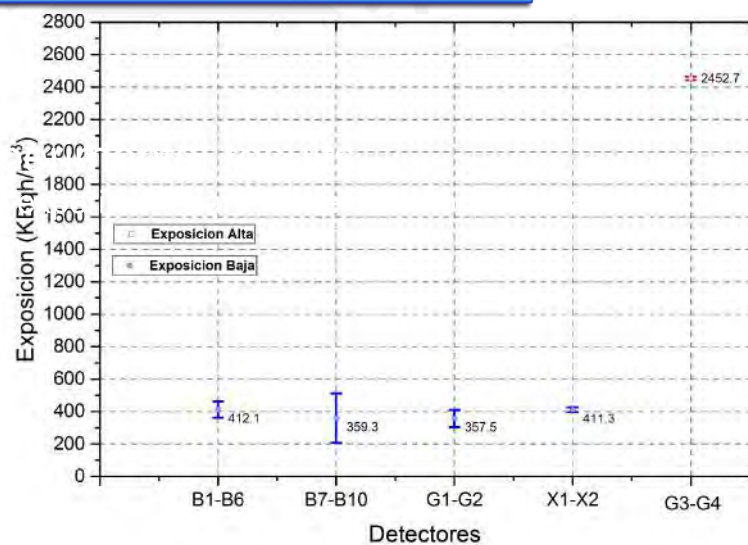


Figure17: Calibration factor for G2 monitors.

Experimental results

Intercomparasion (Universidad de Cantabria (LARUC))

Figure 18: The result of intercomparison was 1.3 times the reference exposure.



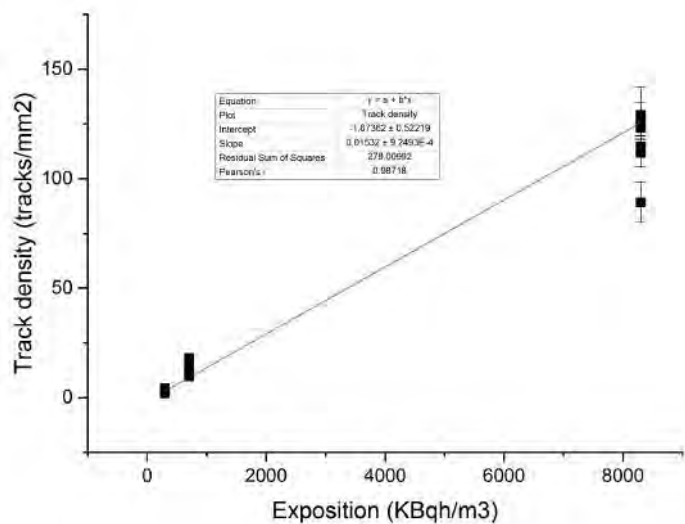
reference exposure (kBqm/m ³)	275.0	1886.7
Mean exposure (kBqm/m ³) ±%	357.5 ±15.0	2452.7 ± 0.6

Experimental results G2

Intercomparasion (Universidad de Cantabria (LARUC))

Figure 19: After eliminate atypical value the result of intercomparasion was 1.13 times the reference exposure.

$$CF_{G2} = 0.01532 \pm 9.2493E^{-4} \frac{\text{Tracks/mm}^2}{\text{KBqh/m}^3}$$



reference exposure (kBqm/m ³)	275.0	1886.7
Mean exposure (kBqm/m ³) ±%	305.5 ± 10.6	2123.7 ± 0.6

Conclusions

- .The G2 can discriminate thoron, radon daughters and avoid aerosols.
- .The results were appropriate however, the tests continue to guarantee compliance with the accuracy criteria.
- .It is possible to calibrate detectors using soil and uranium ore.

References

- [1] <https://www.canada.ca/en/health-canada/services/environmental-workplace-health/reports-publications/radiation/radon-your-home-health-canada-2009.html>
- [2] Matthews, K. M., Kim, C. K., & Martin, P. (2007). Determination of ^{210}Po in environmental materials: a review of analytical methodology. *Applied Radiation and Isotopes*, 65(3), 267-279.
- [3] Ziegler, J. F., & Ziegler, J. SRIM & TRIM (2013).
- [4] Nikezic, D., & Yu, K. N. (2006). Computer program TRACK_TEST for calculating parameters and plotting profiles for etch pits in nuclear track materials. *Computer Physics Communications*, 174(2), 160-165.

Acknowledgment



PONTIFICIA
UNIVERSIDAD
CATÓLICA
DEL PERÚ



CIENCIAACTIVA
Financia y Co-Financiamiento del Concytec



CONCYTEC
GOBIERNO NACIONAL DE CIENCIA,
TECNOLOGÍA E INNOVACIÓN TECNOLÓGICA

Appendix C

Academic Achievements

Publications

1. **Rojas, J.J.**, Pérez, B., López, M.E., (2022). An approach to the measurement of radon permeability and transmission factor using CR-39 detectors inside a diffusion chambers exposed in a new-build radon chamber. Radiation Physics and Chemistry, submitted and review. <https://dx.doi.org/10.2139/ssrn.4252598>
2. Bonifaz, A. P., Moliné, O. B., Schneider, J. O., La Rosa, B. L. R., **Hanco, J. R.**, Rojas, V. G., & Herrera, M. E. L. (2020). Simple and low cost alternative method for detecting photoneutrons produced in some radiotherapy treatments using SSNTDs. Applied Radiation and Isotopes, 161, 109169. <https://doi.org/10.1016/j.apradiso.2020.109169>
3. Vilcapoma, L. L., López Herrera, M. E., Pereyra, P., Palacios, D. F., Pérez, B., **Rojas, J.**, & Sajo-Bohus, L. (2019). Measurement of radon in soils of Lima City-Peru during the period 2016-2017. Earth Sciences Research Journal, 23(3), 171-183. <https://doi.org/10.15446/esrj.v23n3.74108>
4. **Rojas, J.**, Palacios, D., Pereyra, P., Pérez, B., Bohus, L. S., & López, M. E. (2018). A semi-empirical approach to estimate the parameters determining the LR-115 detector response in radon measurements. Radiation Measurements, 118, 36-42. <https://doi.org/10.1016/j.radmeas.2018.08.005>
5. Chacin, G., Sajo-Bohus, L., **Hanco, J. R.**, & Espinosa, G. (2018). Jung's Theorem Applied in Nuclear Track Methodology. Journal of Nuclear Physics, Material Sciences, Radiation and Applications, 6(1), 51-55. <https://doi.org/10.15415/jnp.2018.61008>

Events

- **The XVIII International Symposium on Solid State Dosimetry** held from September 24 to 28, 2018 at Oaxaca, Oax., México. "Analysis of CR39 and LR 115 nuclear track detector response to neutron flux of an $^{241}\text{Am}/\text{Be}$ source using natural boron as converter"
- **XIV International Symposium on Radiation Physics** held from May 23 to 25, 2018 at Puebla, México. "Development of LR-115-based radon monitors and their calibration using soil as radon source in a chamber and the comparison with Monte Carlo simulation"
- **XI Congreso Regional de Seguridad Radiológica y Nuclear.** April 2018, La Habana Cuba. "Determinación del factor de emanación de radón en los granos del suelo a través de simulación Monte Carlo"
- **1st International Symposium on Environment ionizing radiation and its impact** held from January 16 to 20, 2017 at Cuenca, Ecuador. "Enfoque semi-empírico para la calibración de detectores LR-115 en cámaras de difusión para mediciones de radón"

Stage

- **Instituto Peruano de Energía Nuclear (IPEN) - en convenio con Universidad Nacional de Cordova (Argentina).** November 2018, "Training Course in Nuclear Reactors"
- **Universidad Autónoma de Zacatecas, Unidad Académica de Estudios Nucleares.** May to July 2018, México. "Training in Monte Carlo Methods"
- **Universidad Nacional Autónoma de México** Departamento de física experimental. May 2018, "detectors recognition to measure radon at laboratory"

Funding

1. **Doctoral Scholarship.** CONCyTEC N° - 000236 - 2015 - FONDECYT - August 2016 to July 2019.
2. **Master Scholarship.** CONCyTEC N° - 012 - 2013 - FONDECYT - April 2014 to December 2015.

Bibliography

- [1] R Shweikani and G Raja. Design, construct and test of a calibration radon chamber. *Radiation measurements*, 40(2-6):316–319, 2005.
- [2] S Heidary, S Setayeshi, M Ghannadi-Maragheh, and A Negarestani. Monitoring and measurement of radon activity in a new design of radon calibration chamber. *Radiation measurements*, 46(8):694–700, 2011.
- [3] Juan Pablo Bonetto, Analia Canoba, and Fabio Lopez. Radon measurements in argentina. 2014.
- [4] Marta Fuente, Daniel Rabago, Sixto Herrera, Luis Quindos, Ismael Fuente, Mark Foley, and Carlos Sainz. Performance of radon monitors in a purpose-built radon chamber. *Journal of Radiological Protection*, 38(3):1111, 2018.
- [5] P Pereyra, ME Lopez, B Perez, J Rojas, J Martinez, and K León. Characterization of lr-115 type 2 detectors for monitoring indoor radon 222: Determination of the calibration factor. 2016.
- [6] JM Stajic and Dragoslav Nikezic. Theoretical calculation of radon emanation fraction. *Nuclear Instruments and Methods in Physics Research Section B: Beam Interactions with Materials and Atoms*, 336:19–25, 2014.
- [7] Oscar Baltuano, Marco Munive, Jorge Martínez, Susana Gonzáles, Yuri Hernández, and José Solís. Desarrollo de un prototipo económico para monitorear radón en instalaciones industriales y viviendas. 2013.
- [8] Zhang Xiongjie, Zhang Ye, Liu Yang, and Tang Bin. Evaluation of the uniformity of concentration of radon in a radon chamber. *Applied Radiation and Isotopes*, 110:183–188, 2016.
- [9] P Ditmar and AA Van Eck Van Der Sluijs. A technique for modeling the earth’s gravity field on the basis of satellite accelerations. *Journal of Geodesy*, 78(1):12–33, 2004.
- [10] Miroslav Ješkovský, Jakub Kaizer, Ivan Kontul’, Galina Lujaniené, Monika Müllerová, and Pavel P Povinec. Analysis of environmental radionuclides. In *Handbook of Radioactivity Analysis: Volume 2*, pages 137–261. Elsevier, 2019.
- [11] Guillaume Samuel Bineng, Shinji Tokonami, Masahiro Hosoda, Yvette Flore Tchunte Siaka, Hamadou Issa, Takahito Suzuki, Hiromi Kudo, and Oumarou Bouba. The importance of direct progeny measurements for correct estimation of effective dose due to radon and thoron. *Frontiers in Public Health*, 8:17, 2020.
- [12] JD Harrison and JW Marsh. Effective dose from inhaled radon and its progeny. *Annals of the ICRP*, 41(3-4):378–388, 2012.

- [13] Marelene F Rayner-Canham and Geoffrey W Rayner-Canham. Rutherford, the ‘true discoverer of radon’. *Bulletin for the History of Chemistry*, 29(2):89–90, 2004.
- [14] James L Marshall and Virginia R Marshall. Rediscovery of the elements rutherford and radon.
- [15] J Mc Laughlin. An historical overview of radon and its progeny: applications and health effects. *Radiation protection dosimetry*, 152(1-3):2–8, 2012.
- [16] Ludwig Pincussen. Biologische lichtwirkungen, ihre physikalischen und chemischen Grundlagen. *Ergebnisse der Physiologie*, 19(1):79–289, 1921.
- [17] Hajo Zeeb, Ferid Shannoun, World Health Organization, et al. *WHO handbook on indoor radon: a public health perspective*. World Health Organization, 2009.
- [18] World Health Organization. *WHO handbook on indoor radon: a public health perspective*. World Health Organization, 2009.
- [19] Alberto Ruano-Ravina, Karl T Kelsey, Alberto Fernández-Villar, and Juan M Barros-Dios. Action levels for indoor radon: different risks for the same lung carcinogen?, 2017.
- [20] World Health Organization et al. Protection of the public against exposure indoors due to radon and other natural sources of radiation. specific safety guide. 2015.
- [21] Instituto Peruano de Energía nuclear IPEN, Reglamento de seguridad radiologica. http://www.ipen.gob.pe/site/regulacion/normatividad/ds009_97em.pdf. Accessed:2016-02-27.
- [22] IPEN. Decreto supremo n° 009-97-em, sep 1989.
- [23] Worawat Poltabtim, Chutima Kranrod, and Shinji Tokonami. An overview of passive-type detectors for radon and its progeny measurement. *Radiation Environment and Medicine*, 11(2):41–49, 2022.
- [24] Jing Chen and Naomi H Harley. A review of indoor and outdoor radon equilibrium factors—part i: 222rn. *Health physics*, 115(4):490–499, 2018.
- [25] Shinji Tokonami, Takeshi Iimoto, and Ryuhei Kurosawa. Continuous measurement of the equilibrium factor f and the unattached fraction f_p of radon progeny in the environment. *Environment International*, 22:611–616, 1996.
- [26] Jing Chen and Leonora Marro. Assessment of radon equilibrium factor from distribution parameters of simultaneous radon and radon progeny measurements. *Radiation and environmental biophysics*, 50(4):597–601, 2011.
- [27] RC Ramola, MS Negi, and VM Choubey. Measurement of equilibrium factor” f' between radon and its progeny and thoron and its progeny in the indoor atmosphere using nuclear track detectors. *Indoor and Built Environment*, 12(5):351–355, 2003.
- [28] Roger E Stoller, Mychailo B Toloczko, Gary S Was, Alicia G Certain, Shyam Dwaraknath, and Frank A Garner. On the use of srim for computing radiation damage exposure. *Nuclear instruments and methods in physics research section B: beam interactions with materials and atoms*, 310:75–80, 2013.

- [29] D Nikezic, FMF Ng, and KN Yu. Theoretical basis for long-term measurements of equilibrium factors using Ir 115 detectors. *Applied radiation and isotopes*, 61(6):1431–1435, 2004.
- [30] Glenn F Knoll. *Radiation detection and measurement*. John Wiley & Sons, 2010.
- [31] Dragoslav Nikezic and KN Yu. Computer program track_test for calculating parameters and plotting profiles for etch pits in nuclear track materials. *Computer Physics Communications*, 174(2):160–165, 2006.
- [32] Saeed A Durrani and Richard K Bull. *Solid state nuclear track detection: principles, methods and applications*, volume 111. Elsevier, 2013.
- [33] SA Durrani and PF Green. The effect of etching conditions on the response of Ir 115. *Nuclear Tracks and Radiation Measurements (1982)*, 8(1-4):21–24, 1984.
- [34] Jin-lei Sun, Shi-wen Zhang, Song Huang, and Zhan-wei Hui. Design and application of a sikuli based capture-replay tool. In *2018 IEEE International Conference on Software Quality, Reliability and Security Companion (QRS-C)*, pages 42–44. IEEE, 2018.
- [35] VSY Koo, CWY Yip, JPY Ho, D Nikezic, and KN Yu. Deposition fractions of ²¹⁸Po in diffusion chambers. *Applied radiation and isotopes*, 59(1):49–52, 2003.
- [36] Jhonny Rojas, Daniel Palacios, Patrizia Pereyra, Bertin Pérez, Laszlo Sajo Bohus, and María Elena López. A semi-empirical approach to estimate the parameters determining the Ir-115 detector response in radon measurements. *Radiation Measurements*, 118:36–42, 2018.
- [37] KP Eappen and YS Mayya. Calibration factors for Ir-115 (type-ii) based radon thoron discriminating dosimeter. *Radiation measurements*, 38(1):5–17, 2004.
- [38] United States. Environmental Protection Agency. Office of Air and Centers for Disease Control (US). *A Citizen's Guide to Radon: What it is and what to Do about it*, volume 86. US Environmental Protection Agency, Office of Air and Radiation, 1986.
- [39] Edward P Radford and KG St Clair Renard. Lung cancer in swedish iron miners exposed to low doses of radon daughters. *New England Journal of Medicine*, 310(23):1485–1494, 1984.
- [40] Geno Saccomanno, Gerald C Huth, Oscar Auerbach, and Marvin Kuschner. Relationship of radioactive radon daughters and cigarette smoking in the genesis of lung cancer in uranium miners. *Cancer*, 62(7):1402–1408, 1988.
- [41] Jonathan M Samet. Radon and lung cancer. *JNCI: Journal of the National Cancer Institute*, 81(10):745–758, 1989.
- [42] Janet Gaskin, Doug Coyle, Jeff Whyte, and Daniel Krewksi. Global estimate of lung cancer mortality attributable to residential radon. *Environmental health perspectives*, 126(5):057009, 2018.
- [43] A Canoba, FO López, MI Arnaud, AA Oliveira, RS Neman, JC Hadler, PJ Iunes, SR Paulo, AM Osorio, R Aparecido, et al. Indoor radon measurements in six latin american countries. *Geofisica internacional*, 41(4):453–457, 2002.

- [44] Alexandra Giraldo-Osorio, Alberto Ruano-Ravina, Leonor Varela-Lema, Juan M Barros-Dios, and Mónica Pérez-Ríos. Residential radon in central and south america: A systematic review. *International Journal of Environmental Research and Public Health*, 17(12):4550, 2020.
- [45] D Nikezic and KN Yu. Are radon gas measurements adequate for epidemiological studies and case control studies of radon-induced lung cancer? *Radiation protection dosimetry*, 113(2):233–235, 2005.
- [46] Lucia-Adina Truta-Popa, Alexandra Dinu, Tiberius Dicu, Kinga Szacsvai, Constantin Cosma, and Werner Hofmann. Preliminary lung cancer risk assessment of exposure to radon progeny for transylvania, romania. *Health physics*, 99(3):301–307, 2010.
- [47] R Collé, JMR Hutchinson, and MP Unterweger. The nist primary radon-222 measurement system. *Journal of research of the National Institute of Standards and Technology*, 95(2):155, 1990.
- [48] P Kotrappa and F Stieff. One cubic metre nist traceable radon test chamber. *Radiation protection dosimetry*, 128(4):500–502, 2008.
- [49] Mark O Semler and Edwin L Sensintaffar. Quality assurance for radon exposure chambers at the national air and radiation environmental laboratory, montgomery, alabama. Technical report, 1993.
- [50] Jong-Man Lee, Kil Hoon Ahn, Ha Seok Chai, and Tae Soon Park. Development of radon calibration chamber at kriss. *Applied radiation and isotopes*, 61(2-3):237–241, 2004.
- [51] Shinji Tokonami, Tetsuo Ishikawa, Atsuyuki Sorimachi, Hiroyuki Takahashi, and Nobuyuki Miyahara. The japanese radon and thoron reference chambers. In *AIP Conference Proceedings*, volume 1034, pages 202–205. American Institute of Physics, 2008.
- [52] R Subber, HN Noori, FN Ali, HJ Jabbar, and MK Khodier. Constructasa simple radon chamber for measurement of radon detectors calibration factors. *Pelagia research library, Advances in applied Science research*, 6(2):128–131, 2015.
- [53] Paul Kotrappa and Frederick Stieff. Characterization and use of an accumulating type of radon test chamber. *in proceedings of AARST*, 2012.
- [54] MM Radebe. *The design of a radon chamber for the calibration of radon monitors at the Centre for Applied Radiation Science and Technology, Mafikeng, South Africa*. PhD thesis, North-West University (South Africa), 2019.
- [55] Raspberry Pi. Raspberry pi 3 model b. *online*].(<https://www.raspberrypi.org>, 2015.
- [56] Beatriz Ruvira, Beatriz García-Fayos, Belén Juste, José Miguel Arnal, and Gumersindo Verdú. Experimental estimation of the diffusion coefficient in radon barrier materials based on iso/ts 11665-13: 2017. *Radiation Physics and Chemistry*, 193:109993, 2022.
- [57] Christoph Pfeifer, Federica Cavalli, Birgit Huber, Patrick Theato, Leonie Barner, and Manfred Wilhelm. Investigation of the porosity of poly (sodium methacrylate) hydrogels by 1h-nmr t2-relaxation and inverse size-exclusion chromatography. *Macromolecular Chemistry and Physics*, 222(1):2000300, 2021.
- [58] Paul K Kuroda. On the isotopic constitution of radium (ra-223/ra-226) in uranium minerals and recent problems of geochronology. *Annals of the New York Academy of Sciences*, 62(8):179–207, 1955.

- [59] HENRY Bell and WE BALES. A contribution to the geology of uranium. *Uranophane at Silver Cliff Mine, Lusk, Wyoming*, (1009):211, 1954.
- [60] Kainan Sun, Qiuju Guo, and Jianping Cheng. The effect of some soil characteristics on soil radon concentration and radon exhalation from soil surface. *Journal of nuclear science and technology*, 41(11):1113–1117, 2004.
- [61] Ahmad Ciptadi Syuryavin, Seongjin Park, Muttaqin Margo Nirwono, and Sang Hoon Lee. Indoor radon and thoron from building materials: Analysis of humidity, air exchange rate, and dose assessment. *Nuclear Engineering and Technology*, 52(10):2370–2378, 2020.
- [62] Viktor Jobbágy, Timotheos Altzitzoglou, Petya Malo, Vesa Tanner, and Mikael Hult. A brief overview on radon measurements in drinking water. *Journal of environmental radioactivity*, 173:18–24, 2017.
- [63] Abraham Lerman et al. *Geochemical processes. Water and sediment environments*. John Wiley and Sons, Inc., 1979.
- [64] William W Nazaroff and Anthony V Nero. Radon and its decay products in indoor air. 1988.
- [65] G Keller and B Hoffmann. The radon diffusion length as a criterion for the radon tightness. In *IRPA10 conference proceedings, Hiroshima*, 2000.
- [66] AK Narula, SK Goyal, Savita Saini, RP Chauhan, and SK Chakarvarti. Calculation of radon diffusion coefficient and diffusion length for different building construction materials. *Indian journal of physics*, 83(8):1171–1175, 2009.
- [67] International Atomic Energy Agency. Measurement and calculation of radon releases from norm residues, technical reports series no. 474, 2013.
- [68] Akihiro Sakoda, Yuu Ishimori, and Kiyonori Yamaoka. A comprehensive review of radon emanation measurements for mineral, rock, soil, mill tailing and fly ash. *Applied Radiation and Isotopes*, 69(10):1422–1435, 2011.
- [69] KP Eappen, BK Sapra, and YS Mayya. A novel methodology for online measurement of thoron using lucas scintillation cell. *Nuclear Instruments and Methods in Physics Research Section A: Accelerators, Spectrometers, Detectors and Associated Equipment*, 572(2):922–925, 2007.
- [70] C Cosma, F Dancea, T Jurcut, and D Ristoiu. Determination of ^{222}Rn emanation fraction and diffusion coefficient in concrete using accumulation chambers and the influence of humidity and radium distribution. *Applied Radiation and Isotopes*, 54(3):467–473, 2001.
- [71] Jaime Wisniak. Eugène melchior peligot. *Educación química*, 20(1):61–69, 2009.
- [72] Roger F Robison. Radioactive rocks. In *Mining and Selling Radium and Uranium*, pages 57–81. Springer, 2015.
- [73] David John. *Phase relations and crystal chemistry of secondary uranium minerals of the torbernite group*. The University of Manchester (United Kingdom), 1984.
- [74] ML Aceña Barrenechea and MJ Tormo Ferrero. Espectrometría alfa de fuentes• adlacíivas gruesas. 11 posibilidades je aplicación al estudio de equilibrios.

- [75] Oscar Baltuano, Yuri Hernandez, Pablo Mendoza, and Eduardo Montoya. Development of a low cost alpha particle spectrometer. Technical report, 2011.
- [76] Zhang Xiongjie, Zhang Ye, Tang Bin, Wang Renbo, and Qu Jinhui. Methods of kernel parameter calculation for stabilization technology of radon concentration in a closed radon chamber. *Applied Radiation and Isotopes*, 140:267–271, 2018.
- [77] Amit Kumar and RP Chauhan. Back diffusion correction for radon exhalation rates of common building materials using active measurements. *Materials and Structures*, 48(4):919–928, 2015.
- [78] Fabio O Lopez and Analia C Canoba. A passive method for the determination of the equilibrium factor between radon gas and its short period progeny; metodo pasivo para la determinacion del factor de equilibrio entre el gas $\{^{222}\text{Rn}\}$ y sus descendientes de periodo corto. 2001.
- [79] Chi-Feng Lin, Jeng-Jong Wang, Shih-Jung Lin, and Chien-Kung Lin. Performance comparison of electronic radon monitors. *Applied Radiation and Isotopes*, 81:238–241, 2013.
- [80] Marco Caresana, Francesco Cortesi, and Stefano Coria. Study of a discriminative technique between radon and thoron in the radout detector. *Radiation Measurements*, 138:106429, 2020.
- [81] Carlo Sabbarese, Fabrizio Ambrosino, and V Roca. Analysis by scanner of tracks produced by radon alpha particles in cr-39 detectors. *Radiation Protection Dosimetry*, 191(2):154–159, 2020.
- [82] S Frutos-Puerto, MC Hurtado-Sanchez, J de la Torre Pérez, E Pinilla-Gil, and C Miró. Radon alpha track counting on solid state nuclear track detector by an imagej-based software macro. *Applied Radiation and Isotopes*, 173:109695, 2021.
- [83] AA Azooz, SH Al-Nia’emi, and MA Al-Jubbori. A parameterization of nuclear track profiles in cr-39 detector. *Computer Physics Communications*, 183(11):2470–2479, 2012.
- [84] Daniele Franci and Tommaso Aureli. A method to account for track overlap in cr-39 detectors. *Radiation protection dosimetry*, 158(1):107–110, 2014.
- [85] TV Ramachandran, BY Lalit, and UC Mishra. Measurement of radon permeability through some membranes. *International Journal of Radiation Applications and Instrumentation. Part D. Nuclear Tracks and Radiation Measurements*, 13(1):81–84, 1987.
- [86] BK Sahoo, BK Sapra, SD Kanse, JJ Gaware, and YS Mayya. A new pin-hole discriminated $^{222}\text{Rn}/^{220}\text{Rn}$ passive measurement device with single entry face. *Radiation Measurements*, 58:52–60, 2013.
- [87] D Pressyanov, S Georgiev, I Dimitrova, K Mitev, and T Boshkova. Determination of the diffusion coefficient and solubility of radon in plastics. *Radiation protection dosimetry*, 145(2-3):123–126, 2011.
- [88] Marcin Wójcik and Grzegorz Zuzel. Radon permeability through nylon at various humidities used in the borexino experiment. *Nuclear Instruments and Methods in Physics Research Section A: Accelerators, Spectrometers, Detectors and Associated Equipment*, 524(1-3):355–365, 2004.

- [89] Wafaa Arafa. Permeability of radon-222 through some materials. *Radiation measurements*, 35(3):207–211, 2002.
- [90] Dragoslav Nikezic, KN Yu, and JM Stajic. Computer program for the sensitivity calculation of a cr-39 detector in a diffusion chamber for radon measurements. *Review of Scientific Instruments*, 85(2):022102, 2014.
- [91] Dietrich Hermsdorf. Evaluation of the sensitivity function v for registration of α -particles in padc cr-39 solid state nuclear track detector material. *Radiation measurements*, 44(3):283–288, 2009.

